UNIVESITY OF THESSALY

SCHOOL OF ENGINEERING

DEPARTMENT OF CIVIL ENGINEERING

NUMERICAL INVESTIGATION OF WEAK-AXIS
I PROFILE CONNECTIONS

by

KATIANA KONTOLATI

Supervisor: Assist. Prof. Olympia Panagouli

Department of Civil Engineering, University of Thessaly

A thesis submitted in partial fulfilment of the

requirements for the degree of

Diploma in Civil Engineering

Volos, September 2017

ΠΑΝΕΠΙΣΤΗΜΙΟ ΘΕΣΣΑΛΙΑΣ

ΠΟΛΥΤΕΧΝΙΚΗ ΣΧΟΛΗ

ΤΜΗΜΑ ΠΟΛΙΤΙΚΩΝ ΜΗΧΑΝΙΚΩΝ

Διπλωματική εργασία

ΑΡΙΘΜΗΤΙΚΗ ΠΡΟΣΟΜΟΙΩΣΗ ΣΥΝΔΕΣΕΩΝ ΑΣΘΕΝΟΥΣ ΑΞΟΝΑ ΔΙΑΤΟΜΩΝ ΔΙΠΛΟΥ ΤΑΥ

ΚΑΤΙΑΝΑ ΚΟΝΤΟΛΑΤΗ

Επιβλέπων: Επικ. Καθηγήτρια Ολυμπία Παναγούλη

Τμήμα Πολιτικών Μηχανικών, Πανεπιστήμιο Θεσσαλίας

Υπεβλήθη για την εκπλήρωση μέρους των

απαιτήσεων για την απόκτηση του

Διπλώματος Πολιτικού Μηχανικού

Βόλος, Σεπτέμβριος 2017

Η έγκριση της διπλωματικής εργασίας από το Τμήμα Πολιτικών Μηχανικών της Πολυτεχνικής Σχολής του Πανεπιστημίου Θεσσαλίας δεν υποδηλώνει αποδοχή των απόψεων του συγγραφέα (Ν. 5343/32 αρ. 202 παρ. 2).

Examination Committee

First Member (Supervisor)	**Dr. Olympia Panagouli** Assist. Professor, Department of Civil Engineering University of Thessaly
Second Member	**Dr. Euripidis Mistakidis** Professor, Department of Civil Engineering University of Thessaly
Third Member	**Dr. Konstantinos Tzaros** Lecturer, Department of Civil Engineering University of Thessaly

Acknowledgments

Firstly, I would like to thank my supervisors, Assist. Professor Olympia Panagouli and Professor Euripidis Mistakidis for their continuous guidance regarding my thesis. Most importantly, I want to thank them for their kind support, the opportunities they gave me, their valuable advices and the immense enthusiasm I have acquired through them about research. My sincere gratitude also goes to Dr. Apostolis Koukouselis, who guided me into the world of numerical modelling and steered me in the right direction whenever I needed it. I would also want to thank for his participation in the examination committee, Dr. Konstantinos Tzaros. Finally, I must express my gratitude to my family, whose unparalleled love and support keep motivate me to achieve my goals.

Μέλη Τριμελούς Εξεταστικής Επιτροπής

Πρώτος Εξεταστής
(Επιβλέπων)

Δρ. Ολυμπία Παναγούλη
Επικ. Καθηγήτρια, Τμήμα Πολιτικών Μηχανικών
Πανεπιστήμιο Θεσσαλίας

Δεύτερος Εξεταστής

Δρ. Ευριπίδης Μυστακίδης
Καθηγητής, Τμήμα Πολιτικών Μηχανικών
Πανεπιστήμιο Θεσσαλίας

Τρίτος Εξεταστής

Δρ. Κωνσταντίνος Τζάρος
Λέκτορας ΠΔ407/80, Τμήμα Πολιτικών Μηχανικών
Πανεπιστήμιο Θεσσαλίας

Ευχαριστίες

NUMERICAL INVESTIGATION OF WEAK AXIS
I PROFILE CONNECTIONS

Katiana Kontolati

University of Thessaly, Department of Civil Engineering, 2017

Supervisor: Dr. Olympia Panagouli, Assist. Professor

ABSTRACT

An important part of the design of steel structures is the analysis and design of the various connections. In general, beam to column connections of I profiles along the strong axis are usually bolted end plate ones. Although connections along the weak axis of the column are typically designed as simple ones, in certain cases it is necessary for them to be able to carry moments. The connection of the beam directly to the web of the column may lead to construction difficulties, especially in the case that a strong axis connection exists at the same position. An alternative is to use two end plates so that the beam is connected to the two flanges of the column. In this case however, due to the lack of guideline in the relevant Eurocode 3 part 1-8 [1], the design of such a connection may be a cumbersome procedure. An alternative design approach is to employ numerical models. The scope of this study is the investigation of the behavior of such a connection by the means of detailed numerical models, capable of taking into account the different phenomena that may arise, such as material nonlinearity and contact between the various connection components. The investigation focuses on the impact of the thickness of the end-plates and stiffener and the grade and diameter of the bolts on the capacity and ductility of the studied connection. After testing various configurations, a full-strength connection was finally achieved. Finally, conclusions regarding the applicability of the FEA on such connections and the advantages in the use of the proposed configuration are presented.

Key Words
Steel connections, Weak-axis connections, Finite Elements, Non-Linear Analysis

ΑΡΙΘΜΗΤΙΚΗ ΠΡΟΣΟΜΟΙΩΣΗ ΣΥΝΔΕΣΕΩΝ ΑΣΘΕΝΟΥΣ ΑΞΟΝΑ ΔΙΑΤΟΜΩΝ ΔΙΠΛΟΥ Τ

Κατιάνα Κοντολάτη

Πανεπιστήμιο Θεσσαλίας, Τμήμα Πολιτικών Μηχανικών, 2017

Επιβλέπων Καθηγήτρια: Δρ. Ολυμπία Παναγούλη, Επίκ. Καθηγήτρια

ΕΚΤΕΤΑΜΕΝΗ ΠΕΡΙΛΗΨΗ (EXTENDED ABSTRACT IN GREEK)

Αναπόσπαστο κομμάτι στον σχεδιασμό των μεταλλικών κατασκευών αποτελούν οι θέσεις αποκατάστασης συνέχειας, γνωστές και ως συνδέσεις. Παραδοσιακά, συνδέσεις δοκού-υποστυλώματος διατομής διπλού ταυ κατά τον ισχυρό άξονα του υποστυλώματος υλοποιούνται μέσω κοχλιωτής σύνδεσης με μετωπική πλάκα. Παρόλο που οι συνδέσεις στον ασθενή άξονα του υποστυλώματος συνήθως θεωρούνται απλές, επιτρέποντας την ανάπτυξη στροφών που προκύπτουν λόγω των δράσεων σχεδιασμού, ενίοτε η ανάγκη παραλαβής ροπής και στους δύο άξονες του υποστυλώματος (ισχυρό και ασθενή) γίνεται επιτακτική.

Η πιο διαδεδομένη διάταξη σύνδεσης ασθενούς άξονα, αποτελεί αυτή κατά την οποία η δοκός συνδέεται απευθείας στον κορμό του υποστυλώματος. Η εν λόγω διάταξη, έχει μελετηθεί κατά κόρον τις προηγούμενες δεκαετίες από αρκετούς ερευνητές οι οποίοι θέσπισαν μία νέα συνιστώσα, αυτή του 'κορμού του υποστυλώματος σε κάμψη και διάτρηση' (Gomes et al. [2], Steenhuis et al. [39]). Επιπλέον, εξήγαγαν αναλυτικές σχέσεις για τον υπολογισμό της αντοχής και στροφικής δυσκαμψίας αυτής, βασισμένοι στη θεωρία των γραμμών διαρροής. Παρόλα αυτά, η συγκεκριμένη σύνδεση ασθενούς άξονα, χαρακτηρίζεται κατά την αστοχία από μία εκτός επιπέδου κάμψη του κορμού του υποστυλώματος η οποία οδηγεί στον σχηματισμό πλαστικοποιήσεων στην περιοχή, οι οποίοι με τη σειρά τους δυσχεραίνουν σημαντικά τον σχεδιασμό μίας δεύτερης σύνδεσης στον ισχυρό άξονα του υποστυλώματος. Επιπλέον, προβλήματα δημιουργούνται και κατά την κατασκευή αυτής, στην περίπτωση που υπάρχει ήδη μία σύνδεση στον ισχυρό άξονα.

Εναλλακτική λύση αποτελεί η σύνδεση της δοκού στα πέλματα του υποστυλώματος με την χρήση δύο μετωπικών πλακών. Οι ελάχιστες μελέτες που έχουν διεξαχθεί πάνω στην εν λόγω διάταξη, έχουν κυρίως εστιάσει στην συμπεριφορά της ισχυρής σύνδεσης, παρουσία της εναλλακτικής ασθενούς, καθώς αυτή επιβάλλεται σε καμπτικά φορτία (Cabrero and Bayo [46],[47], Loureiro et al. [48]). Εξαιτίας λοιπόν, της περιορισμένης βιβλιογραφίας πάνω στο εν

iv

λόγω ζήτημα αλλά και της έλλειψης οδηγιών σχεδιασμού από τον σχετικό κανονισμό (Ευρωκώδικας 3, μέρος 1.8), ο προσδιορισμός της αντοχής και της συνολικής συμπεριφοράς είναι σχετικά δύσκολη υπόθεση.

Μία διαφορετική προσέγγιση για τον υπολογισμό μια τέτοιας σύνδεσης, αποτελεί η χρήση αριθμητικών προσομοιωμάτων και ο προσδιορισμός της συμπεριφοράς μέσω της μεθόδου των Πεπερασμένων Στοιχείων. Σκοπός της παρούσας εργασίας, είναι η διερεύνηση της συμπεριφοράς και των μηχανισμών αστοχίας μίας τέτοιας σύνδεσης στον ασθενή άξονα μέσω μίας παραμετρικής ανάλυσης. Για τον σκοπό αυτό, η σύνδεση προς μελέτη προσομοιώθηκε μέσω τρισδιάστατων αριθμητικών μοντέλων, τα οποία είναι ικανά να λάβουν υπόψη τη μη γραμμική συμπεριφορά των υλικών αλλά και την επαφή μεταξύ των διάφορων στοιχείων της σύνδεσης. Η μελέτη επικεντρώνεται στην επιρροή του πάχους των μετωπικών πλακών, της κατακόρυφης μεταλλικής λεπίδας του υποστυλώματος (stiffener) αλλά και της διαμέτρου και ποιότητας των κοχλιών, τα οποία καθορίζουν σε μεγάλο βαθμό την τελική αντοχή και πλαστιμότητα της σύνδεσης.

Πιο συγκεκριμένα, ο κόμβος ο οποίος μελετήθηκε αποτελείται από μία δοκό HEB300, και ένα υποστύλωμα σύνθετης διατομής (πολύ κοντά στις διαστάσεις της πρότυπης HD360x179). Στη δοκό είναι συγκολλητή μία μετωπική πλάκα πλάτους/ύψους 300x500mm ενώ το πάχος αυτής είναι παράμετρος του προβλήματος. Μία δεύτερη συγκολλητή πλάκα στα πέλματα του υποστυλώματος πλάτους/ύψους 350x500mm και επίσης μεταβλητού πάχους, κοχλιώνεται με την μετωπική πλάκα, μέσω 8 κοχλιών (σε 4 σειρές). Η διάμετρος αλλά και η ποιότητα των κοχλιών είναι και αυτές παράμετροι του προβλήματος. Τέλος, εσωτερικά του υποστυλώματος, τοποθετείται μία κατακόρυφη λεπίδα μεταβλητού ύψους και πάχους, με σκοπό να προσδώσει μεγαλύτερη δυσκαμψία στην σύνδεση. Όσον αφορά το είδος της συγκόλλησης μεταξύ των πελμάτων του υποστυλώματος και της πλάκας η οποία είναι συγκολλητή σε αυτά, φάνηκε μέσω προκαταρκτικών αναλύσεων πως η λύση της απλής εξωραφής δεν επαρκεί καθώς κατά την καμπτική καταπόνηση του κόμβου, δημιουργούνται σε αυτή την περιοχή έντονες πλαστικοποιήσεις και τελικά μία πρόωρη αστοχία της σύνδεσης. Για το λόγο αυτό, είναι απαραίτητη η συγκόλληση μέσω εσωραφής πλήρους διείσδυσης, έτσι ώστε να αποφευχθούν τέτοια φαινόμενα και να γίνει εφικτή η εκμετάλλευση όλων των συνιστωσών της σύνδεσης κατά την παραλαβή φορτίων.

Η εισαγωγή των μοντέλων διαφορετικής γεωμετρίας στο πρόγραμμα πεπερασμένων στοιχείων Marc της εταιρίας MSC, γινόταν για λόγους εξοικονόμησης χρόνου μέσω κώδικα γλώσσας python. Το υποστύλωμα συνολικού ύψους 3 μέτρων, προσομοιώνει ουσιαστικά μισό όροφο πάνω και κάτω, ενώ το μήκος της δοκού επιλέχθηκε έτσι ώστε η τέμνουσα η οποία αναπτύσσεται στην περιοχή της σύνδεσης κατά την κάμψη αυτού να μην πλαστικοποιεί τον κορμό της δοκού. Δεδομένης της συμμετρίας του φορέα καθώς και της συμμετρίας της φόρτισης, (έμμεση καμπτική ροπή στον κόμβο μέσω επιβαλλόμενης μετακίνησης στο άκρο της δοκού) αποφασίσθηκε να αναλυθεί ο μισός φορέας, κάτι το οποίο

v

μείωσε σημαντικά τον υπολογιστικό χρόνο, δεσμεύοντας φυσικά τους κατάλληλους βαθμούς ελευθερίας στο επίπεδο συμμετρίας. Όσον αφορά το είδος των πεπερασμένων στοιχείων, στην κεντρική και κρίσιμη ζώνη της σύνδεσης, στην οποία και αναπτύσσονται κυρίως οι πλαστικοποιήσεις, χρησιμοποιήθηκαν ισοπαραμετικά στοιχεία ανώτερη τάξης τετράεδρα, δεκακομβικά σε αντίθεση με το υπόλοιπο μοντέλο, στο οποίο έγινε χρήση των βασικών τετράεδρων τετράκομβων στοιχείων. Επιπλέον, στην κρίσιμη αυτή ζώνη χρησιμοποιήθηκε πυκνότερος κάναβος για περισσότερη ακρίβεια. Τέλος, το σπείρωμα των κοχλιών προσομοιώθηκε με έναν κύλινδρο ισοδύναμης διατομής, κάτι το οποίο θεωρήθηκε πως δεν επηρεάζει τα αποτελέσματα σε σημαντικό βαθμό.

Ολοκληρώνοντας την προσομοίωση του κόμβου σε αριθμητικό μοντέλο, είναι απαραίτητο να ορισθούν οι βασικές παράμετροι μη-γραμμικότητας του προβλήματος, έτσι ώστε να επιτευχθεί η καλύτερη αναπαράσταση αυτού. Η πρώτη μορφή μη-γραμμικότητας πηγάζει από την μη γραμμική σχέση μεταξύ τάσεων και παραμορφώσεων. Πρότυπες καμπύλες τάσεων-παραμορφώσεων όλκιμων υλικών μπορούν να βρεθούν στον αντίστοιχο Ευρωκώδικα (EC3). Ωστόσο, οι καταστατικοί νόμοι του Ευρωκώδικα, θεωρούνται καταλληλότεροι για την περίπτωση του σχεδιασμού, μιας και αποτελούν μία συντηρητική απεικόνιση της συμπεριφοράς του υλικού. Μία πιο ρεαλιστική προσέγγιση κατά την δημιουργία αριθμητικών προσομοιωμάτων, είναι η υιοθέτηση καταστατικών νόμων προερχόμενοι από πειράματα που έχουν προέλθει από πειράματα. Έτσι λοιπόν, για τους κοχλίες ποιότητας 8.8 και 10.9, χρησιμοποιήθηκε μία τρι-γραμμική προσέγγιση από την βιβλιογραφία (Dessouki et al. [52]) με 12% και 8% αντίστοιχα, παραμόρφωση αστοχίας (ISO 898-1 [53]). Για τον δομικό χάλυβα S275, ο οποίος χρησιμοποιήθηκε σε όλα τα υπόλοιπα μέρη του κόμβου, υιοθετήθηκε μία πολύ-γραμμική προσέγγιση βασισμένη σε πειράματα [54], με παραμόρφωση αστοχίας 15%. Δεδομένου ότι η ανάλυση θα οδηγήσει σε μεγάλες παραμορφώσεις (2$^\text{η}$ πηγή μη-γραμμικότητας), οι παραπάνω πειραματικές τιμές τάσεων-παραμορφώσεων μετατράπηκαν με κατάλληλους μετασχηματισμούς έτσι ώστε να ληφθούν υπόψη οι παραμορφωμένες επιφάνειες. Τέλος, σαν κριτήριο αστοχίας επιλέχθηκε το Von Mises, πλέον ιδανικό για την αναπαράσταση του φαινόμενου της διαρροής σε όλκιμα υλικά.

Η τρίτη και τελευταία πηγή μη-γραμμικότητας στο μοντέλο, προέρχεται από το φαινόμενο της επαφής, το οποίο εμφανίζεται ιδιαίτερα σε κοχλιωτές συνδέσεις, λόγω της επαφής της κεφαλής των κοχλιών με τις πλάκες, την επαφή του σώματος του κοχλία με την άντυγα των οπών αλλά και το πιθανό ενδεχόμενο ανάπτυξης τριβής μεταξύ των πλακών. Με σκοπό την ρεαλιστική αναπαράσταση του φαινόμενου της επαφής, όλα τα σώματα θεωρήθηκαν παραμορφώσιμα ενώ για την επαφή μεταξύ τους επιλέχθηκε η "node-to-segment" αλληλεπίδραση, κατά την οποία κάθε εξωτερικός κόμβος επιφάνειας θεωρείται πιθανός κόμβος επαφής, ενώ τα segments αποτελούνται από τις ακμές και επιφάνειες των σωμάτων. Για την επαφή μεταξύ κοχλιών και πλακών επιλέχθηκε η αλληλεπίδραση

vi

"touching", ενώ σαν μοντέλο τριβής το δι-γραμμικό Coulomb, το οποίο βασίζεται στις σχετικές μετακινήσεις μεταξύ των σωμάτων επαφής, με συντελεστή τριβής 0,6.

Στο σύνολο 14 μοντέλα αναλύθηκαν, στα οποία μεταβάλλονταν καταλλήλως οι παράμετροι του προβλήματος, δηλαδή το πάχος των πλακών, η διάμετρος και ποιότητα των κοχλιών αλλά και οι διαστάσεις της εσωτερικής λεπίδας. Πιο συγκεκριμένα, η διαδικασία που ακολουθήθηκε, περιλαμβάνει αρχικά τον εντοπισμό των κρίσιμων συνιστωσών της σύνδεσης κατά την καταπόνηση αυτής. Έπειτα οι κατάλληλες παράμετροι του προβλήματος μεταβάλλονται με στόχο την βελτίωση της γενικής συμπεριφοράς και γίνονται διαδοχικές συγκρίσεις μεταξύ των αποτελεσμάτων. Με τον τρόπο αυτό, εξετάζονται οι παράμετροι του προβλήματος και διερευνώνται πλήρως οι πιθανές μορφές αστοχίας. Κατά την διαδικασία αυτή, θεωρήθηκε κρίσιμη η προσπάθεια διατήρησης του κορμού του υποστυλώματος στην αρχική του κατάσταση, έτσι ώστε να μπορεί να διευκολυνθεί ο σχεδιασμός της βασικής σύνδεσης ισχυρού άξονα.

Η πρώτη σύγκριση μεταξύ των Μοντέλων 0 και 1, αποσκοπεί στην εκτίμηση της αποτελεσματικότητας της κατακόρυφης εσωτερικής λεπίδας για την βελτίωση της γενικής συμπεριφοράς. Πράγματι, η τοποθέτηση αυτής οδήγησε σε αύξηση της ροπής αντοχής κατά 20,46% αλλά και μείωση των πλαστικοποιήσεων στην περιοχή της συγκόλλησης μεταξύ της πλάκας του υποστυλώματος και τα πέλματα αυτού. Η ένταση κατανεμήθηκε πιο ομοιόμορφα, αξιοποιώντας έτσι όλα τα μέρη της σύνδεσης και αλλάζοντας την μορφή αστοχίας από αστοχία της συγκόλλησης στα πέλματα σε ταυτόχρονη αστοχία της μετωπικής πλάκας (η οποία στο άνω μέρος της μπορεί να προσομοιωθεί με ένα ισοδύναμο βραχύ T) αλλά και των κοχλιών στην άνω σειρά. Η μεγάλη καταπόνηση των κοχλιών οφείλεται εν μέρει και στην ανάπτυξη των δυνάμεων επαφής (prying forces) μεταξύ των δύο πλακών οι οποίες με τη σειρά τους οφείλονται στο σχετικά μη-επαρκές πάχος της μετωπικής πλάκας η οποία κάμπτεται σημαντικά.

Με την αύξηση των πάχους της μετωπικής πλάκας από 20 σε 25mm, η παραμόρφωση αυτής μειώνεται αισθητά ενώ η ένταση συγκεντρώνεται κυρίως στους κοχλίες της άνω σειράς που τελικά οδηγούν και την σύνδεση σε αστοχία. Ακολούθως, η διάμετρος των κοχλιών μεταβλήθηκε από Μ24 σε Μ30 και αυτό προκάλεσε μία αύξηση της καμπτικής αντοχής που έφτασε μέχρι και το 34%. Ωστόσο, η αλλαγή αυτή επέφερε μία έντονη καταπόνηση της εσωτερικής λεπίδας και του κορμού του υποστυλώματος (σ<315MPa) στο οποίο υπάρχει αισθητή παραμόρφωση χωρίς όμως την ανάπτυξη πλαστικών παραμορφώσεων. Η αστοχία των εν λόγω συνδέσεων εξακολουθεί να προέρχεται λόγω της μη επάρκειας των κοχλιών στην άνω σειρά και για το λόγο αυτό η ποιότητα των κοχλιών μεταβλήθηκε από 8.8 σε 10.9. Η τροποποιημένη ποιότητα των κοχλιών φάνηκε να μην επηρεάζει ιδιαίτερα την αντοχή και στροφική δυσκαμψία της σύνδεσης. Αντιθέτως, προκάλεσε μία σημαντική αύξηση της στροφικής ικανότητας (μέχρι και 53%), ενώ στα νέα μοντέλα φάνηκε μία αυξημένη καταπόνηση της εσωτερικής λεπίδας και της πλάκας του υποστυλώματος η οποία κάμπτεται

κατά τον κατακόρυφο άξονα. Για ακόμη μία φορά τα μοντέλα αστόχησαν λόγω της μη επάρκειας των κοχλιών στην άνω σειρά.

Εν συνεχεία, η μεταβολή των διαστάσεων της κατακόρυφης εσωτερικής λεπίδας από 161x500x10mm σε 161x750x16mm (πλάτος, ύψος, πάχος αντίστοιχα), βελτίωσε αισθητά τον τρόπο κατανομής των εσωτερικών εντάσεων, καθώς σχεδόν μηδένισε τις πλαστικοποιήσεις στην λεπίδα και κορμό του υποστυλώματος, ενώ αυτές πλέον συγκεντρώθηκαν κυρίως στην πλάκα του υποστυλώματος μέσω της εκτεταμένης κάμψης αυτής. Η αλλαγή του πάχους της πλάκας του υποστυλώματος, η οποία αποτελεί και την τελευταία παράμετρο του προβλήματος, μείωσε τις τελική στροφική ικανότητα των μοντέλων χωρίς σημαντική προσφορά στην αύξηση της καμπτικής ροπής. Αυτό που παρατηρείται, είναι η έντονη ένταση που αναπτύσσεται στους κοχλίες της δεύτερης σειράς καθώς και η ανάπτυξη τάσεων (σ<292MPa) στα πέλματα και κορμό της δοκού HEB300.

Όλα τα μοντέλα, σύμφωνα με την τελική ροπή αντοχής τους θεωρούνται, σύμφωνα με την κατηγοριοποίηση των κόμβων του EC3, ως συνδέσεις μερικής αντοχής. Έτσι, θεωρήθηκε αναγκαίο να σχεδιασθεί και αναλυθεί μία σύνδεση πλήρους αντοχής. Η σύνδεση αυτή περιλαμβάνει κοχλίες M36 10.9, μετωπική πλάκα πάχους 32mm, πλάκα υποστυλώματος πάχους 25mm και κατακόρυφη εσωτερική λεπίδα διαστάσεων 161x750x20mm. Πράγματι, η αντοχή της σύνδεσης αυτής ξεπέρασε την πλαστική ροπή της συνδεόμενης δοκού (κατά 5,36%), και έτσι κατηγοριοποιείται ως σύνδεση πλήρους αντοχής. Η εικόνα της σύνδεσης κατά την αστοχία, αποδεικνύει τον σχηματισμό πλαστικής άρθρωσης στο άκρο της δοκού, μέσω των εκτεταμένων πλαστικοποιήσεων, ενώ επιπλέον παρατηρείται και τοπικός λογισμός του κάτω πέλματος της δοκού.

Συμπερασματικά, είναι εμφανές ότι το φαινόμενο της επαφής είναι πολύ έντονο σε μία κοχλιωτή σύνδεση και απαιτεί μεγάλη προσοχή, τόσο στο αρχικό στάδιο της προσομοίωσης όσο και στην επεξεργασία και ερμηνεία των αποτελεσμάτων. Φυσικά, αποτελεί και τον βασικό παράγοντα του ιδιαίτερα μεγάλου χρόνου ανάλυσης των μοντέλων. Φαίνεται λοιπόν, ότι η ανάλυση των κόμβων μέσω της μεθόδου των Πεπερασμένων Στοιχείων, είναι εφικτή αλλά όχι ιδιαίτερα πρακτική στα χέρια ενός μελετητή. Όσον αφορά την συμπεριφορά της σύνδεσης, έγινε προφανές πως η τοποθέτηση της κατακόρυφης εσωτερικής λεπίδας είναι απαραίτητη για την αποφυγή φαινομένων πλαστικοποίησης του υλικού στην περιοχή των κρίσιμων συγκολλήσεων (μεταξύ πελμάτων υποστυλώματος και πλάκας αυτού). Κυρίαρχη μορφή αστοχίας αποτελεί αυτή λόγω αστοχίας των κοχλιών (ιδίως στην πρώτη σειρά). Για το λόγο αυτό, η διάμετρος των κοχλιών φάνηκε η βασική παράμετρος αύξησης της αντοχής της σύνδεσης. Αντίθετα, οι υπόλοιπες παράμετροι, κυρίως προκάλεσαν την μεταβολή της κατανομής των εσωτερικών εντάσεων σε διαφορετικά μέρη της σύνδεσης και είχαν επίσης επιρροή στην πλαστιμότητα αυτής. Τέλος, με την ολοκλήρωση της διερεύνησης, αποδείχθηκε πως μία τέτοια διάταξη μπορεί να μορφώσει μία σύνδεση πλήρους αντοχής με την αύξηση των κατάλληλων παραμέτρων.

Ο υπολογισμός της καμπύλης ροπών-στροφών μίας σύνδεσης ροπής ασθενούς άξονα μέσω της μεθόδου των Πεπερασμένων Στοιχείων χαρακτηρίζεται από μεγάλο υπολογιστικό κόστος. Για το λόγο αυτό, η ανάπτυξη μιας διαδικασίας αντίστοιχη με αυτή του Ευρωκώδικα για την ανάλυση συνδέσεων ισχυρού άξονα, θεωρείται απαραίτητη. Αυτό απαιτεί την "διάσπαση" της σύνδεσης σε κατάλληλες συνιστώσες και στην ανάπτυξη αναλυτικών σχέσεων για τον υπολογισμό της αντοχής αυτών είτε ανήκουν στην εφελκυόμενη, θλιβόμενη ή διατεμνόμενη ζώνη της σύνδεσης. Επιπλέον, δεδομένου ότι στην παρούσα εργασία εξετάσθηκε μία μεμονωμένη σύνδεση ασθενούς άξονα, είναι εμφανής η ανάγκη διερεύνησης ενός κόμβου (εσωτερικού η γωνιακού) παρουσία συνδέσεων και στους δύο άξονες με σκοπό να εξεταστούν φαινόμενα αλληλεπίδρασης. Τέλος, σημαντική θεωρείται και η ανάλυση της εν λόγω σύνδεσης, παρουσία σταθερού θλιπτικού φορτίου στο υποστύλωμα, κάτι ούτως ή άλλως δεδομένο σε πραγματικές συνθήκες.

Λέξεις Κλειδιά

Μεταλλικές συνδέσεις, Σύνδεση ασθενούς άξονα, Πεπερασμένα Στοιχεία, Μη Γραμμική Ανάλυση

ix

Table of Contents

1. INTRODUCTION

In the design of steel structures, of paramount importance is the design of connections. Their presence on the structure determine its response characteristics such as displacements, internal forces as well as failure load and failure mode. Unlike cast-in-place reinforced concrete which ensures monolithic properties to the structure, in steel structures the design and construction of connections its necessary and demands extensive effort and time. Inadequate connections can be the "weak link" of the structure and cause its failure without even affect the steel members.

In connections, various configurations are used ensuring sufficient transmission of internal forces. The configuration depends upon the type of connecting elements, magnitude of forces and moments, available equipment, erection, fabrication and cost considerations. In modern steel structures, connections are primarily made either by bolting or welding. Bolted connections allow a great variety of structural solutions and are deemed to be economical and more appropriate constructed in field regarding safety. Welding, on the other hand is easier to make, requires a few, if any, holes in the connected members and it is usually shop fabricated. In both cases, the geometry of these connections is highly intricate, as it is shown in Figure 1.
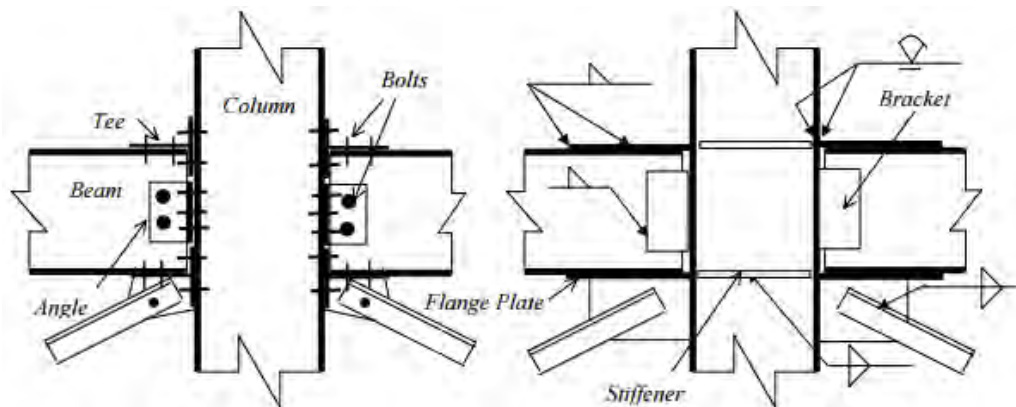
Figure 1. *Complexity in the geometry of bolted (left) and welded (right) connections (Source: Google search)*

Typically, in cases that both columns and beams are of double tee profiles, the connections are realized by a bolted end plate. Although, usually connections to the minor axis of the column are designed not to carry moments (simple connections), in some cases it is inevitable to have moment carrying connections in both the minor and the major axis of the column so that the necessary structural rigidity against lateral loads is achieved (Figure 2). Although a lot of research exists for major axis connections, in the case of minor axis connections the relevant research is somewhat limited.

1

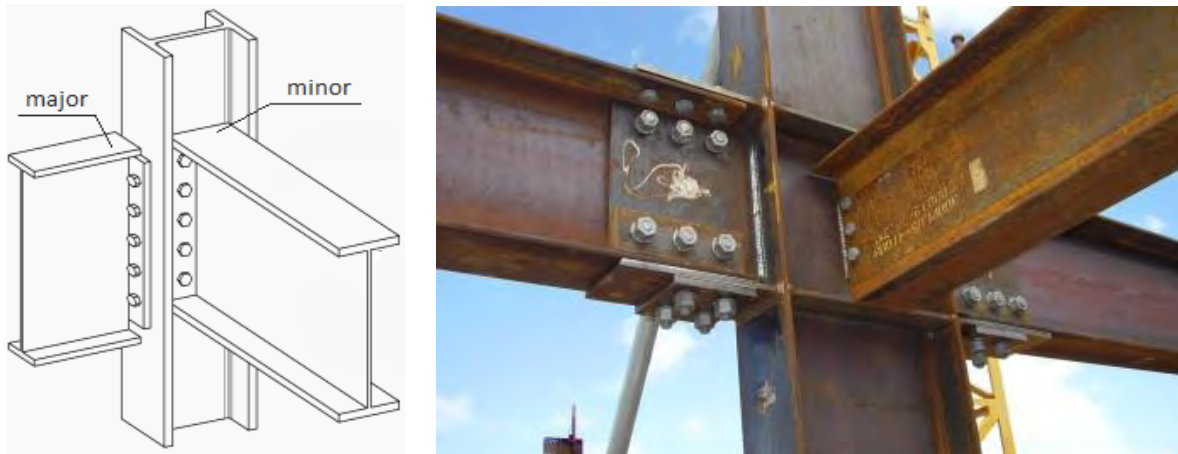*Figure 2. Joints with connections on both major and minor axis of the column*
(Source: Google search)

In more detail, in cases that bracing is not possible for a variety of reasons, usually architectural, the required rigidity of the structure is usually achieved by moment resisting frames also along the minor axis of the structure. Usually, in these cases two alternatives exist, have two end plates, one welded to the two flanges of the column and one to the beam bolted to each other or connect the beam directly to the web of the column (see Figure 3a). Usually, the construction of the second connection (Figure 3b) is more difficult as in the case that a strong axis connection also exists, manufacturing conflicts appear.
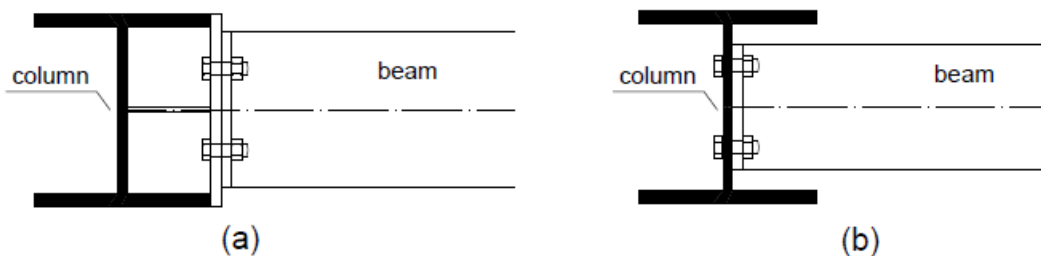

Figure 3. Minor axis connections with double end-plate (a) and direct connection of the beam to the column's web (b)

For the design of major axis steel connections, the relevant Eurocode (Eurocode 3 part 1-8 [1]) provides an approach based on the component method. In this method, the response of a connection is calculated by the geometrical and mechanical properties of its components. The mechanical models are based on association of springs in series and/or parallel. The component method provides efficient solutions for major axis connections but it fails to describe the behavior of its weak-axis counterpart. However, from a theoretical point of view, the procedure that the component method follows can be applied to any type of joint.

For the estimation of the capacity and the understanding of failure mechanisms of a weak-axis connection, when the beam is directly bolted to the column web, analytical models and design methods based on yield line analysis and plate theory have been proposed.

2

Conversely, such research has not yet been performed regarding minor axis connections where the beam is connected to the column two flanges. Only a limited amount of research has been performed for this particular connection configuration and the interaction between major- and minor-axis connections in 3-D joints. These types of connections have not yet been covered in Eurocode 3 for design purposes. An alternative design approach, is to use finite element models to determine both the capacity and the rigidity of the connection. This approach however is not easily applicable in every day engineering practice as it is both time consuming and requires advanced simulation and engineering skills.

The purpose of this thesis is the investigation of the behavior of the developed double end-plate minor axis connection (Figure 3a). More specifically, detailed numerical 3D models will be formulated capable of taking into account the different phenomena that may appear such as material-geometrical nonlinearity and the contact interaction between the various components of the connection. The investigation focuses on the impact of the geometry of the key components on the capacity and response of the connection, such as the thickness of the end-plates the dimensions of the vertical-stiffener and the size and grade of the bolts.

In Chapter 1, an introduction to the problem at hand is made. In Chapter 2, an overview of connections and joints as well as the methodology and classification of Eurocode 3 focusing on bolted end-plate connections is presented. In the sequel, a state of the art literature review regarding weak-axis connections is provided.

In Chapter 3, the formulation of the numerical models is discussed. First, the geometry of the connection is presented as well as the parameters whose impact on the behavior of the connection will be investigated. Next, the results of the necessary investigation regarding the finite element discretization are presented and finally the numerical models as well as the material properties and boundary conditions incorporated in the analyses are thoroughly presented.

In Chapter 4, the results of the investigation are presented. First, the imperativeness of the use of the vertical-stiffener is highlighted. Subsequently, the influence of the thickness of the end-plates, the dimensions of the vertical stiffener and the diameter and grade of bolts is thoroughly discussed by relevant comparisons between the various models. In addition, a presentation on how to achieve a full-strength connection is presented.

In Chapter 5, the drawn-conclusions from the investigation are presented with a focus on the reliability, usability and efficiency of the finite element method in the design of such connections as well as the key-components that affect their capacity, rigidity and ductility. Finally, suggestions for further investigation are presented.

2. THEORETICAL FRAMEWORK

2.1 Joints and connections

A steel structure consists of prefabricated usually linear members, which are transferred on the construction site in order to be connected with each other. Similarly, every prefabricated part is composed by the connection of smaller parts. The aim of connections is the proper configuration of the smaller parts and the restoration of the continuity of the different members. In Figure 4 different kind of major axis joint configurations are presented.
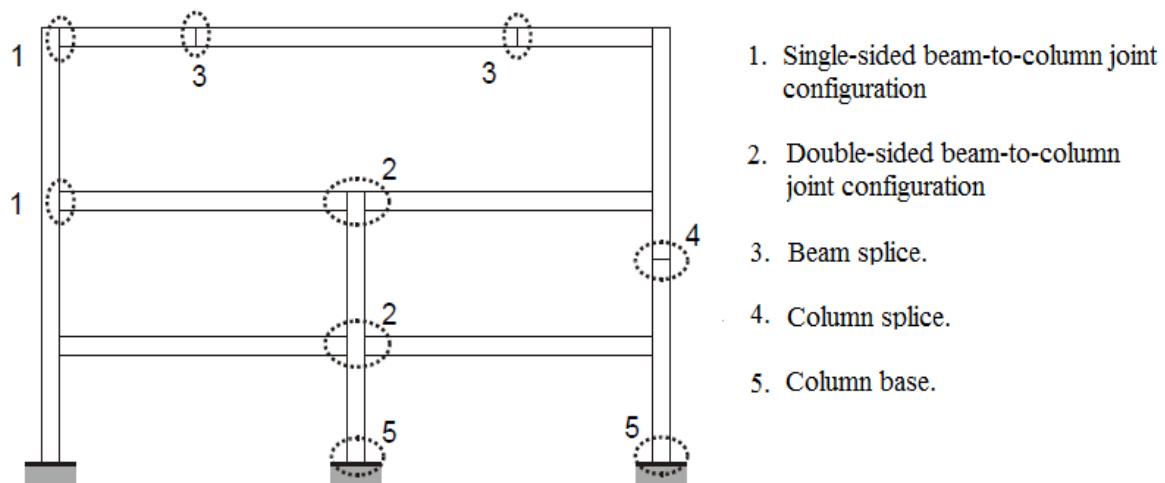

Figure 4. Major axis joint configurations (Source: Eurocode 3 part 1-8, Fig.1.2)

1. Single-sided beam-to-column joint configuration

2. Double-sided beam-to-column joint configuration

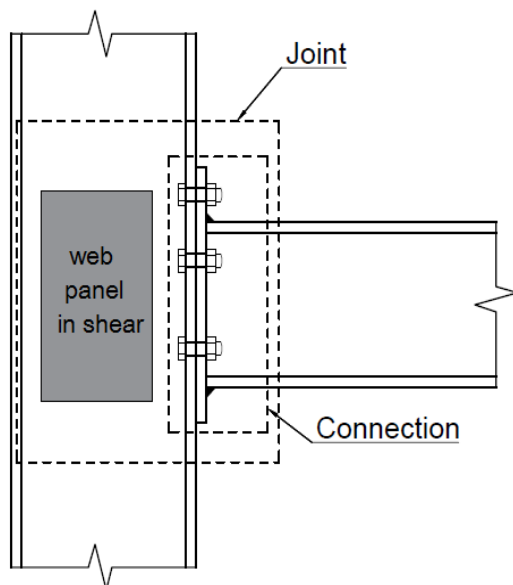3. Beam splice.

4. Column splice.

5. Column base.

Figure 5. Difference between joint and connection

As the terms **joints** and **connections** are used interchangeably in practice, a distinction between those two is essential. A ***connection*** comprises structural elements (bolts, end-plates) used for joining different members of a structural steel frame work. It is assumed, that the connection is located exactly at the region where the fastening action occurs (e.g. at the interface between the edge of the beam and the column in a beam-column joint). The term ***joint*** is used to describe both the connection and the interaction zone between the connected members, namely the panel zone of the column web (e.g. joint = web panel in shear + connection).

4

2.2 Classification of joints

Traditionally, steel frame designers assumed that beam-to-column joints are either rigid or pinned, despite that the actual rotational behavior of joints is often intermediate between the two extreme situations. These assumptions allow a great simplification in structural analysis and design, but they disregard the actual behavior of joints. Although computational capabilities have been exceedingly improved the last two decades, most of steel frames are still being designed by this hypothesis. This leads to the conclusion that frames designed with the pinned joint assumption do not exploit the limited yet existent stiffness, while frames designed with the rigid joint assumption often lead to an increase of the final cost due to the installation of multiple stiffeners, in order to achieve the required stiffness.

Depending on the internal forces that they transmit, connections are divided into:

Simple Connections

This type of connection, receives and transmits only axial and shear forces, allowing the resulting rotations under design loads, without developing significant moments. An example is the pinned beam-to-column connection, which transmits shear force from the beam to the column, as well as the pinned connection in trusses, which distributes the axial forces from the members to the joints (Figure 6).
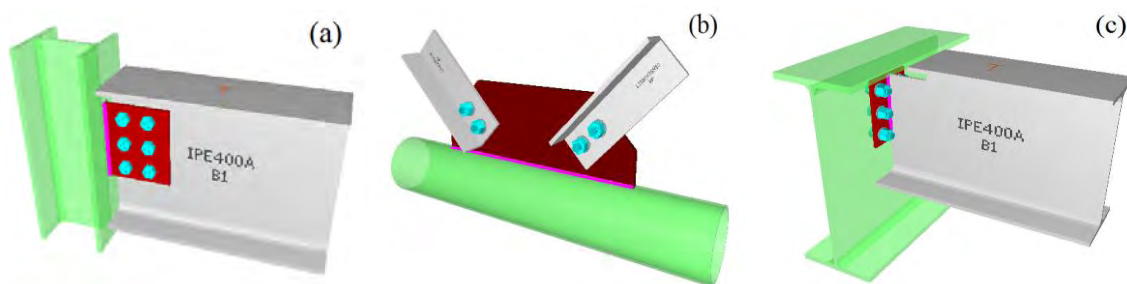
Figure 6. Fin plate (a), KT Gusset plate (b) and flexible end plate (c) simple connections (Source: Limocon v3.63 connection software)

Moment Connections

A moment connection can receive and transmit not only forces but also moments. Typical examples are restorations of continuity (splice connections), steel frame beam-to-column connections which transfer shear and moment from the beam to the column and of course column base connections (Figure 7). It is worth mentioning that moment connections are invariably pricier than simple connections, because they involve much more fabrication effort.

5

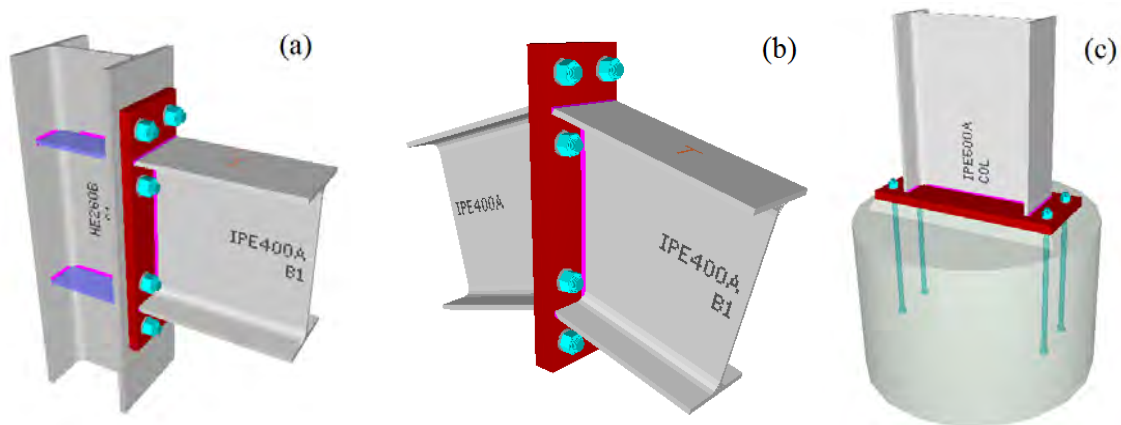*Figure 7. Moment connections (bolted end plate (a), bolted end plate apex (b) and base plate (c)) (Source: Limocon v3.63 connection software)*

2.2.1 Classification by stiffness

In the case of elastic design, the classification system requires only the rotational stiffness criterion leading to three categories: nominally pinned, rigid or semi-rigid. The first two categories considered the traditional ones while the intermediate third category has been introduced to fill the gap between pinned and rigid connections and it is now accepted in the relevant codes.

To classify connections, a comparison between connection's initial rotational stiffness and the frame's stiffness needs to be made (Figure *9*). The total response of a joint can be represented by the relevant moment-rotation diagram (M-φ), where the first is the transmitted bending moment $M_{j,Ed}$ and the second the relative rotation $φ_{ED}$, which is equal to the beam rotation minus the column rotation (Figure 8). The slope of the elastic range of this specific diagram represents the initial stiffness $S_{j,ini}$ of the connection. The calculation of the ultimate moment resistance of a connection $M_{j,Ed}$ will be analyzed in section 2.3.3, by means of the component method which is included in Eurocode 3.
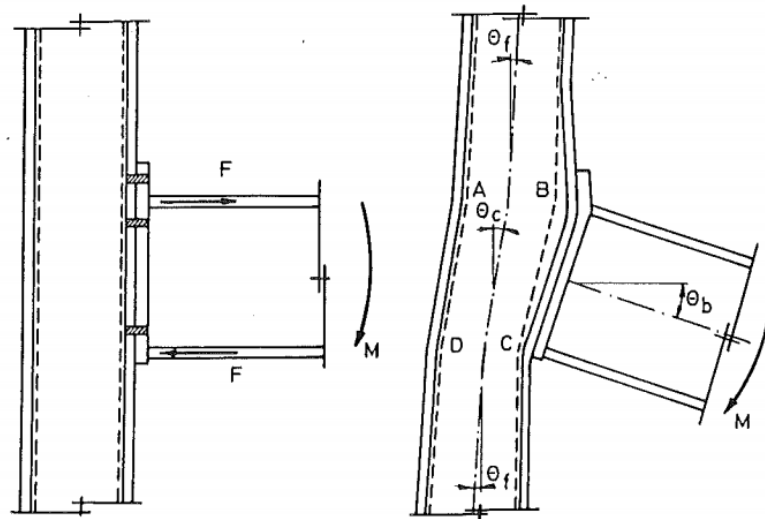
6

Figure 8. Deformation of a major axis joint [3]

Nominally pinned Connections

Nominally pinned connections are assumed to transfer the shear and eventually the normal force from the beam to the column and should allow the relative rotations between the connected members to be developed. This type of connection is widely used when lateral stiffness of structure is achieved by appropriate bracing systems.

Rigid Connections

Connections classified as rigid may be assumed to have sufficient rotational stiffness to justify analysis based on full continuity. In addittion, the corresponding parameter S of such connections is considered to be almost infinite.

Semi-rigid Connections

Connections that can be included in this category, are those where the relative rotation between the connected member and the joint is changing according to the transferred bending moment M to the member. Semi rigid joints, provide a predictable degree of interaction between members, based on the design moment-rotation characteristics of the joint. The simplest way to simulate the behavior of such connections is by using rotational springs between the connected members. The rotational stiffness of the spring S is the parameter that connects the transferred moment $M_{j,Ed}$ with the relative rotation φ_{Ed}. The economic and structural benefits of semi-rigid connections are well known and much has been written about their use in braced systems. However, because of their highly non-linear behavior, they are seldom used by designers.
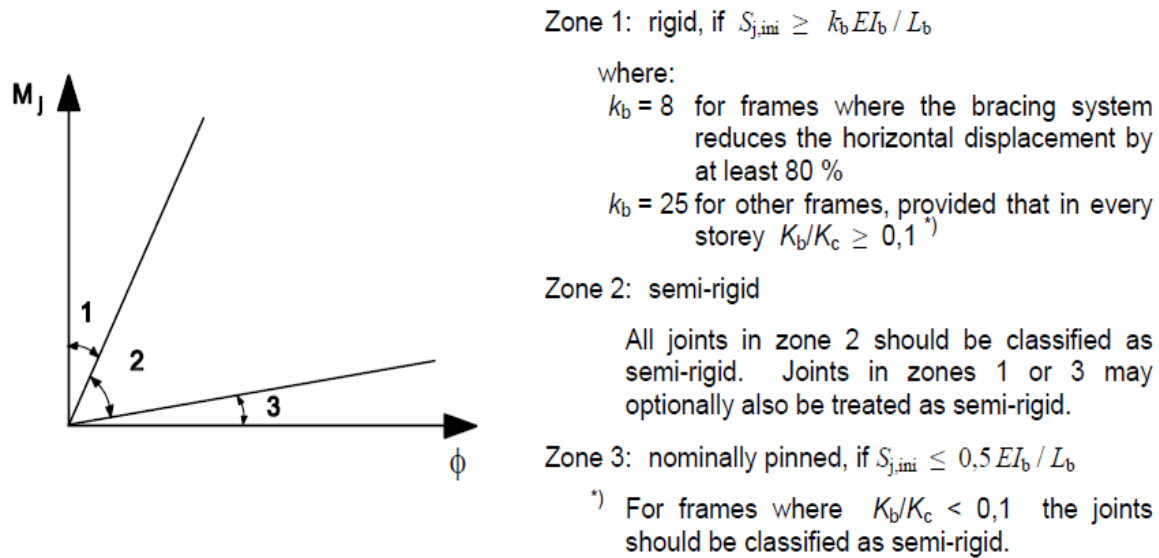
7

Zone 1: rigid, if $S_{j,ini} \geq k_b EI_b / L_b$

where:

$k_b = 8$ for frames where the bracing system reduces the horizontal displacement by at least 80 %

$k_b = 25$ for other frames, provided that in every storey $K_b/K_c \geq 0.1$ [*]

Zone 2: semi-rigid

All joints in zone 2 should be classified as semi-rigid. Joints in zones 1 or 3 may optionally also be treated as semi-rigid.

Zone 3: nominally pinned, if $S_{j,ini} \leq 0.5 EI_b / L_b$

[*] For frames where $K_b/K_c < 0.1$ the joints should be classified as semi-rigid.

Figure 9. Classification of joints by stiffness (Source: Eurocode 3 part 1-8, Fig.5.4)

where:

K_b is the mean value of I_b/L_b for all the beams at the top of that storey;

K_c is the mean value of I_c/L_c for all the columns in that storey;

I_b is the second moment of area of a beam;

I_c is the second moment of area of a column;

L_b is the span of a beam (centre-to-centre of columns);

L_c is the storey height of a column.

2.2.2 Classification by strength

In case of structural design based on rigid-plastic analyses, the classification criterion is based on joint flexural resistance is of concern. the **Design Moment Resistance $M_{j,Rd}$**, is equal to the maximum value of the M-φ curve in terms of moment resistance According to the relevant part of the Eurocode 3, connections can be classified by their strength into two categories: full strength and partial strength connections. It is also suggested that if the design moment resistance $M_{j,Rd}$ of the connection does not exceed 25% of the design moment resistance of the beam, the connection should be classified as nominally pinned (for a full-strength connection, provided that the joint has additionally sufficient rotational capacity).
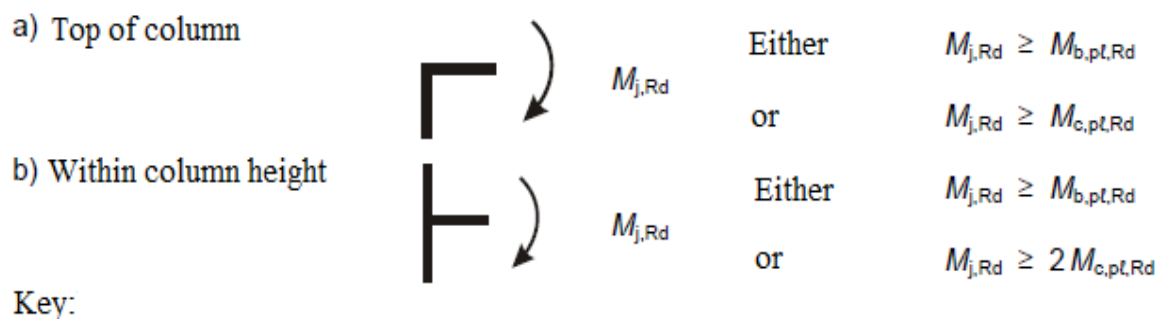
Full-Strength Connections

A connection should be classified as full-strength in case that its design moment resistance $M_{j,Rd}$ at least exceeds the ones of the connected members. Such connection must meet the criteria given in Figure 10. A plastic hinge will be formed in the adjacent member, but not in the connection. Examples of such connections, are column and beam splices, where the

8

design moment resistance of the connection is greater than the one of the relevant member or beam-to-column joints, where the design moment resistance of the joint is greater than the ones of the connected members

Partial-strength Connections

A joint which does not meet the criteria of a full-strength joint or a nominally pinned should be classified as a partial-strength joint. A plastic hinge will be formed in the connections and in such case, sufficient rotation capacity is required. A characteristic example is beam-to-column joints, where the design moment resistance of the joint is less than the design moment resistance of the connected beam.

a) Top of column

$M_{j,Rd}$

Either $\quad M_{j,Rd} \geq M_{b,pl,Rd}$

or $\quad M_{j,Rd} \geq M_{c,pl,Rd}$

b) Within column height

$M_{j,Rd}$

Either $\quad M_{j,Rd} \geq M_{b,pl,Rd}$

or $\quad M_{j,Rd} \geq 2 M_{c,pl,Rd}$

Key:

$M_{b,pl,Rd}$ is the design plastic moment resistance of a beam;
$M_{c,pl,Rd}$ is the design plastic moment resistance of a column.

Figure 10. Full strength Joints criteria (Source: Eurocode 3 part 1-8, Fig.5.5)

It should be noted at this point, that the use of semi-rigid joints in structural analyses instead of the conventional nominally pinned and rigid ones, will not only affect the structure's deformations but it will also have a substantial impact on the distribution and magnitude of the internal forces throughout the structure.

Additional classification methods have been introduced for beam-to-column connections such as the proposed method from Nethercot et. al. [4] , in which the moment resistance and rotational stiffness are considered simultaneously. Lastly, a parameter according to which connections can be classified, is their plastic rotation supply. Respectively to member profiles, joints can be characterized by their plastic behavior, that is their ability to resist local instabilities and brittle failures. **Full ductility connections** are able to develop a plastic rotation supply equal or greater than that of the connected member, while **partially ductile connections** less than that. The practical interest of this classification is the assessment of whether an elastoplastic analysis can be performed or not, until the collapse of the structure due to the formation of enough plastic joints.

2.3 Modelling of joint behavior

As already emphasized in the previous section, steel structures are usually designed by assuming that the connections are either fully rigid or ideally pinned. Nevertheless, in spite of their obvious rigidity, allow a certain degree of rotation and deformation or, in spite of their apparent deformability, provide a certain degree of rotational restrain. In other words, all actual beam-to-column joints behave as semi-rigid ones. The most important input data for the analysis and design of semi-rigid frames is the moment versus rotation curve M-φ. A thorough understanding of this curve for each connection can ultimately lead to more reliable prediction of load effects and subsequently to more economic structural solutions.

In this framework, an accurate modelling of the beam-to-column joint behavior is of essence. In order to achieve such high level of accuracy and closely reproduce the behavior of joints, the panel zone and each connection should be modelled separately. The shear deformation of the panel zone is taken into account by means of a diagonal spring element located in the middle, while the rotational springs at the two sides of the column account for the deformability of each of the connections. For simplification purposes, the modelling of the joint can be represented by only two rotational spring, whose moment-rotation characteristics accounts for both the behavior of the connections and the panel zone [1] (Figure 11).
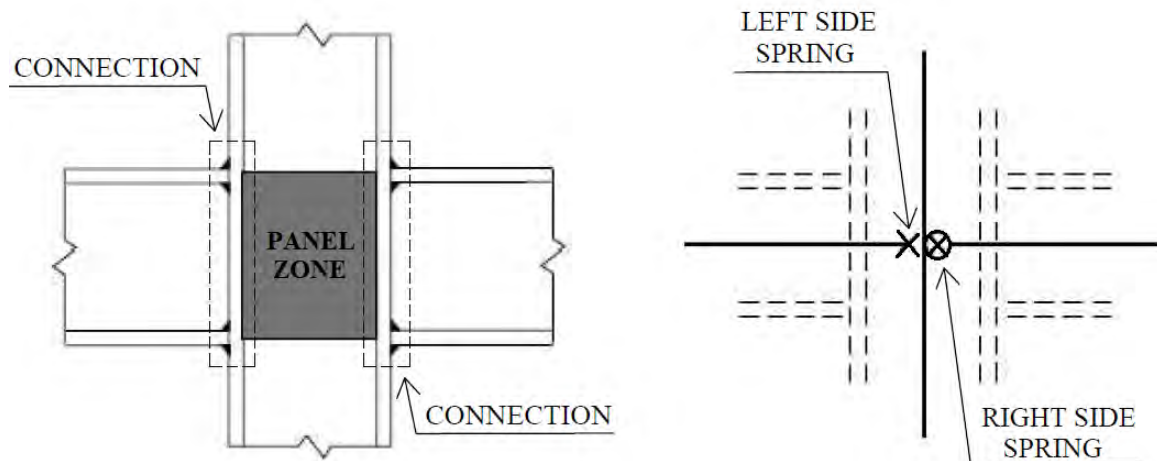

Figure 11. Modelling of the joint by means of separate rotational springs

For simplified methods of structural analysis, spring elements with linear or bilinear behavior can be used whereas more advanced methods need to rely on a more accurate modelling of the joint behavior and in this case the use of multilinear or curvilinear M-φ curves is suggested. Of course, the selected moment-rotation behavior in the modelling of the beam-to-column joint, depends on the type of the global structural analysis to be performed. In elastic analyses, where only the joint classification according to stiffness is of concern, the

joint can be modelled with the use of linear spring element while if rigid plastic analysis is used, the joint resistance is of concern and the joint modelling can be based in a bilinear M-φ curve. Finally, when elastic-plastic analysis is performed the representation of joint's behavior can be bilinear, multilinear or non-linear.

2.3.1 Methods of predicting moment-rotation curves

Different approaches can be used for predicting the joint rotational behavior and each of them needs to be combined with a mathematical representation of the moment-rotation curve [5] . These methods can be divided into the five following categories:

- empirical models;
- analytical models;
- mechanical models;
- finite element models;
- experimental testing.

Empirical models

Empirical models are based on the use of empirical formulations relating the parameters involved in the mathematical representation of the moment-rotation curve to the geometrical and mechanical properties of the beam-to-column joints. Selected data from experimental testing, finite elements or from other methods can be used to obtain these empirical formulations by means of regression analyses.

Several empirical models have been developed and suggested throughout the years, with the first being that by Frye and Morris (1975) [6] which is based on an odd-power polynomial expression of the M-φ curve with parameters that include the mechanical and geometrical properties of the joint. Later, a new empirical model was developed based on a wide parametric analysis by means of the finite element method (Krishnamurthy et al. (1979) [7] . This approach was applied to the case of an extended end-plate connection with four bolts in the tension zone and led to a simple power representation of the moment-rotation curve. Kukreti, Murray and Abolmaali (1987) [8] , adopted the above approach and provided insights about flush end-plate connections and also for extended end-plate with eight bolts in the tension zone and a stiffened end-plate.

Finally, a different approach has been used by Faella, Piluso and Rizzano (1997) [9] for extended end-plate connections. The authors analyzed more than 110.000 different extended end-plate beam-to-column joints by means of a mechanical model based on the Eurocode's 3 component method. For the empirical model, the mathematical representation of the M-φ curve that was adopted is the one that is also suggested in the Eurocode 3 and will be discussed further later (Section 2.3.2 The Component method in bolted end-plate connections).

11

However, these empirical models are only applicable for specific configurations that were used for the calibration of the relevant formulations and given that, this method has a major drawback. In addition, this method fails to present the contribution of each component to the overall response and to explain the failure mode of the joint. For these reasons, more advanced methods have been developed, that manage to overcome these obstacles.

Analytical models

The basis of these kind of models is the prediction of moment-rotation curves directly from the joint properties (mechanical and geometrical). A simplified connection model needs to be created, capable of predicting the initial connection stiffness, the plastic mechanism that the researcher has observed in a specific connection and the maximum moment resistance. The main advantage of analytical models is their ability to produce the moment-rotation curve with high accuracy, without resort to testing.

An extensive research has been made by Chen et al. [10], [11] (1988a; 1988b) , on the semi-rigid behavior of connections with angles. The authors, who developed analytical expressions for the calculation of initial stiffness and ultimate bending moment, assumed that the connection lies on a rigid support and not to a deformable column. In other words, it should be considered that those expressions are referred to the connection's behavior rather than the joint's one.

Perhaps the most complete study for end-plate connections, that also includes the column deformations is that of Yee and Melchers (1986) [12]. They separated the joint into five different effects of action:

- flexural deformation of the end plate;
- flexural deformation of the column flange;
- bolt extension;
- shear deformation of the panel zone;
- deformation due to the compression zone of the column web.

The following failure modes, that aim to provide the weakest connection element, have been proposed:

- tension bolt failure;
- formation of a plastic mechanism in the end plate;
- formation of a plastic mechanism in the tension zone of the column flange;
- shear yielding of the column web;
- column web buckling;
- column web crippling.

12

By computing the deformation, displacement and plastic resistance of each element the authors manage to provide expressions for the calculation of the rotational stiffness and moment resistance of the joint. This procedure, considers to be the predecessor of the well-known and applied "component method", incorporated in the Eurocode 3.

Mechanical models

A mechanical model, also known as spring model, simulates the behavior of a joint or connection by using a set of flexible and rigid components with predefined mechanical characteristics. To produce the expected non-linear response of the joint or connection, relevant inelastic constitutive laws are adopted for the deformable spring elements. These constitutive laws are obtained from empirical relationships, test data, numerical simulations or analytical models.

A major advantage of this method, is that a curve fitting in the knee of the M-φ diagram is unnecessary due to the method's ability to produce multilinear overall behavior, from the successive yielding of the spring elements or joint components. However, this method usually requires the use of computer programs to generate the moment-rotation curve.

Several researchers have developed mechanical models with the aim to provide the response of different joint configurations. Wales and Rossow (1983) [13] suggested a mechanical model that simulates the behavior of double web angle connections under bending moment and axial load. Their model was extended by the work of Chmielowiec and Richard (1987) [14] to include the top and seat angle with double web angles joint configuration.

In order to simulate the behavior of welded and end-plate bolted connections, Tschemmernegg and Humer (1988) [15] created two mechanical models that include several springs, each of which representing a different part of the joint. For the model of the welded joint, two nonlinear springs exist, the "load introduction spring", which accounts for the deformation due to the load transmitted by the beam flanges and the "shear spring", that simulates the deformation of the panel zone. In the case of a bolted end-plate connection, additional springs has been used, namely "connection springs", which account for the new sources of deformation. (Figure 12).
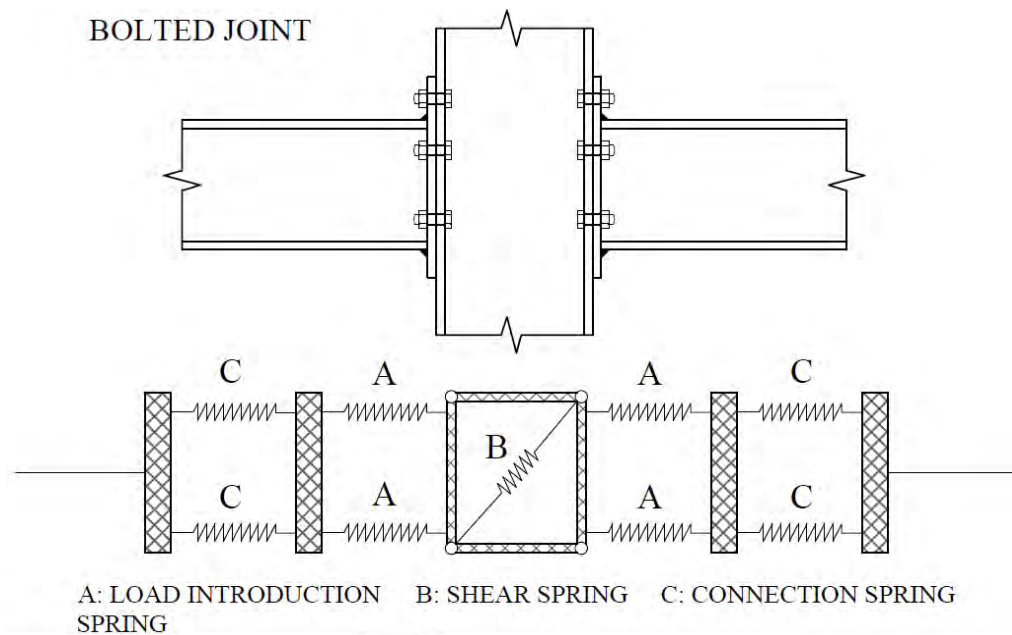
13

Figure 12. Mechanical model of a bolted joint (Tschemmernegg and Hummer, 1988)

For the calibration of a mechanical model of a beam-to-column joint, an identification of the joint components needs to be made. The so-called components are deformable elements with a failure potential in each configuration. These components and their corresponding models have been collected and incorporated in the Eurocode 3 within the component method (Section 2.3.2 The Component method in bolted end-plate connections).

Finite Element Analysis

Finite element technique is a sophisticated approach to predict the behavior of joints, using 2-D and 3-D models that simulate their non-linear behavior. Particularly in the case of bolted connections, the analysis requires the modelling of the following:

- geometrical nonlinearities;
- material nonlinearities;
- contact interaction between bolts and plate;
- friction resistance;
- slip due to bolt-to-hole clearance;
- welds;
- imperfections (residual stresses).

In the case of welded beam-to-column joints, the finite element technique has proven to provide sufficiently accurate results. Conversely, when it comes to bolted joints the above requirements are not always fully attained. Despite the significant progress that has been

14

achieved the past few years, the complex mechanisms behind semi-rigid bolted connections still need to be investigated and understood in order to be modelled properly.

The first study of into joint behavior using the Finite Element Method, conducted by Bose et. al. [16] and was related to welded beam-to-column joints. The model, among others included plasticity, strain hardening and buckling. The following years, researchers focused their studies predominantly in bolted connections. Krishnamurthy and Grabby [17] , created the first 3-D numerical model of a joint while Sherbourne and Bahaari [18] developed a model to investigate the behavior of bolted end-plate connections. Bursi and Jaspart modelled T-stub connections [19] and isolated extended end-plate connections [20,21] .Choi and Chung [22] , created a model of a double extended end-plate connections in which the column flange was included. Bahaari and Sherbourne [23] and Sumner et al. [24] developed detailed 3-D models to investigate 8-bolt and 4-bolt extended unstiffened end-plate connections. Swanson et al. [25] used 2-D as well as 3-D models to investigate the behavior of T-stub flanges. Gantes and Lemonis [26] studied bolted T-stub connections while Abolmaali et al. [27] modelled flush end-plate connections. Maggi et al. [28] conducted a parametric analysis regarding bolted extended end-plate connections and Kukreti and Zhou [29] using 3-D finite element models quantified the influence of semi-rigid connections characteristics on steel frame behavior. Dai et al. [30] studied five different type of joints: fin plate, flexible end-plate, flush end-plate, web cleat and extended end-plate on fire conditions.

Considering the aforementioned numerical studies on bolted beam-to-column joints the following three observations can be made [31] :

- End-plate joints are the most studied;

- Most of the models include: geometric and material nonlinearity; bolts contact and pre-tensioning;

- Although computational capabilities allow the calibration of 3-D models, other finite elements have been used: 2D plane stress and shell elements and truss and beam elements for columns, beams and bolts.

Experimental testing

The prediction of the moment rotation characteristics of beam-to-column joints can be also achieved by means of experimental testing. More importantly, this method is used to assess the reliability of empirical, analytical, mechanical and finite element models. It should be noted though that this method does not predict accurately the true joint behavior in building frames. The stress distribution in the panel zone of the column web in tested specimens is constantly modified. This particular process differs from the one in joints integrated in building frames. Additional differences are related to the internal actions induced in the

building erection process, to the geometrical imperfections and the numerous loading conditions which joints, as a part of a building are required to withstand.

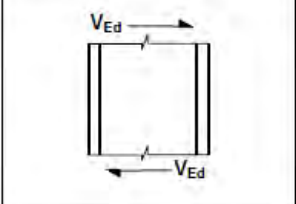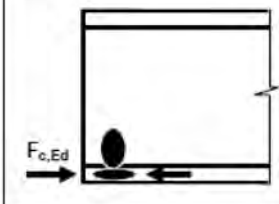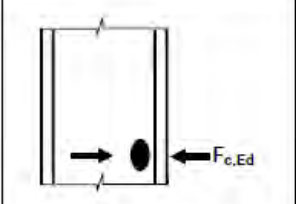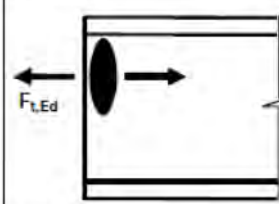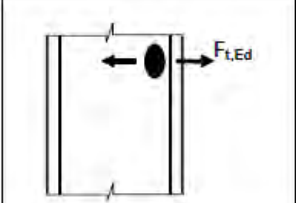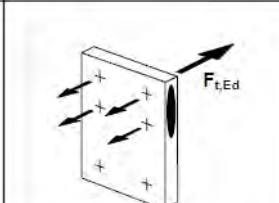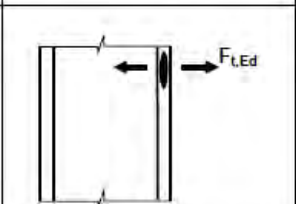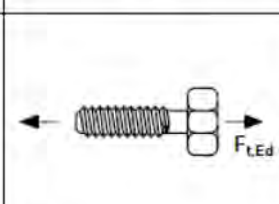### 2.3.2 The Component method in bolted end-plate connections

In order to design a bolted end-plate connection, a proper identification of the basic components that influence its function needs to be made. Eurocode 3 comprises 20 different components in total that each of them can be used in the mechanical modelling of various configurations. In case of an extended bolted end-plate connection the overall behavior can be obtained considering eight individual components, as it is shown in Table 1. Each of these components can be described by its own level of strength and stiffness in tension, compression or shear.

The application of the component method requires the following three steps (Jaspart, 2000 [32]):

1. Identification of the active components is the studied joint;

2. Evaluation of the mechanical properties of each of these components (specific characteristics or the whole deformability curve);

3. Assembly of the components for the calculation of the mechanical characteristics of the whole joint (specific characteristics or the whole deformability M-φ curve).

Some of these components are highly dependent on the number of the bolt rows in tension but also on the location of each bolt row. These components are the end-plate in bending, the column flange in bending, the bolts in tension, the column web in tension and the beam flange in tension. To evaluate the contribution of these components, the behavior of each bolt row as both a single row and as belonging to a bolt group needs to be made.

Table 1. Basic bolted end-plate joint components (Source: Eurocode 3, part 1-8, Table 6.1)

The most important components of extended end-plate bolted connections (end-plate and column flange in bending) can be analyzed using the so-called T-stub model (Figure 13). These equivalent T-stubs play a fundamental role in the prediction of the moment rotation curve. To obtain the force-displacement diagram of a T-stub, the evaluation of its behavior subjected to axial forces needs to be made.
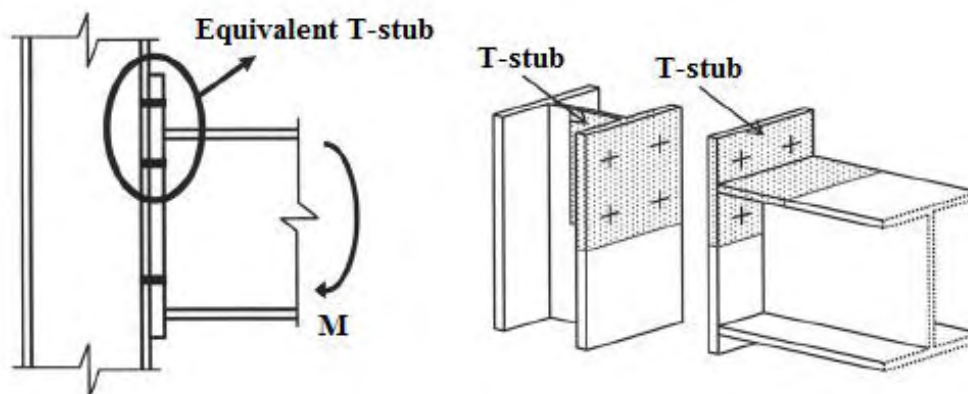
Figure 13. T-stub identification for extended end-plate bolted connection [33]

17

The joint **moment resistance $M_{j,Rd}$** is calculated by means of the following relationship:

$$M_{j,Rd} = \sum_{i=1}^{n} h_i F_{i,Rd} \tag{1}$$

where:

$F_{i,Rd}$ is the resistance of the i-th bolt row;

n is the number of bolt rows in tension;

h_i is the distance of the i-th bolt row from the center of compression.

The **rotational stiffness S_j,** which for a moment $M_{j,Ed}$ less than the design moment resistance $M_{j,Rd}$ of the joint and provided that the axial force in the connected member N_{Ed} does not exceed 5% of the design resistance $N_{pl,Rd}$ of its cross-section, may be obtained with sufficient accuracy from the following expression:

$$S_j = \frac{E*z^2}{\mu*\Sigma_i \frac{1}{k_i}} \tag{2}$$

where:

k_i is the stiffness coefficient for basic joint component i ;

z is the level arm, which for bolted connection is the distance between the center of compression and the bolt-row in tension (with only one bolt-row active in tension);

μ is the stiffness ratio, where $S_j= S_{j,ini}$ if $\mu=1$, otherwise if $M_{j,Ed} \geq {}^2\!/_3\, M_{j,Rd}$

$\mu=(1{,}5 M_{j,Ed}/ M_{j,Rd})^\psi$ ($\psi=2.7$ for bolted end plate connections).

Finally, the moment-rotation diagram that Eurocode 3 adopts is the trilinear approximation shown in Figure 14a. However, most computer design programs, are based on the bilinear approximation of the moment-rotation curve. For this reason, Eurocode 3 also suggest the use of the bilinear diagram (Figure 14b). The stiffness modification factor η, is based in the type of the connection. For bolted end-plate joints η=2.
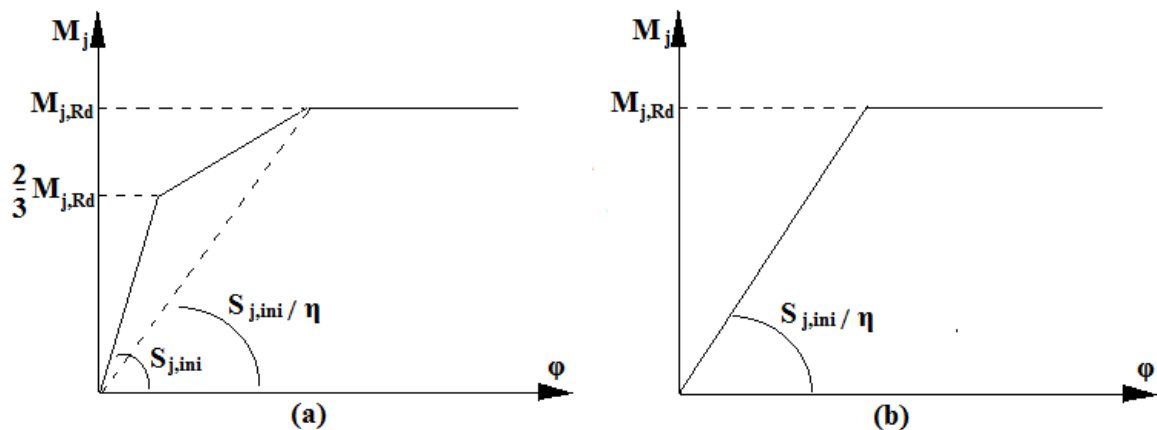
18

Figure 14. Trilinear (a) and bilinear (b) approximation of the Eurocode 3 representation of the moment-rotation curve [1]

2.4 Weak-axis connections and 3-D joints

2.4.1 Beam connected to column web

In beam-to-column minor-axis joints a common design solution is to connect the beam directly to the column web. Part 1-8 of Eurocode 3, limits the component method and considers this joint only as an internal node with balanced moments in the two directions and thus no bending moment transmitted to the column through its web. However, given the existence of external joints and that in internal ones usually moment in both sides is unequal, the column web exhibits an out-of-plane deformation and this phenomenon needs to be examined.

Initially, such joints were recognized as pinned ones. In 1934, the laboratory studies of Young and Jackson [33] showed that this idealization is not in accordance with the joints' actual structural behavior. Few decades later, a series of tests performed by Rentschler, Chen and Driscoll Jr. [34] demonstrated the critical role of the column web in out-of-plane bending in the joints' response. This was also confirmed in the later studies of Chen and Lui [35] , Janss et al. [36] , Davison et al. [37] and Kim [38] . The analytical approach presented by Gomes, Jaspart and Maquoi [2] regarding the accurate calculation of the ultimate moment-resistance of minor-axis joints is considered to this date the most important and will be discussed later.

A beam-to-column minor-axis joint where the beam is directly connected to the column web, can be either welded or bolted. In both cases, the mechanisms of such joints can also be observed in the case of connections between a beam and a RHS section (Figure 15). Hereafter, a presentation of the minor-axis joint moment resistance and rotational stiffness is going to be made with a focus on connections of I profile sections.
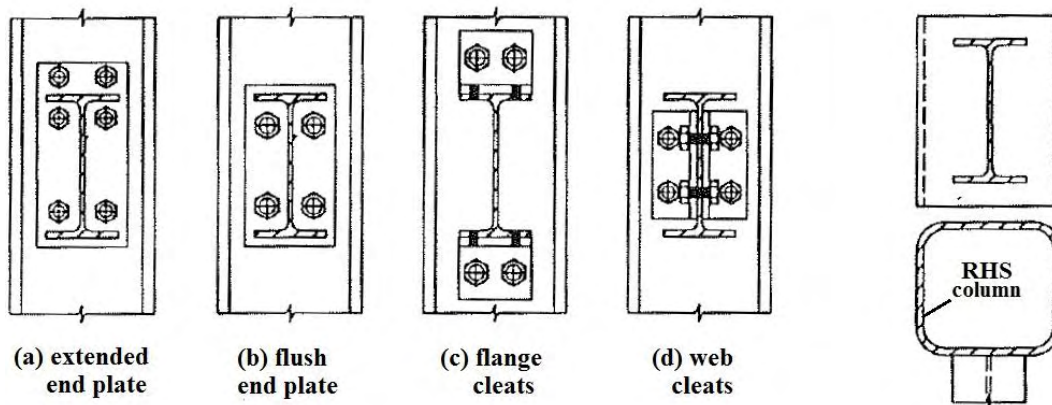
Figure 15. Beam to I-section column and beam to RHS section column joints [2]

Strength of minor-axis joints

A minor-axis joint similarly to its major-axis counterpart, can be decomposed into a number of active components. More specifically, for an end-plated minor-axis joint, the five following components need to be taken into consideration (Steenhuis et al. 1998 [39]) :

- column web in bending and punching;

- bolts in tension;

- end plate in bending;

- beam web in tension;

- beam flange and web in compression.

The strength and stiffness properties of all these components can be determined from Eurocode 3 method, except for the component "column web in bending and shear punching". In 1996, Gomes, Jaspart and Maquoi [2] published and extensive research in the behavior of this specific component and proposed a method that predicts its failure modes. Their study contains expressions for both bolted and welded joints based on the Johansen yield line theory. Hereafter, this method is going to be presented, focusing on minor-axis bolted joints.

The most common case of failure in minor-axis joints, is the one due to the out-of-plane deformation of the column web. The failure mechanisms of the column web can be divided into two main groups: *Local* and *Global* mechanisms. When local failure occurs, a yield line pattern should be observed only in the tension or compression zone, while in case of global failure both zones are involved (Figure 16).
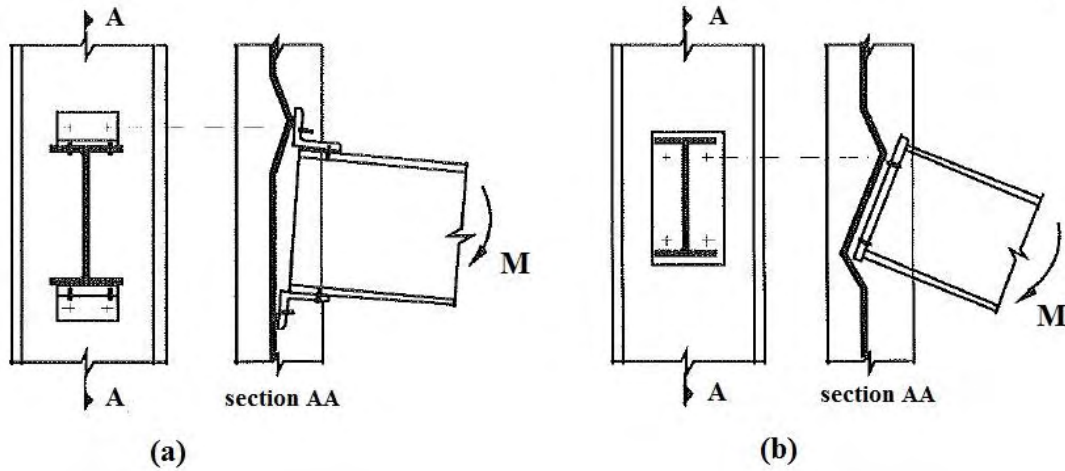
20

Figure 16. Local (a) and Global (b) failure mechanisms in a minor-axis joint

Local failure

The local failure mechanism is the one associated to the minimum plastic force:

$$F_{local,Rd} = min \ (\ F_{punch,Rd} \ ; \ F_{comb,Rd} \ ) \quad (3)$$

where $F_{punch,Rd}$ is the punching shear resistance;

$F_{comb,Rd}$ is the resistance to combined punching shear and bending,

given by equations (4) and (5) respectively.

For bolted connections, the punching perimeter of the column web depends on the diameter of the bolt head and the number n of bolts in the tension zone. The resistance in shear punching is given by the following expression:

$$F_{punch,Rd} = n \ \pi \ d_m \ t_{wc} \ f_y \ / \ (\sqrt{3} \ \gamma_{\mu 0} \ ) \quad (4)$$

where t_{wc} is the thickness of the column web;

f_y is the yield strength of column web;

$\gamma_{\mu 0}$ is the partial safety factor for steel.

In equation (5), the resistance against combined flexural and punching shear mechanisms is presented. When x=0, this combined mechanism is transformed into the pure flexural one (flexural yield lines in Figure 17). For bolted connections, the dimensions *b* and *c* of the equivalent rectangle are defined by equations (7).

21

$$F_{comb,Rd} = k \, t_{wc}^2 \, f_y \left[\frac{\pi \sqrt{L \, (a+x)} + 2c}{\alpha + x} + \frac{1.5 \, c \, x + x^2}{\sqrt{3} \, t \, (\alpha + x)} \right] / \gamma_{\mu 0} \qquad (5)$$

where
$$k = \begin{cases} 1 & if \ \frac{(b+c)}{L} > 5 \\ 0.7 + 0.6 \frac{(b+c)}{L} & if \ \frac{(b+c)}{L} \leq 5 \end{cases} \qquad (6)$$

$\alpha = L - b$

x   can be calculated by relevant expressions in Ref. [2]

In bolted connections, when a single beam is connected to the column web, the tension load acts in a specific rectangular area (Figure 17). The dimensions of the equivalent rectangular are:

$$\begin{cases} b = bo + 0.9dm \\ c = co + 0.9dm \end{cases} \qquad (7)$$

where b_o and c_o are the distances between bolts centers and d_m is the mean diameter of the bolt ($d_m = \frac{d1+d2}{2}$).

Global failure

Global failure mechanisms involve both tension and compression zones and the corresponding failure force may be obtained as:

$$F_{global,Rd} = (\, F_{comb,Rd} \, / \, 2 \,) + (\, t_{wc}^2 \, f_y \, / \, 4 \,) \left(\frac{2 \, b}{z} + \pi + 2\rho \right) / \gamma_{\mu 0} \qquad (8)$$

where $F_{comb,Rd}$ is given by equation (5);

    z is the distance between the center of tension and compression zone and

$$\rho = \begin{cases} 1 & if \ z/(L-b) \leq 1 \\ \frac{h}{L-b} & if \ 1 \leq z/(L-b) \leq 10 \end{cases} \qquad (9)$$

The two mechanisms of global failure are often assumed to be symmetrical and in this case the failure load can be calculated once. However, when the dimensions b x c of the compression zone are different from those in tension zone, equation (8) should be applied twice, one for each zone and the final load will be an intermediate value.
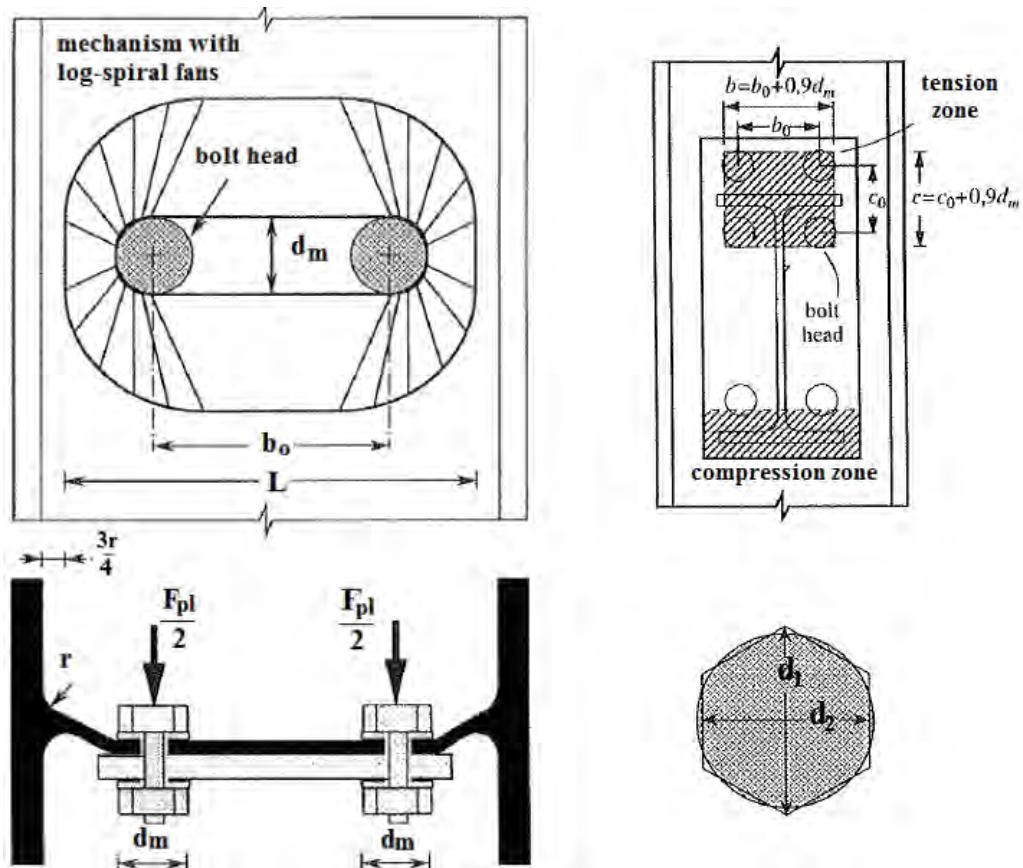
Figure 17. Flexural mechanism in the tension zone of a bolted connection (left) and dimensions of equivalent rectangle and bolt (right) [36].

Ultimate moment

The ultimate moment resistance of the joint can be obtained by $M_{pl} = z$ x min ($F_{local,Rd}$, $F_{global,Rd}$). When there is not axial force in the beam, the compression and tension forces are equal. In this case, the dimension c of the equivalent rectangular in the compression zone (Figure 17) will be determined in order to have the same plastic load with the tension zone. For simplification purposes, it can also be assumed that these two zones have the same b x c dimensions. Finally, the distance between the compression and tension zone is the one between the centers of their equivalent rectangles.

The above-mentioned method, is deemed to be the most fundamental one for the estimation of a minor-axis joint response. However, several researchers have presented alternative methods and provided additional insights in this matter. A mechanical model of a minor-axis joint proposed by Lima et al. (2001) [40] in the basis of the component method, that was after compared with finite element modelling results, confirmed the importance of the column web thickness for the joint strength and stiffness. On the other hand, the authors found the stiffeners in the column web equally important. Given that, they concluded that designers should position the stiffeners as close as possible to the bolt's top row.

23

Rotational stiffness and capacity of minor-axis joints

The rotational stiffness of a minor-axis joint is calculated according to equation (2). As it is previously mentioned (section 2.4) a minor-axis joint can be dissembled into five active components. Each of these components is characterized by a stiffness factor. These factors can be obtained by Eurocode 3 except in the case of the column web in bending and punching component, whereas neither the relevant coefficient nor the component have been included yet.

Expressions that predict with high accuracy the components' stiffness have been proposed by Neves and Gomes (1994) [41] . For the estimation of the component coefficient, the authors modelled the column web as a plate supported at the junction with the flanges and free in the others boarders (strip model) . An effective width (l_{eff}) is estimated according to the column geometry (Figure 18). The factors can be calculated for a minor-axis joint alone, or for the case when the column flange is restrained by a major-axis beam. A simplified evaluation of the joint post-yielding rotational capacity can be found on Ref. [41], [42].

An alternative approach has been proposed in 2009 by Lima et. al [40] , in which reflection photoelasticity experiments were performed for the evaluation of the actual value of the effective width (Figure 18). It is worth mentioning that it was the first time that such technique was implemented for the investigation of minor-axis joints. The findings were later compared to FEM simulations. The technique was found to be superior than the conventional experimental methods, due to its ability to produce the evolution of the principal stress distribution in the column web at each step and even display the development of yield lines, thus obtain with good accuracy the effective width and the column web stiffness factor.
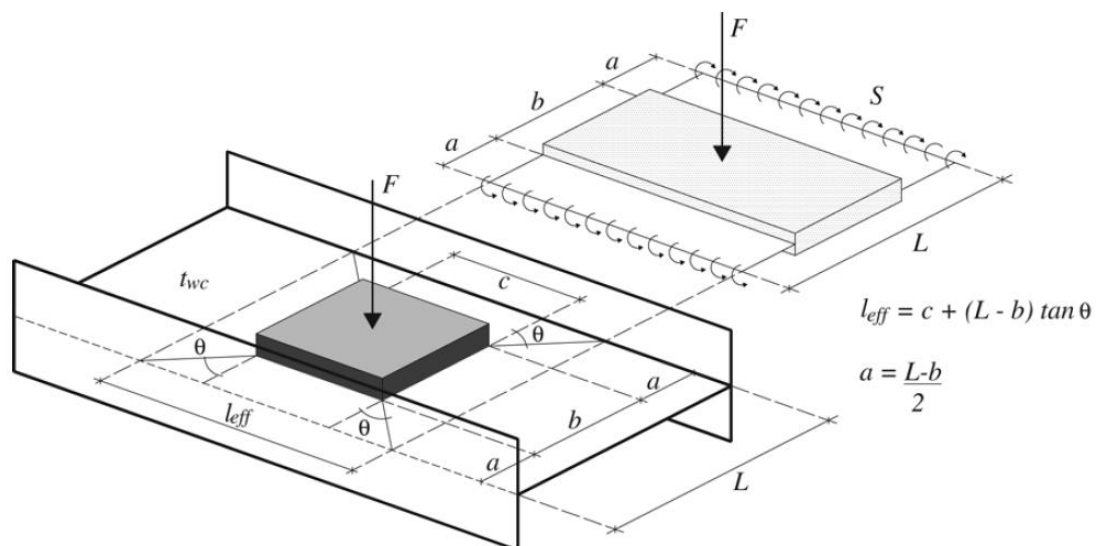

$$l_{eff} = c + (L - b)\tan\theta$$

$$a = \frac{L-b}{2}$$

Figure 18. Strip model for the stiffness of the column web in transverse bending

24

Despite the above advances for the estimation of minor-axis joint stiffness, Silva (2008) [44] mentioned that some developments are still required to achieve a better understanding concerning: (i) the incorporation of a simplified large-displacement formulation including membrane effects for the evaluation of the post-limit response; (ii) the establishment of a method that deals with the problem of web panels connecting beams with various levels of bending moment and (iii) the consistent validation of the procedure for a wide range of configurations and loading.

2.4.2 Beam connected to column flanges

An alternative design scheme in order to transfer the beam's moment to the minor-axis of an I section column is to connect the beam to the column's two flanges. In comparison with major-axis connections the literature provides few insights about the minor-axis counterpart and their simultaneous existence in three-dimensional joints.
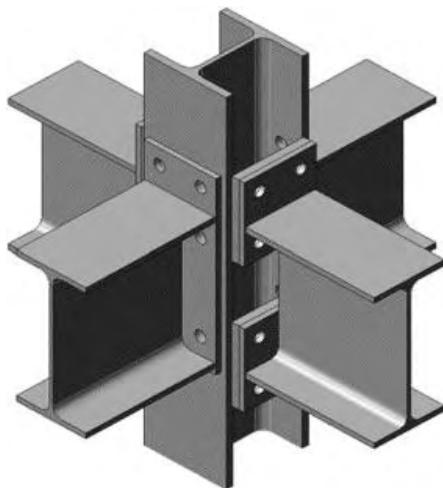

Figure 19. Cabrero and Bayos' studied connections [46]

Cabrero and Bayo [46],[47] performed an experimental study for a proposed design for 3-D joints where the minor-axis connections are bolted to a plate welded to the column flanges (additional plate) (Figure 19). In the proposed joint, minor-axis connections consist of two partial end-plates with a gap to access and tighten the bolts properly if the column size is not big enough. The use of this doubled end-plate minor-axis connection in 3-D joints is characterized by several advantages. The connections in the two axes of the column do not hinder with each other so they can be design separately. Furthermore, the additional plate acts as a stiffener for the major-axis connection. From the tests that they conducted, they found that the thickness of the additional end-plate is a key parameter to the joints' behavior and that Eurocode 3, overestimates the rotational stiffness of tested major-axis connections. Finally, the authors developed an elastic model for the additional plate in bending in both the upper and lower zone.

A few years later, Loureiro et al. [48] , provided additional insights about the above mentioned connection by using extended continuous end-plates (similar to the one studied in this thesis, Figure 20), instead of two partial in the tension and the compression zone. The authors performed experiments for external, internal and corner joints. From these tests, they

concluded that a symmetrical load in the minor-axis results in a significant increase (1,7%-7,6%) of the initial stiffness in the major-axis joint, due to the tensioning effect in the column flanges. Conversely, in external and corner joints, the shear in the column web due to the asymmetrical loading, results in a reduction of the initial stiffness of the major-axis joint. When the geometry, end-plate thickness and bolts are chosen to ensure a complete yield of the end-plate in bending in the major-axis connection, the failure mode is not affected by the presence of additional plates and load in the minor-axis connections. From a

Figure 20. Loureiro et al. studied 3-D joint [48]

series of numerical tests, the authors showed that the additional end-plates stiffen the column flange in bending and that its height plays a significant role in the behavior of the major-axis joint, thus it must be considered in 3-D joint design. For these reasons, and for the accurate calculation of major-axis joints' stiffness in 3-D joints, EC3 needs to include in the component method an additional coefficient that accounts for the end-plates in the minor-axis connections.
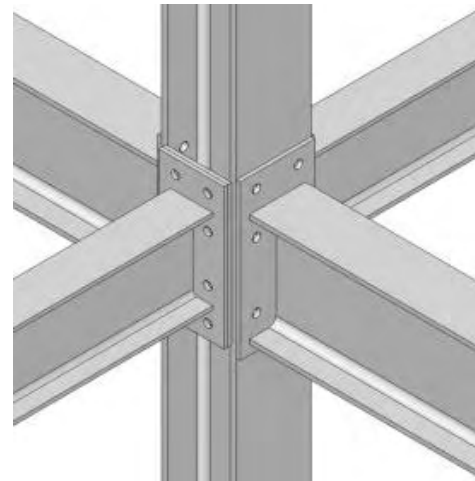
The analytical evaluation of the resistance and stiffness of such joints is a complex task due to the advent of a new component, the E-stub. This component if formed by the column flange in bending, whose two sides are welded with the additional end-plates of the minor-axis connections. Loureiro et al. [49], studied the elastic and plastic behavior of this new component whose location is the same as the column T-stub in 2-D joints. The authors proposed a mechanical model of the E-stub, accounting for the column flanges in bending and the column web and plates in tension, that provided accurate results.
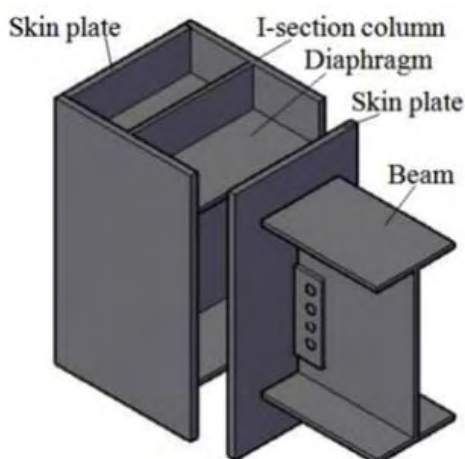

Figure 21. Lu et al. developed weak axis connection [50]

Finally, a very recent study by Lu, Xu, Zhou and Zheng [50], provided insights about a developed weak-axis beam-to-column connection. The proposed minor-axis connection is presented in Figure 21 and shows the several plates and stiffeners inside the column. The mechanical properties and failure mechanisms were examined through a series of experiments in full scale frame joint specimens under monotonic load. The box strengthened joint region was found to be rigid enough so that plastic hinge forms in the beam away from the joint area. The joint region and

26

column remain in elastic state and the overall performance of the joint can be characterized as highly ductile. Additionally the authors tested 10 cruciform joint specimens, with the proposed configuration in both sides of columns' weak axis, five of which were bare steel joints and the rest composite ones, under seismic loads [51] . An important conclusion was that the welding quality between the various components is essential in order for the joints to perform effectively under seismic equivalent loads.

From all the previous, it has become understandable that the concept of semi-rigid minor-axis joints is accepted and adopted the past few years and by that designers have managed to exploit the semi-rigidity of them. Nevertheless, a lot of research still needs to be done in this area to cover alternative joint configurations and to examine them in various load types.

2.5 Final remarks

The analysis of the behavior of steel joints is very complex and incorporates a plethora of phenomena, ranging from material non-linearity (plasticity), geometrical non-linearity (local instability), non-linear contact and slip and numerous intricate configurations. For simplification purposes it is usual for the designers to adopt an idealize moment-rotation curve where only three parameters are of concern: moment resistance ($M_{j,Rd}$), initial stiffness ($S_{j,ini}$) and rotational capacity (φ_{cd}). Since the 1970's, much study has been devoted to the evaluation of the strength and stiffness of semi-rigid major-axis joints while most recently emphasis has been given in the ductility of joints.

Regarding weak-axis connections, when the beam is connected directly to the column web, the analytical and experimental work of many scientists have clearly shown the crucial contribution of the column web panel out-of-plane deformation to the joint response and proven its plate-like behavior (Figure 22a). Conversely, only few studies have been conducted for the alternative design approach, that is when the beam is connected to the column flanges with the use of two end-plates. The use of this dual end-plate weak-axis connection in 3-D joints is characterized by several advantages. The connections in the two axes can be assembled easier as they do not hinder with each other and no holes on the column web are required. Furthermore, the additional plates act as stiffeners for the strong-axis connection and provide further resistance for the column web in shear, tension and compression. Studies have been mainly focused in the configurations of Figure 22 b, c. and especially on the coupling effects between connections in the two axes rather than to the investigation and examination of the failure mechanisms observed in individual weak-axis connections.
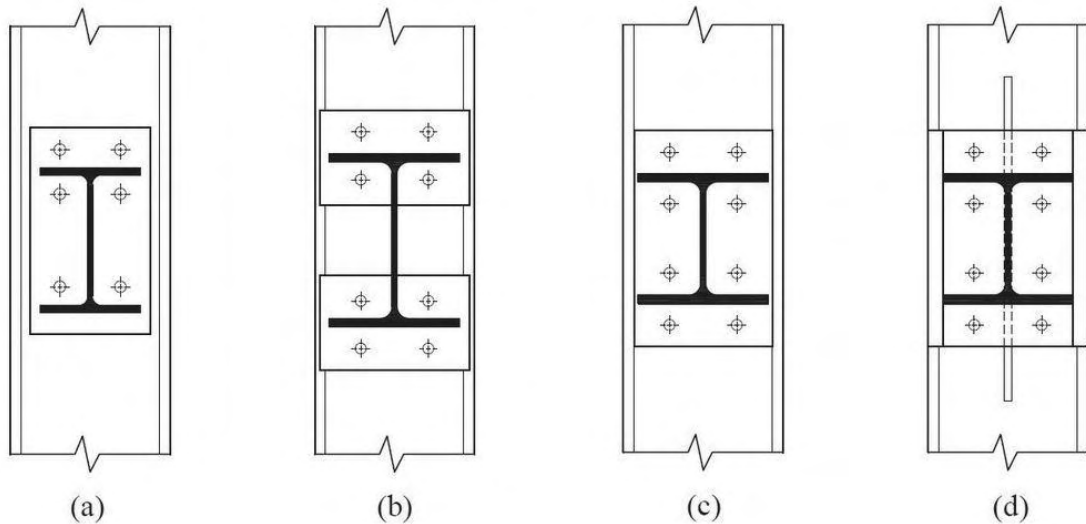
27

Figure 22. Weak-axis connection configurations

In this paper, the studied connection consists of a uniform attached plate, welded to the column flanges, bolted to an end-plate connected to the beam. An additional vertical stiffener has been added (Figure 22d) to increase the strength of the column-attached plates and curtail the stress concentration in the welds between the column and its attached-plate, especially in column sections of significant heights (e.g. h>300mm). In the sequel, the study will be focused in the interaction of such connection in the presence of a second one in the strong axis of the column.

A parametric analysis on an individual connection has been conducted by means of numerical models in order to fully comprehend its structural capacity, ductility, vulnerability and its failure mechanisms. The finite element method has been extensively implemented for the investigation of semi-rigid connections (major and minor) and has proven to be an efficient and reliable method. For both major and minor-axis joints, the findings of numerous approaches and the suggestions of researchers have given the designers the knowledge to exploit to the utmost the joint characteristics. Given that this method allows us to perform numerous analyses, a series of tests have been performed in this thesis and the results will be discussed in Chapter 4. The key components of such connections will be thoroughly analyzed and simplistic designing methods will also be presented.

28

3. FORMULATION OF THE NUMERICAL MODEL

3.1 Geometry of the weak-axis connection

The aim of this study is to simulate and investigate the behavior of a connection in the minor axis of the column, essential to be understood if it is to be designed in a moment resisting frame, mainly on cases when bracing is not possible. The studied connection that is presented is a beam-to-column one, part of a steel frame where no bracing exists.

The geometry of the connection under investigation is presented in Figure 23. In more detail, the connection consists of a HEB300 beam connected to a welded profile column with dimensions very close to those of the HD360x179 standard profile. The beam is attached to an end-plate with dimensions 300x500 and thickness of 20mm/25mm. The column has a plate with dimensions 370x500 attached to its flanges by means of welding (full penetration welds). This plate is referred in the sequel as column-attached plate and for its thickness two cases were also considered (20mm/25mm). For all the studied models, full penetration welds were considered for the connection of this plate to the column flanges. A vertical stiffener of 161mm width and height/thickness of 500mm/750mm and 10mm/16mm respectively, reinforces the attached plate and connects it to the web of the column.
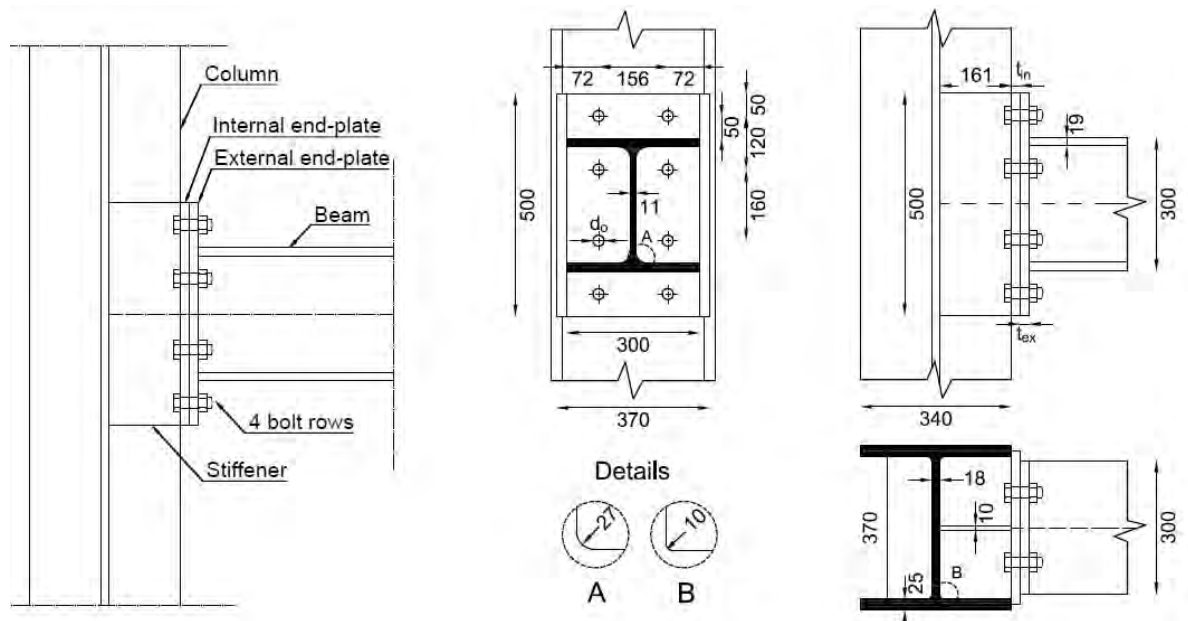

Figure 23. Dimensions of the extended double end-plate weak axis connection

The two assemblages (the beam with the end-plate and the column with the attached plate and the stiffener) are bolted together by means of standard ISO 4017 bolts M24, M30 and M36 (see Table 3), arranged in two columns and 4 rows, for which various alternatives were considered. In total, 14 different models were analyzed and assessed, resulting from a combination of the above-mentioned parameters. These models are presented in Table 2.

29

Table 2. Geometric details of the analyzed weak-axis connections

|	Bolt type	End-plate thickness (mm)	Column-plate thickness(mm)	Column stiffener dimensions (mm)
Model 0	M24 8.8	20	20	-
Model 1	M24 8.8	20	20	161x500x10
Model 2	M24 8.8	25	20	161x500x10
Model 3	M30 8.8	20	20	161x500x10
Model 4	M30 8.8	25	20	161x500x10
Model 5	M30 10.9	20	20	161x500x10
Model 6	M30 10.9	25	20	161x500x10
Model 7	M30 8.8	25	20	161x750x16
Model 8	M30 10.9	20	20	161x750x16
Model 9	M30 10.9	25	20	161x750x16
Model 10	M30 8.8	25	25	161x750x16
Model 11	M30 10.9	20	25	161x750x16
Model 12	M30 10.9	25	25	161x750x16
Model 13	M36 10.9	32	25	161x750x20
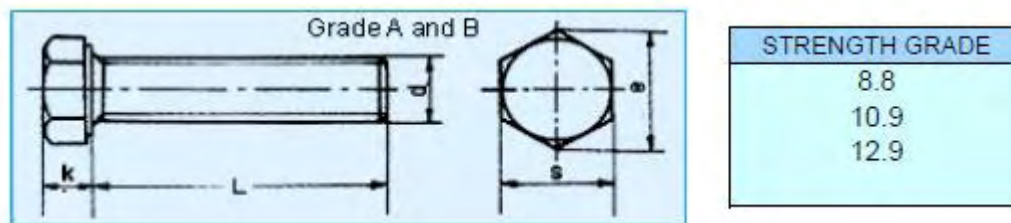
Figure 24. Bolts' geometrical details according to ISO 4017

Table 3. Geometrical details of bolts M24, M30 and M36

Hexagon head screws – ISO 4017			
Thread size	k (mm)	e (mm)	d_b (mm)
M24	15	41,60	21,20
M30	18,7	50,85	26,73
M36	22,5	60,79	32,25

30

3.2 Numerical simulation of the connection

The design of semi-rigid steel frames depends on the joint characteristics, as it has been extensively discussed in the previous chapter. The determination of those characteristics is a complex task due to the numerous connection types and details as well as the corresponding parameters that must be accounted for. The improvement of the electronic system of computation made the use of numerical analyses possible both for the field of research and design. The past few decades, several researchers have studied different beam-to-column joint configurations using numerical models based on the Finite Element Method (FEM) and provided thorough insights by predicted their mechanical behavior (Section 2.3.1). In the current study, numerical models of the double end-plate minor-axis connection have been formulated and analyzed with the use of the software package MSC/Marc [46]. In the following section, the basic principles of the Finite Element Method regarding numerical simulation and analysis are briefly presented.

3.2.1 The Finite Element Method (FEM)

The description of various physics phenomena is achieved by the use of partial differential equations (PDE's). For the vast majority of problems and geometries these equations cannot be solved with analytical methods. Given that, methods that provide approximate solutions have been constructed and used as an alternative approach. The two most common methods are the one proposed by Rayleigh and Ritz and the Galerkin Method.

The Finite Element Method (FEM), is a sub-indent of the above-mentioned methods and it is highly advantageous as it handles complex geometries with great efficiency and it can be programmed in computers easily. The basis of this method, lies on the substitution of the initial geometric filed, to a set of elements (finite elements), each with specific geometric properties and coordinates. These elements are represented by a stiffness matrix constructed using knowledge of the strength of materials. Using these matrices, we are able to construct a system of algebraic equations and by solving it obtain the structures' nodal displacements.

The application of this method requires the following steps:

1. Formulation of the geometric model of the problem;

2. Discretization of the model to smaller parts (finite elements) with specified geometrical, mathematical and physical properties;

3. Determination of the boundary conditions of the problem;

4. Formulation of the problem equations;

5. Solving of the equations (linear or non-linear) with a pre-selected numerical method.

In order to solve the above-mentioned equations, a solution procedure must be performed. Linear systems are expressed with equation 10.

$$K\,u = F \tag{10}$$

where K is the elastic stiffness matrix;

F is the applied load vector and

u is the displacement vector.

The Finite Element Method can be used for non-linear problems as well. In the following section, non-linear systems and a corresponding solution procedure are briefly presented.

3.2.2 Non-linear analysis

Non-linear analysis is usually more complex and expensive than linear analysis and a non-linear problem can never be formulated as a set of linear equations. In general, the solutions of non-linear problems require incremental solutions and iterations (recycles) within each increment to ensure that equilibrium is satisfied at the end of each step. The most common iteration procedure and the one that it is also used in the current study is the Newton-Raphson. This method can be used in structural analysis by considering the following set of equations in which R, K and F are functions of u.

$$K(u)\,\delta u = F - R(u) \tag{12}$$

where u is the nodal-displacement vector;

F is the external nodal-load vector;

R is the internal nodal-load vector (following from the internal stresses) and

K is the tangent stiffness matrix.

$$R = \sum\nolimits_{elem} \int \beta^{T} \sigma \, dV \tag{13}$$

where β is the differential operator that transforms displacements to strains and

σ is the current generalized stresses.

The tangent stiffness matrix and the relevant residual is calculated at each increment and the process is repeated until the convergence criteria are satisfied. Figure 25 graphically demonstrates the Newton-Raphson iteration technique in one dimension to find the roots of the function $F(u) - 1 = \sqrt{u} - 1 = 0$, starting from increment 1 where $F(u_0) = 0.2$ to increment 2 where $F(u_{last}) = 1.0$.
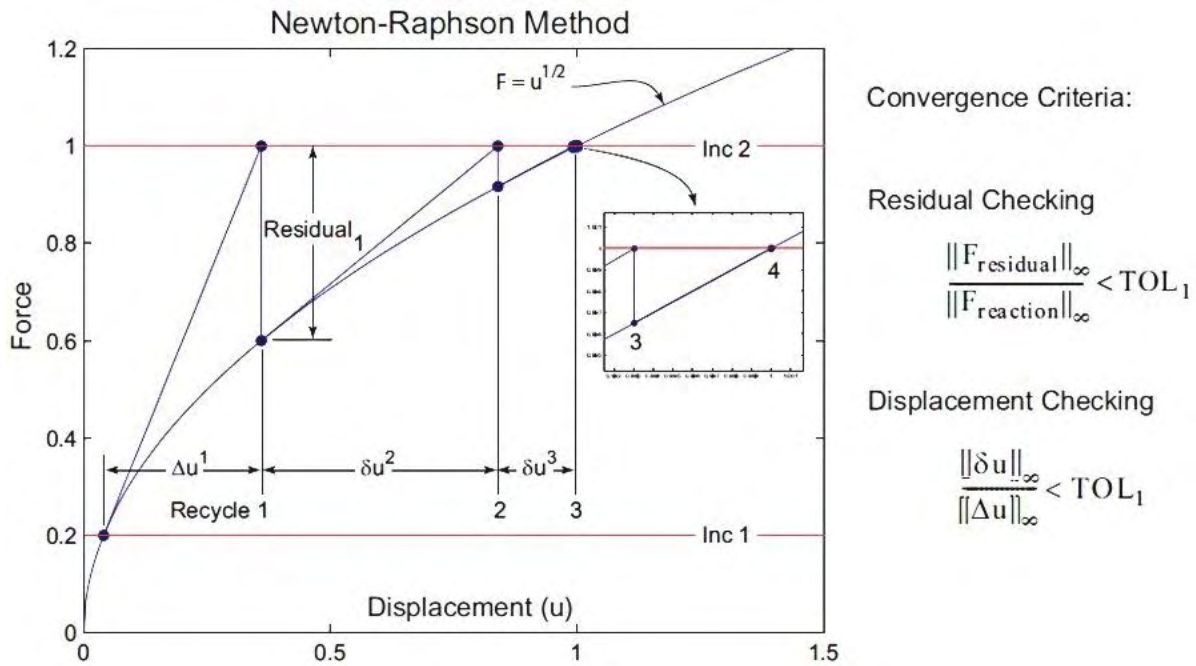
32

Figure 25. Graphical representation of Newton-Raphson iteration technique [45]

3.2.2.1 Material nonlinearity

The first source of non-linearity is the material one and it stems from the nonlinear relationship between stresses and strains. As opposed to an isotropic linear elastic material, which can be defined by two constants: Young's modulus E and Poisson's ratio ν, the nonlinear behavior of a material needs a more complex mathematical representation (constitutive law). This representation is obtained predominantly by experimental data and for the most common materials like elastomers and metals, a plethora of models exists. Other material model of significant importance in engineering problems are: composites, viscoplastics, creep, soils, concrete, powder and foams.

To fully specify a material's non-linear behavior a failure criterion needs to be adopted. The failure of materials is usually classified as brittle or ductile. Steel is characterized, after the elastic range by a ductile yield. The magnitude of the yield stress is generally obtained from a uniaxial test. However, the stresses in a structure are usually multiaxial. A measurement of yielding for the multiaxial state of stress is called the yield condition. Although many forms of yield conditions are available, the von Mises criterion is the most widely used. The criterion's success is attributed to the continuous agreement with the observed behavior of common ductile materials. The von Mises criterion states that yield occurs when the equivalent stress σ_{eq}, equals the yield stress σ_y. The equivalent stress can be expressed from the following two Equations.

For an isotropic material:

33

$$\sigma_{eq} = [\ (\ \sigma_1 - \sigma_2\ )^2 + (\ \sigma_2 - \sigma_3\ )^2 + (\ \sigma_3 - \sigma_1\ )^2\ ]^{\frac{1}{2}} / \sqrt{2} \qquad (14)$$

where σ_1, σ_2 and σ_3 are the principal Cauchy stresses.

$$\sigma_{eq} = [\ (\ \sigma_x - \sigma_y\ )^2 + (\ \sigma_y - \sigma_z\ )^2 + (\ \sigma_z - \sigma_x\ )^2 + 6\ (\ \tau^2_{xy} + \tau^2_{yz} + \tau^2_{zx}\ )\ ]^{\frac{1}{2}} / \sqrt{2} \qquad (15)$$

where σ_x, σ_y, σ_z, τ_{xy}, τ_{yz} and τ_{zx} are the non-principal Cauchy stresses.

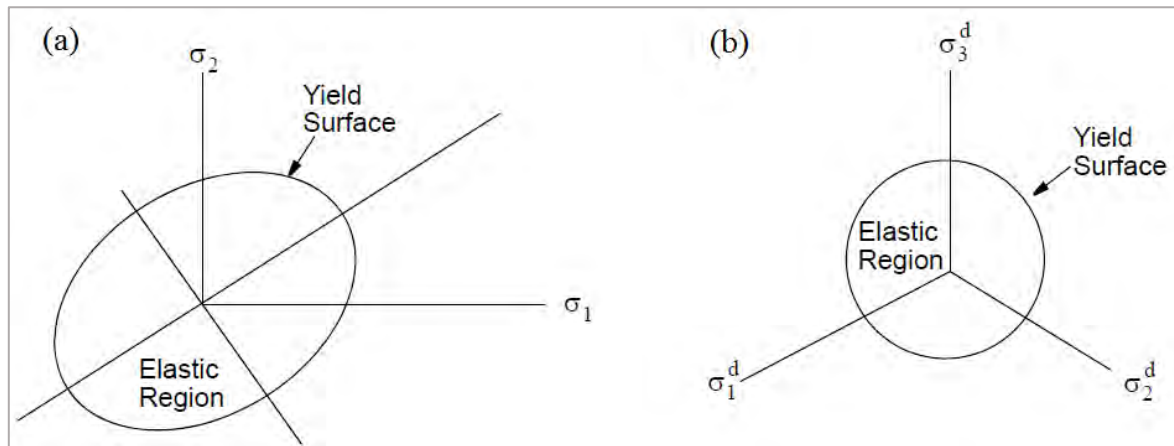Figure 26a and b, demonstrates the von Mises yield surface that encircles the elastic region of the material.

Figure 26. von Mises yield surface [45]

3.2.2.2 Geometric nonlinearity

The second source of nonlinearity results from the non-linear relationship between strains and displacements as well as stresses and forces. Geometric nonlinearity leads to two type of phenomena: change in structural behavior and loss of structural stability. Generally, there are two natural classes of large deformation problems:

1. large displacement - small strain problem and

2. large displacement - large strain problem

For the large displacement, small strain problem, changes in the stress-strain law can be neglected, but the contributions from the nonlinear terms in the strain displacement relations cannot be neglected. For the large displacement, large strain problem, the constitutive relation must be defined in the correct frame of reference and is transformed from this frame of reference to the one in which the equilibrium equations are written.

34

3.2.2.3 Non-linear boundary conditions

The third and final source of nonlinearity can be associated with three types of problems: contact, non-linear support and non-linear loading. During the loading procedure of a structure or a connection, contact between different parts is occurred, occasionally accompanied with friction development. The analysis involving gap and friction must be carried out incrementally. Iterations can also be required in each (load/time) increment to stabilize the gap-friction behavior. The problem of contact appears in bolted connections in a great extent due to the interaction of bolts and plates, the slip caused by the bolt-to-hole clearance and the friction phenomenon between the plates. In case of non-linear supports the modelling can be made either by non-linear springs or elastic foundations. Finally, the directions and the areas of the loads are constantly changing when the structure is deformed. Due to this fact, disregarding the non-linear loads in specific structures could result in a significant error.

3.2.3 Discretization and grid sensitivity

During the discretization process, two things need to be specified. First, the number of the elements and second the type of them. When a model contains curves, corners and sharp edges, a common technique is to increase the number of elements to achieve an efficient representation of the actual geometry and generally obtain improved results. However, such action can result in a lengthy analysis time and a large number of data, something that needs to be avoided if a high number of analyses is to be performed. Usually, in cases when the model lacks intricate curves and edges, an alternative method is to induct higher-order elements. Either way, knowing the nature of the investigated problem is of essence in order to obtain trustworthy results.

In the studied connection, numerous analyses were performed, using various element types and mesh density, to achieve the best-possible effectiveness. Each part of the connection (column, beam, welds, plates, bolts, stiffener) was modeled separately. Initially, the discretization of the whole model was achieved using a four-node isoparametric three-dimensional tetrahedron with three global degrees of freedom (x,y,z) (Figure 27. Forms of four-node (a) and ten-node (b) 3-D tetrahedron elements). The use of this element was combined with a finer mesh but because the strains are constant throughout it, it resulted in a poor representation of the effects of action in the critical areas and the contact phenomenon between the two plates.

For these reasons, a more accurate element was chosen for the critical areas, the ten-node isoparametric tetrahedron again with three global degrees of freedom (x,y,z) (Figure 27b). Each edge of this element, forms a parabola so that four nodes define the corners of the

element and a further six nodes define the position of the mid-point of each edge. This element was found to be advantageous when used in the non-linear analysis. Given that, the ten-node tetrahedron element was used with a fine mesh in the zone that was considered critical (e.g. yield areas). This zone is presented in Figure 28 and it includes the connection as well as a wider beam and column region.
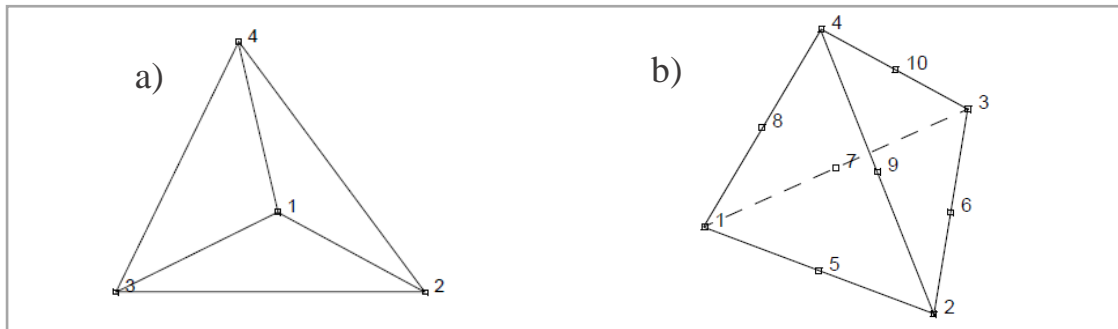

Figure 27. Forms of four-node (a) and ten-node (b) 3-D tetrahedron element

For both element types, the geometry of each element in the model is determined by a pre-chosen algorithm embedded in the software package. A considerable differentiation can be observed in the small size of elements in the curved welds of the column and the beam compared to those in other parts of the connection that are comparatively larger.

Given both the symmetry of the connection and the symmetry of the load, it was decided to analyze the one-half of the numerical model. The plane of symmetry passes through the column, beam, plates and stiffener and the appropriate boundary conditions in the cross-section will be presented in Section 3.2.7.2. By exploiting the models' symmetry, the computation time was considerably reduced and more analyses were able to be performed.

Several analyses were performed prior to the main investigation to fully apprehend the models' grid density needs. These analyses clearly showed the sensitivity of the model regarding the bolts discretization. A considerable fluctuation in the structural response of the joint was observed when the selected mesh factor was altered and for this reason a series of analyses were performed each time with an increased number of elements in the bolts. When the response of the joint was not further changed, the final grid factor was obtained. However, in order to maintain a reasonable analysis time, it was decided to apply these factors only in the two upper bolt rows, that are critical parts in terms of force distribution.

36

3.2.4 Finite Element Model of the connection

For the simulation of the various alternatives of the considered joint, 3D solid finite elements were used within the MSC Marc software environment. In order to reduce the computational cost, the symmetry of the problem was utilized and thus only one half of the original connection was simulated. After a mesh sensitivity investigation that has been presented in Section 3.2.3, a combination of four-node and ten-node isoparametric tetrahedra were used for the discretization of the problem at hand. The different meshes were connected using the built-in capability of MSC Marc to connect non-conforming meshes. The modelling was extended to include parts of the column below and above the connection. A typical story height of 3m was considered and half of the upper and lower parts of the column were simulated, equipped with a simple support at their ends.

Concerning the modelling of the bolts, ten-node isoparametric tetrahedral elements were used. Instead of simulating the threaded part of the bolts, the shank diameter was reduced so that it corresponds to the reduced tension area. This simplification does not affect the obtained results. The welds between the beam end-plate and beam, stiffener and column were not simulated but considered as 'glued' for simplification purposes. The Young's modulus was set equal to 200GPa and the Poisson's ratio equal to 0.3 for all the different steel grades.
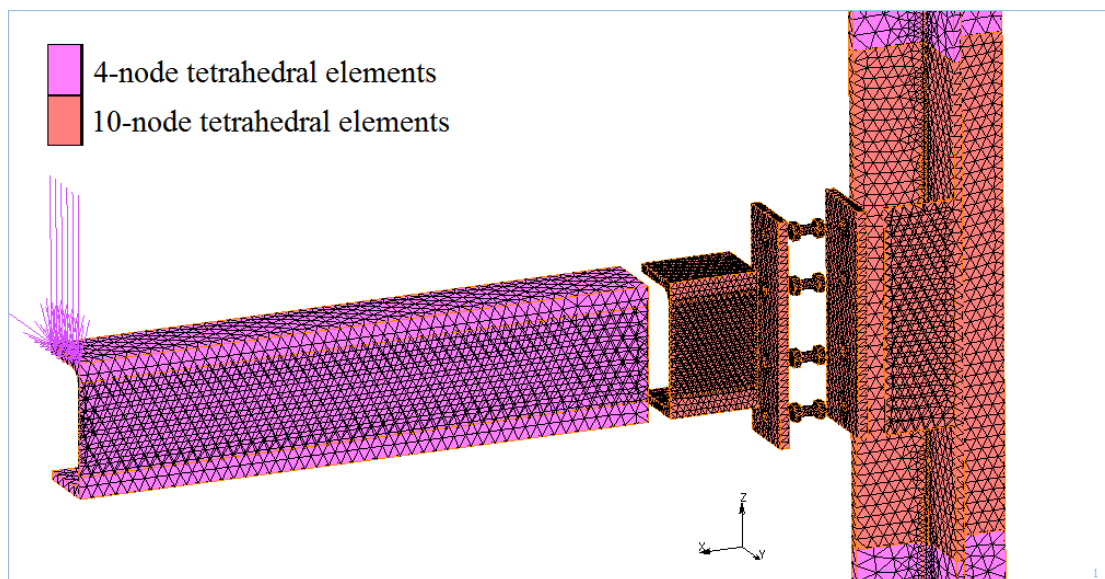

Figure 28. Numerical model of the single minor-axis connection

As it has been mentioned before, the geometry of some parts of the connections will be altered parametrically throughout the study in order to examine the joints' behavior. In Table 5, a presentation of the finite elements of each part in a typical model is being made. The finite elements in a typical bolt at the upper row were around 9820 while in the lower bolt rows around 2420.

37

Table 4. Number of finite elements in each part of the minor-axis connection

number of finite elements			
column	upper column part	middle and stiffener	lower column part
	10922	40377	11020
beam	left beam part		right beam part
	9979		8986
end-plates	end-plate to column		end-plate to beam
	25122		23734
bolts each (M24)	bolts in two upper rows		bolts in two lower rows
	9820		2420

3.2.6 Material properties

For a realistic simulation of the studied problem, proper material needs to be adopted both for the steel components and high-strength bolts. The non-linear material curves can be obtained from Eurocode 3 recommendations or from standard tensile tests of steel. However, this is more appropriate when used for design purposes. A more realistic approach would be to apply in the numerical model, stress-strain relationships obtained from experimental tests.

The steel used for column, beam, end-plates and stiffener was S275. On the other hand, the bolts' strength and diameter were parameters of the problem. M24 and M30 bolts were used, of 8.8 and 10.9 grade, in different combinations. Young's modulus and Poisson's ratio remained constant throughout the study at 210GPa and 0,3 respectively.

For 8.8 and 10.9 bolt materials, the constitutive relationship that was adopted was the trilinear one proposed by Dessouki et al. [52], while the strain values after fracture were obtained from ISO 898-1 [53] as 12 and 9% respectively. For steel S275, a multilinear approximation based on experimental tests was adopted [54] with a fracture strain at 15%. The stress-strain curves are presented in Figure 29a - b and their characteristic values in Table 5.

Since the analyses will lead to a large deformation of the components, it is essential to consider the deformed area thus the non-linear relationship of *true stress* versus *true strain* needs to be considered. However, according to the uniaxial material test for steel, the data obtained are in their nominal form (engineering). For this reason, values in Table 5 will be converted from engineering to true stresses and strains according to the following expressions:

38

$$\sigma_{true} = \sigma_{nom} \, (\, 1 + \varepsilon_{nom} \,) \qquad (16)$$

$$\varepsilon_{true} = \ln \, (\, 1 + \varepsilon_{nom} \,) \qquad (17)$$

where σ_{true} is the true stress

         ε_{true} is the true strain

         σ_{nom} is the nominal stress

         ε_{nom} is the nominal strain

Finally, in order to input into Marc the strain values, the ones from Eq. 17 need to be decomposed into elastic and plastic strains ($\varepsilon_{el,true}$, $\varepsilon_{pl,true}$). The true elastic strain is equal to the true stress (σ_{true}) divided by the Young's modulus (E) and the true plastic strain can be obtained from the following expression:

$$\varepsilon_{pl,true} = \varepsilon_{true} - \varepsilon_{el,true} = \ln \, (\, 1 + \varepsilon_{nom} \,) - \sigma_{true} / E \qquad (18)$$
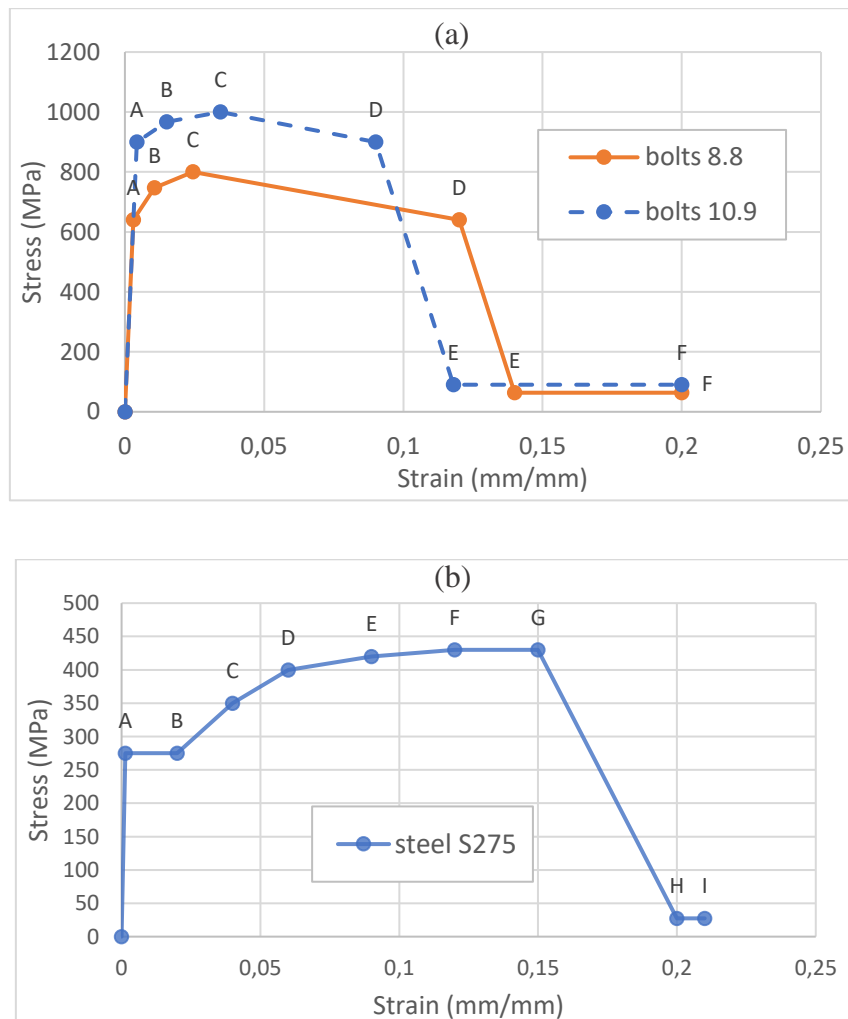
Figure 29. Stress-strain curves for (a) 8.8 and 10.9 bolts and (b) steel S275

39

Table 5. Characteristic values of stress-strain curves

		A	B	C	D	E	F	G	H	I
S275	σ (Mpa)	275	275	350	400	420	430	430	27,5	27,5
	ε (%)	0,13	2	4	6	9	12	15	20	21
8.8	σ (Mpa)	640	747,2	800	640	64	64	-	-	-
	ε (%)	0,305	1,067	2,44	12	14	20	-	-	-
10.9	σ (Mpa)	900	967	1000	900	90	90	-	-	-
	ε (%)	0,429	1,5	3,43	9	11,8	20	-	-	-

3.2.7 Boundary conditions

3.2.7.1 Contact status

Contact plays a cardinal role in the total behavior of steel connections. Through contact forces are allowed to be transmitted and after possible local failures to be redistributed until the joint achieves its maximum capacity. An efficient representation of the actual contact phenomenon between the various components is of essence in order to attain reliable results.

All the different components of the connection, including bolts were defined as deformable. In addition, the selected contact procedure was the "node-to-segment", in which each node in the exterior surface is treated as a potential contact node. The potential segments composed by edges or faces, are considered as piece-wise linear (PWL).

Three in total contact interactions were used to simulate the actual phenomenon. The "touching" (T) interaction was adopted for the contact between the plates while the "glued" (G) one to connect the parts of the column and beam that had been separated and assigned with different mesh grid and finite element order. Finally, in order to avoid the free move of the bolts in the initial steps an interaction called "glued but actually touching" (G/T) was adopted between the end plates and the bolts of the minor-axis connection. In addition, it was considered that friction may be occur and for this reason a relevant coefficient of 0.6 was used in this specific interaction. In Table 6, a representation of the three interactions between the various components is being made. The table is obviously a symmetrical one.

Table 6. Contact interactions between the components

		1	2	3	4	5	6	7	8	9	10	11
1	beam left		G					G				
2	beam right	G										
3	column low				G							
4	column-stiffener			G		G	G					
5	column up				G							
6	plate to column				G			T	G/T	G/T	G/T	G/T
7	plate to beam	G					T		G/T/	GT	G/T	G/T
8	bolt (1st row)						G/T/	G/T				
9	bolt (2nd row)						G/T	G/T				
10	bolt (3rd row)						G/T	G/T				
11	bolt 7 (4th row)						G/T	G/T				

3.2.7.2 Supports

The boundary conditions accounting for the supports of the connection were divided into two main groups. The restrains in the upper and lower nodes of the column as well as the ones in the columns' symmetry plane.

The pinned nodes of the column were simulated with the use of RBE2's. An RBE2 is a rigid link were a number of nodes are rigidly connected to a retained node. The retained node can have loads and boundary conditions applied to it. The tying can be done for some or all degreed of freedom. After connecting the upper and lower nodes of the column to two master nodes, the translations in all three directions were then restrained for these two nodes. Finally, in order to sustain the proper consistency in the cross-section area of the column, three restrains were assigned. The displacement in *y-axis*, rotations in *x-* and *z-axis*.

3.2.7.3 Load application and analysis

All the analyses regarding the single connections were displacement controlled. A vertical displacement was applied at the free edge of the 1.5 m long beam, leading to a moment capacity of the beam which does not need to be reduced due to the presence of shear (the shear stresses that develop in the beam web are comparatively low). All the models were analyzed using a large strain total Lagrange formulation. The two main assemblages and the eight bolts were considered as different deformable bodies that may come into unilateral contact. Between the parts that come into contact, Coulomb friction is considered with a friction coefficient of 0.6. The computational solution strategy employed incremental load application with a relative convergence criterion based on the residual forces.

4. BEHAVIOUR OF THE WEAK-AXIS CONNECTION

The investigation presented hereafter focuses on the understanding of the behavior of a single weak-axis connection. Given that the proposed configuration (Figure 22d) comprises several structural elements in order to be realized (two end-plates, vertical stiffener), it would be highly complex to try to produce mechanical models for each of its components. For this reason, the finite element method was exploited and a parametric analysis has been conducted in order to fully comprehend the various failure mechanisms, characterize the structural response and determine the key parameters, fundamental in joint design.

In total 14 models were analyzed, the geometry and numerical models of which were presented in Sections 3.1 and 3.3.4 respectively. In the sequel, results obtained from the analyses are going to be presented by means of the load-displacement, moment-rotation curves, the state of the connection (Von Mises stress and plastic strains) during the loading procedure and until the ultimate capacity and finally the prying action. The ultimate strength (failure load) in the analysis is assumed to be the maximum load obtained from load-displacement curve. Much attention is going to be given not only in the condition of the connection at the ultimate state, but also in every single increment of the analysis for serviceability purposes. Extreme deformations should be avoided in joint design.

During the presentation of the results, an explanation of the procedure followed will be made. More specifically, reasons why certain parts of the connection were decided to be strengthened at each new model are discussed. After presenting the post-processing results of the FEA, a comparison between the 14 models is going to lead to important conclusions. Finally, with respect to what it has been discussed in Section 2.5, the effectiveness of the proposed weak-axis connection and the several advantages are going to be thoroughly evaluated. In addition, the efficiency of the added vertical stiffener (innovation of this thesis) is going to be assessed. It should be reminded that the vertical stiffener has been added in order to prevent stress concentration in the two weld zones (thus an early failure) between the column flanges and its attached plate and it should primarily being used in columns with relatively significant heights. (Figure 22d).

4.1 Model 0 – Performance without the column stiffener's existence

Prior to the main investigation, that is examine the behavior of the proposed weak-axis connection, is was decided to first analyze a model with an absence of the vertical column stiffener in order to later compare it with the main results and thus realize its significant utility. The connection of the Model 0 consists of a 20mm thickness end-plate and a 20mm thickness column-attached plate (width and height of the plates remains constant throughout the study). The eight in total bolts used in this model are M24 of 8.8 grade. The FE model of Model 0 is presented in Figure 30. It is reminded that for computational cost purposes only the half connection was analyzed.
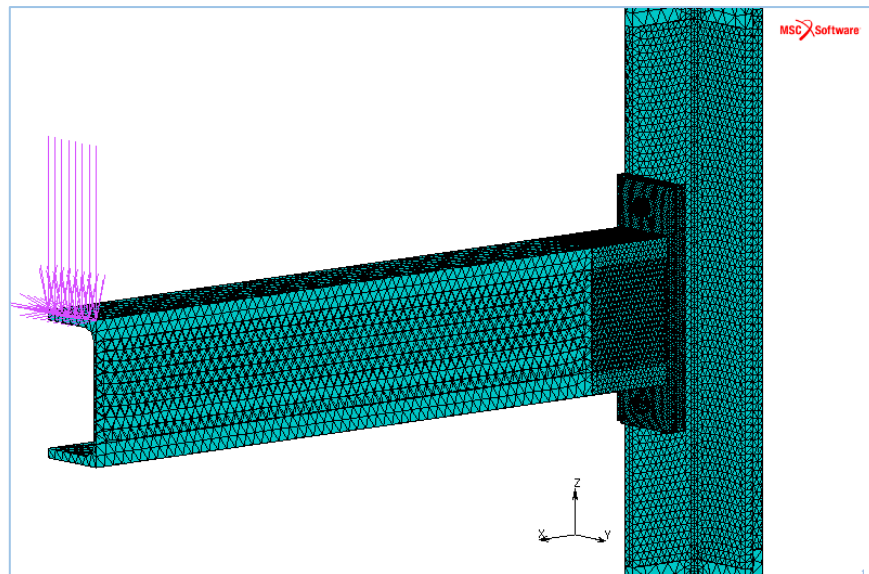
Figure 30. Finite Element Model 0 - absence of column's vertical stiffener

The incremental analysis was displacement controlled. The displacement on the edge of the beam was gradually increasing until reaching the connections ultimate capacity. The force (reaction)-displacement curve was first obtained by exporting the results in excel. This curve is presented in Figure 31. The reaction force at the edge of the beam reaches at the maximum point of the curve 151,10kN which corresponds to a 153mm displacement. However, a better understanding of the connection's behavior can be achieved by observing its moment-rotation curve, presented in Figure 32.
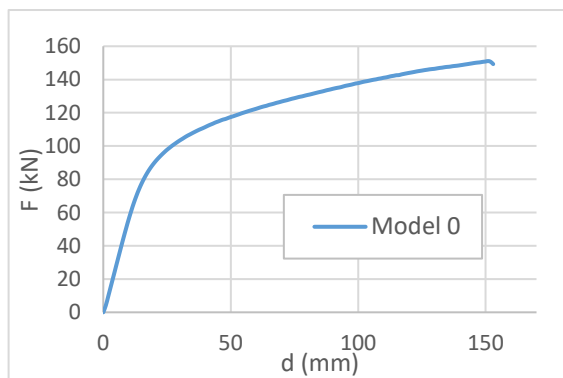
Figure 31. Model 0 - Reaction force-displacement diagram
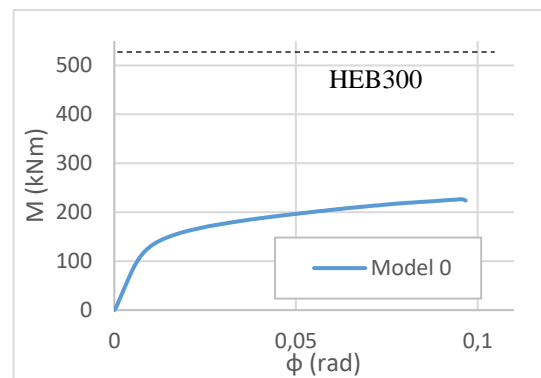
Figure 32. Model 0 - Moment-rotation curve and beam's plastic moment

The curve initiates with a linear response until reaching the beginning of the non-linear region, approximately at 53% of its ultimate limit state. Subsequently, rotation increases considerably until the maximum value of 0.097rad that corresponds to 226,66kNm of bending moment.

A brief analysis of the above figures, shows that this configuration is characterized by a relatively to the beam's plastic moment (513,97kNm), low ultimate capacity (only 44.1%).

43

Such smooth curve also indicates a rather ductile failure of the connection. In the sequel, a presentation of the connection's plastic strains in several increments is going to be presented.

From the following figures, one can observe the development of plastic strains mainly in the region between the column flanges and its attached plate, but also in a vertical area in the middle of this plate that can be attributed to its significant bending around z-axis. This bending is caused due to the absence of a restriction between the column's two flanges. At this point, the rotation of the column-attached plate leads to a considerable bending of the bolts in the two upper rows (also around z-axis). Consequently, bolts become extremely stressed and cause the failure of the connection ($M_{j,u0}$=226,66kNm), at which point the material in the region of the full penetration welds has reached its maximum capacity (15-20% plastic strains).
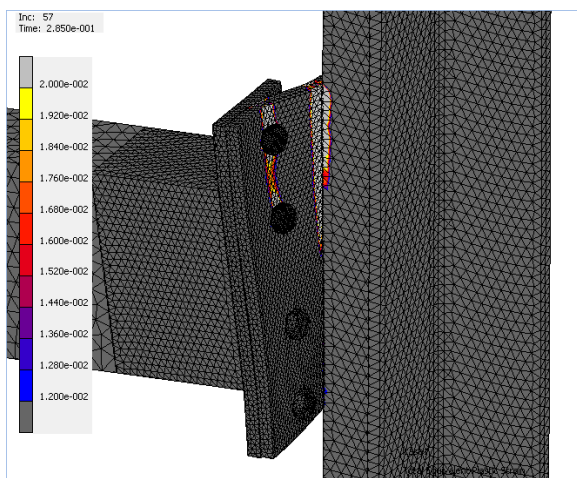
Figure 33. Model 0 - Plastc strains at 80%$M_{j,u0}$ =181.32kNm (x4)
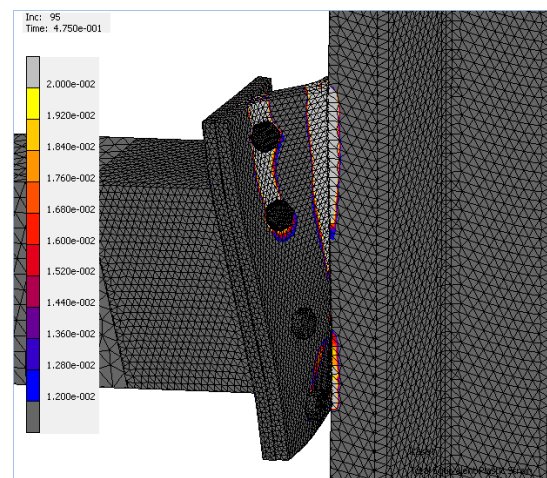
Figure 34. Model 0 - Plastc strains at 90%$M_{j,u0}$ =204kNm (x4)
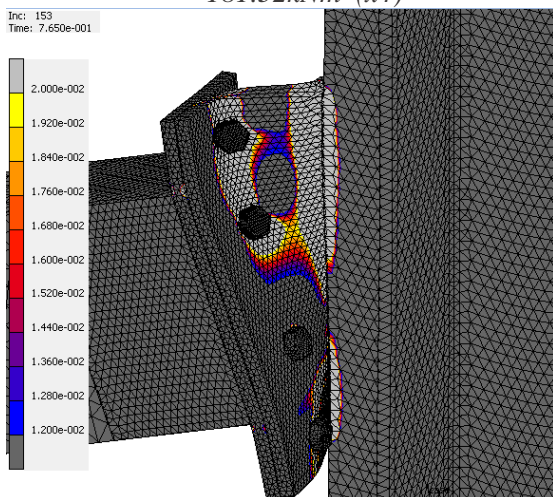
Figure 35. Model 0 - Plastc strains at $M_{j,u0}$=226.66kNm   (x4)
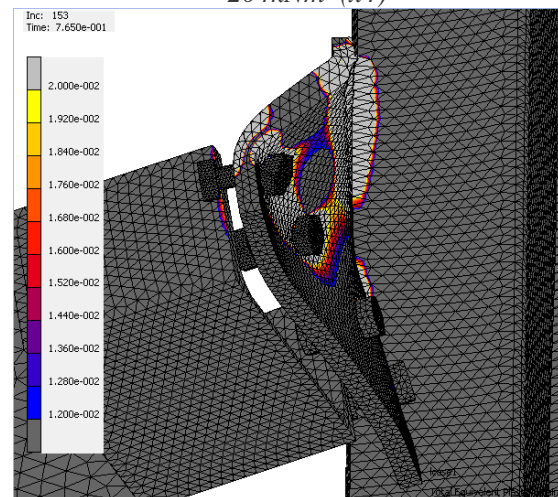
Figure 36. Model 0 - Bending of bolts and column-attached plate at failure (x4)

The above figures, clearly demonstrate the gradual development of plastic strains throughout the connection and basically highlight its weak zones. These include the welds

44

between the flanges of the column and its attached plate and also the plate itself that develops a significant deformation due to the existence of degrees of freedom. However, this plate does not yield completely but rather develops maximum levels of stress at its outer layer. Instead, bolts in the upper row being the ones that carry most of the connection's tension, reach their maximum capacity and finally fail due to simultaneous bending and tension. Focusing on the end-plate behavior, it can be observed that it follows the column-attached plate's shape and exhibits the usual T-stub behavior but rather in a small extent with barely discernible plastic strains.

4.2 Model 1 – Influence of the column stiffener

All in all, one can assume that the configuration of Model 0, presented in the previous section, is characterized by extreme deformations that need to be avoided in joint design as they can pose a serious threat in the entire structure. The connection's ultimate capacity corresponds to a low percentage of the beam's plastic moment and by no means exploits the end-plate's existence. In view of this, Model 1 incorporates a vertical stiffener with dimensions of 161x500x10, that unites the column-attached plate with the column's web and it is parallel to its two flanges. The stiffener is expected herein to provide an indispensable solution to the previous connection's inadequacy.

The first ooutputs that were exported from the analysis were the force-displacement and moment-rotation curves, that are presented in Figures 37,38. The first noticeable discrepancies one can observe in the following diagrams mainly concern the initial stiffness, rotational and moment capacity.
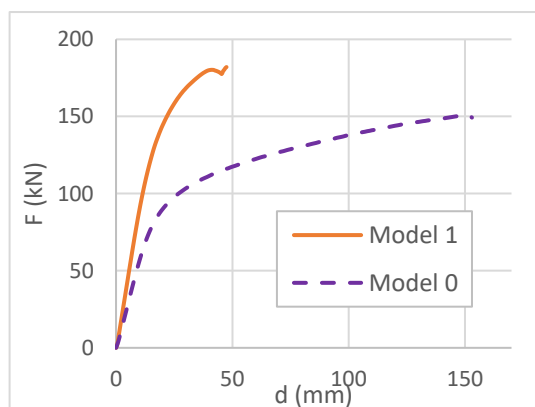

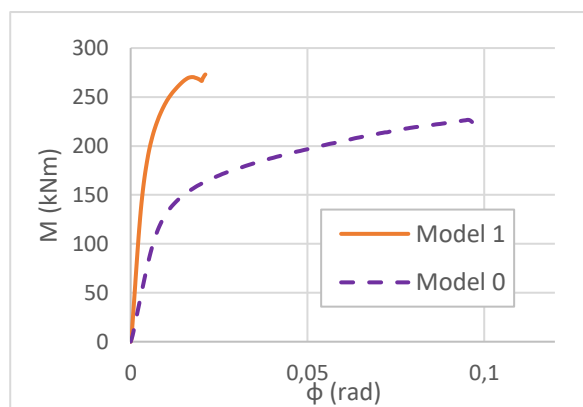*Figure 37. Force-displacement diagram – Model 0-Model 1 comparison*

Figure 38. Moment-rotation diagram – Model 0-Model 1 comparison

The strengthening of the connection due to the added stiffener results in a significant increase of the initial stiffness $S_{j,ini}$ and allows a slight rotation that reaches the maximum value of 0.02rad (five times smaller than the maximum rotation of Model 0). The displacement along x-axis diagrams of Models 0-1 are presented in Figures 39,40 and prove

45

the efficiency of the added stiffener in the well-controlled ductility of the connection. It is clear that the previous model's displacements have been significantly curtailed which also leads to a reduction of the bending action of the column-attached plate and the bolts, thus an early failure. Finally, when a plastic design is of concern, the ultimate flexural resistance of the joint has been considerably altered by a 20,46% increase.
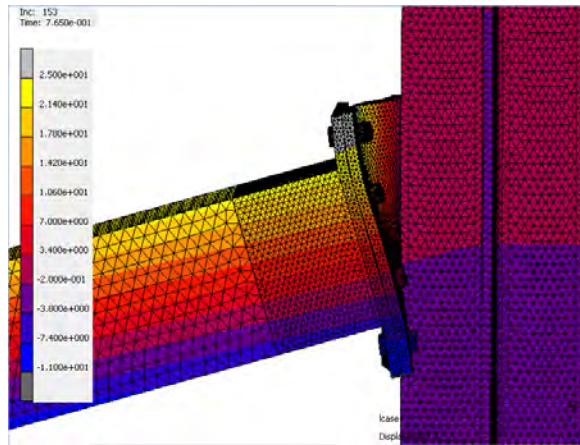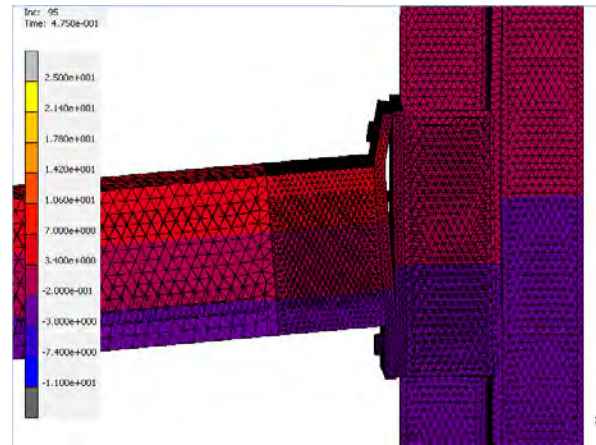

| Figure 39. Model 0 - x-axis horizontal displacements (x4) | Figure 40. Figure 41. Model 1 - x-axis horizontal displacements (x4) |

At this point, a presentation of the development of stresses in Model 1 in 80% and 100% of the maximum moment resistance is going to be made in order to establish the possible differentiation regarding failure mode and the development of the internal stresses and plastic strains.
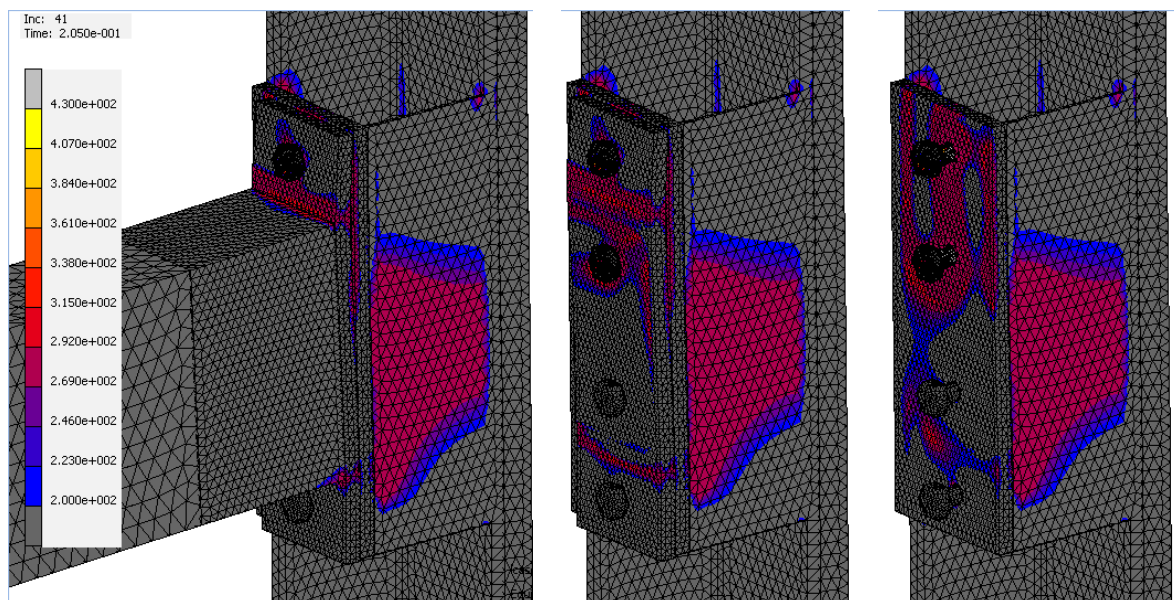
Figure 41. Von Mises Stress of Model 1 at 80%$M_{j,u1}$ =218,43kNm (x4)

46

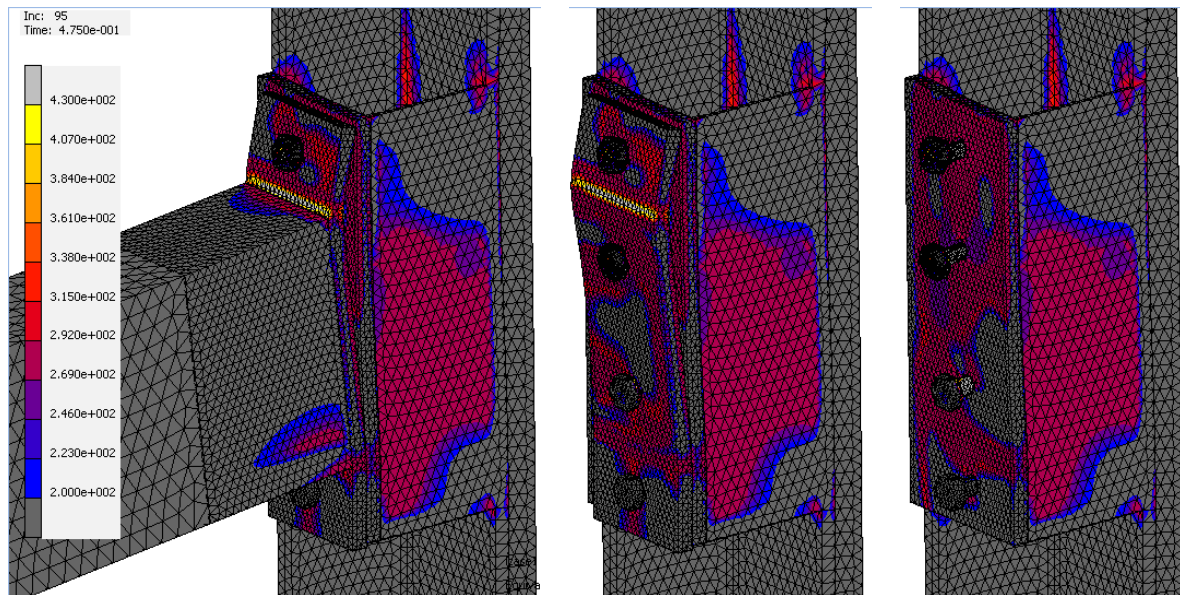*Figure 42. Von Mises Stress of Model 1 at $M_{j,u1}$ =273,04kNm (x4)*

Focusing on Figures 41,42, one can observe the main stress concentration at the added vertical stiffener, a large area of which has reached its yield stress (f_y=275Mpa) from an early stage of the analysis. Essentially, the stiffener plays the role of the column web that a weak-axis connections lacks. Due to that, it can be assumed as the main shear force transferrer, and act as a dominant component that transmits a large amount of load from the beam to the column. For higher load levels, the yielding area has been expanded, the stiffener seems to draw with it the middle part of the column web and as a result it instigates the emergence of small highly stressed zones at the weld areas of the column.

Regarding the column-attached plate, it is clear that a considerable reduction of its deformation has been achieved which stems from the existence of the vertical stiffener. However, by the time the joint has reached its ultimate resistance, this plate has exhibited an almost uniformly stressed behavior that does not have a serious effect on the inner layers.

As far as the end-plate in of concern, it can be said that it manifests a rather typical T-stub behavior, with two main stressed zones parallel to y-axis, above and under the beam's upper flange. By observing the connection at its ultimate limit state, we can see that the excessive bending of the end-plate around y-axis creates a plastic hinge by reaching 430kN of stress. As it is already known from the literature, an equivalent T-stub can have three modes of failure. Failure of the end plate's material formed with the plastic hinge, failure of the bolts or a simultaneous failure of both. In order to recognize the true mode, an examination in the bolts needs to be made.

The two bolts (upper row) that are incorporated in the equivalent T-stub, exhibit a highly stressed behavior. The bolt in the second row, is mostly tensed and a neck is created at the last increments of the analysis. Conversely, the upper bolt besides the amount of tension

47

that receives, it also bends around y-axis due to the prying action between the two plates. The thickness of the end-plate (20mm) has proved to be inadequate and causes the cracking of the bolts. Ultimately, the maximum flexural resistance of the joint reached the value of $M_{j,u1}=273,04$kNm. From all the above, it can be concluded that the connection's behavior was eventually governed by the failure of the T-stub component and more specifically by the simultaneous cracking of bolts and failure of the end-plate.
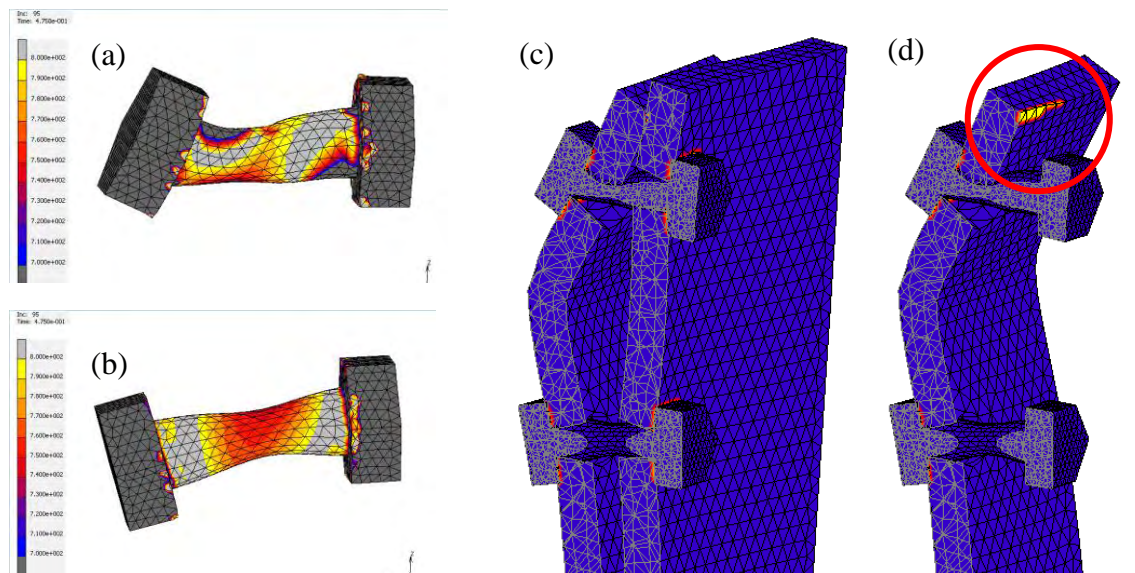
Figure 43. Von Mises Stress at bolts in the upper first (a) and second (b) row and the prying action between the two plates (c,d) (x8)

4.3 Model 2 – Influence of the end-plate's thickness

An analysis of the previous Model's results, already presented in Section 4.1.2, indicates the inadequacy of the connection regarding the performance of the equivalent T-stub, formed by the end-plate, the beam's upper flange and the bolts. However, it has been accepted that the highly stressed condition of the bolts, can be partially attributed to the prying forces developed between the two plates. In order to diminish those forces, it was decided to increase the end-plate's thickness from 20mm to 25mm. With this alteration, a more satisfactory performance of the connection can theoretically be achieved.

The first diagrams, presented in Figures 44,45, depict the new Model's behavior in terms of the reaction force-displacement and moment-rotation curves. From these diagrams, it can be observed a 21,35% increase in the beam's maximum displacement (from 44,5mm to 45mm) and a 14,44% increase in the corresponding reaction force at the edge of the beam (from 182,03KN to 208,31KN). With regard to the moment-rotation curve, we can first notice a significant increase in the connection's initial stiffness that causes an almost negligible differentiation in the rotational capacity. Finally, the ultimate moment resistance of the joint has been altered from $M_{j,u1}=273,04$kNm to $M_{j,u2}=312,46$kNm. This value of the maximum

48

moment of Model 2 corresponds to a 60,79% of the beam's plastic moment and renders the connection as a partially strength one (Eurocode 3-Joint classification by strength [1]).
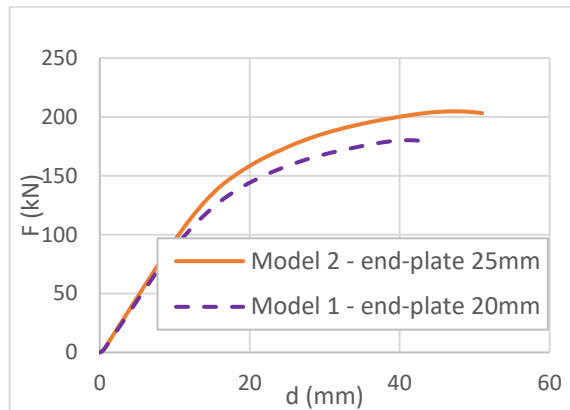

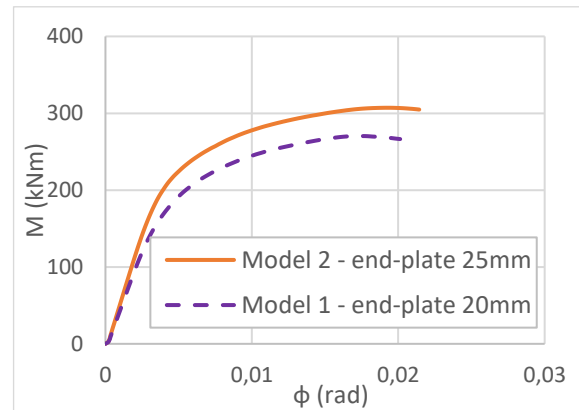*Figure 44. Force-displacement diagram – Model 1-Model 2 comparison*

Figure 45. Moment-rotation diagram – Model 1-Model 2 comparison

In order to observe the distribution of internal forces and the relevant failure modes, its essential to examine once again the condition of the connection of Model 2, during the analysis. The main interest with this configuration, was to achieve a better overall performance by strengthening the critical component, that is the T-stub. This has been achieved by looking Figure 46, where one can notice at the final increment of the analysis, a switch of the internal forces. The vertical stiffener as well as the bolts in the two upper rows seem much more stressed due to the relatively thick end-plate that cannot be deformed as easily as before and thus generate the development of prying forces or create a plastic hinge. In addition, the welds between the column and its attached plate have also reached a high level of stress relatively to the other parts of the connection. Plastic strains have also been expanded to the inner edge of the beam as it can be seen in the Figure below.
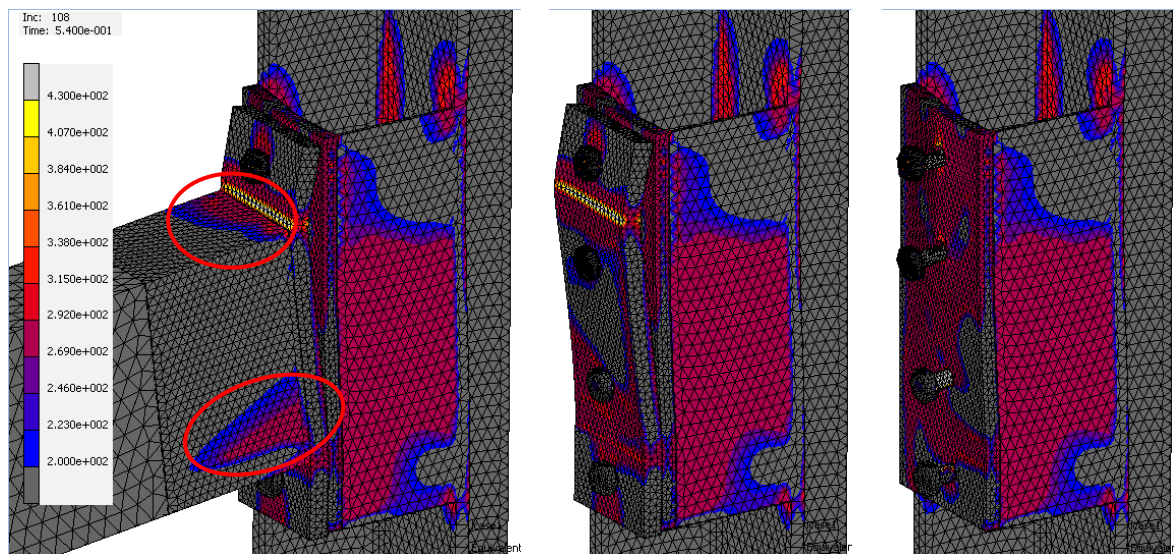

Figure 46. Von Mises Stress of Model 1 at $M_{j,u2}$ =312,46kNm (x4)

49

When the applied displacement reaches the maximum value of 54mm, the ultimate flexural resistance of the joint is obtained ($M_{j,u2}$=312,46kNm), the failure of which is finally attributed to the inadequacy of the bolts in the upper row, despite the extreme stressed condition of the end-plate that does not eventually reaches its limits. The deformed shape of the bolts has not significantly altered, but rather the intensity of stress.
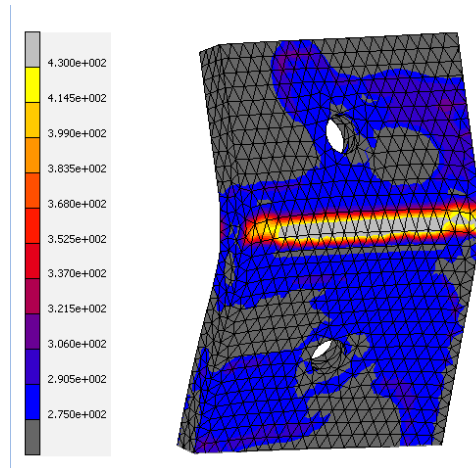

Figure 47. Von Mises stress of Model 1's end-plate (20mm) at $M_{j,u1}$=273,04kNm

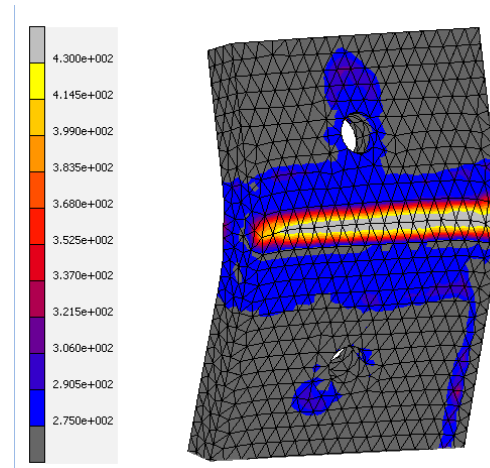*Figure 48. Von Mises stress of Model 1's end-plate (25mm) at $M_{j,u2}$=312,46kNm*

Figures 47,48, present the condition of the equivalent T-stubs of Models 1-2 at the ultimate increment. It is clear that Model 2 exhibits an improved behavior with comparison to Model 1's counterpart. However, the T-stub is still the component that causes the connection's failure due to bolt rupture.

Until this moment of the investigation, three analyses have been performed that have establish the imperativeness of the use of a vertical stiffener in order to avoid an unpleasant stress concertation in the welds between the column and its attached-plate, but also the extreme bending of this plate and thus the bolts. By adding this stiffener, stress is shifted to different components such as the equivalent T-stub formed by the end-plate and beam. After increasing the thickness of this plate and thus improve the joint's overall performance it is considered reasonable to then alter the diameter of the bolts in order to strengthen them and thus avoid their early failure. Table 7, represents the geometry and final results of the three previous Models (0,1,2).

Table 7. Geometry of parameters and response of Models 0,1,2

	Bolt type	End-plate thickness (mm)	Column-plate thickness(mm)	Column stiffener dimensions (mm)	$M_{j,ui}$ (kNm)	$M_{j,ui}/M_{pl,HEB300}$
Model 0	M24 8.8	20	20	-	226.66	44,10
Model 1	M24 8.8	20	20	161x500x10	273.04	53,12
Model 2	M24 8.8	25	20	161x500x10	312,46	60,79

4.4 Models 3 and 4 – Influence of bolt's diameter

The aim of the two new analyses is to examine Models 1 and 2 by altering their bolts' diameter from M24 to M30. It can be assumed that this will increase not only the joint's maximum resistance but also its stiffness. The results are going to be presented by comparing Model 1 with Model 3 and Model 2 to Model 4. Essentially, these pairs can be characterized by the same geometry, except their bolt size. This will allow us to focus on the bolts diameter's effectiveness in the joint's overall performance.

- Model 1/3 comparison (End-plate's thickness 20mm – Bolts 8.8 M24/M30)

The first step in the post-processing analysis is to examine the force-displacement and moment-rotation curves of Models 1 and 3. By observing Figure 49, a clear differentiation in the two Model's behavior can be noticed. The reaction force at the beam's edge has been increased by a 31,27% and the displacement of the beam by an impressive 124,84%. In correspondence, Figure 52 demonstrates the increase in the ultimate moment resistance from $M_{j,u1}=273,04$kNm to $M_{j,u3}=352,47$kNm (20,09%) and the relevant increase in the rotational capacity from 0,02rad to 0,05rad (150%). The maximum flexural resistance of the Model's 3 connection corresponds to a 67,86% of the beam's plastic moment. By comparing this percentage to the one of Model 1 we can see a 14,74% increase.
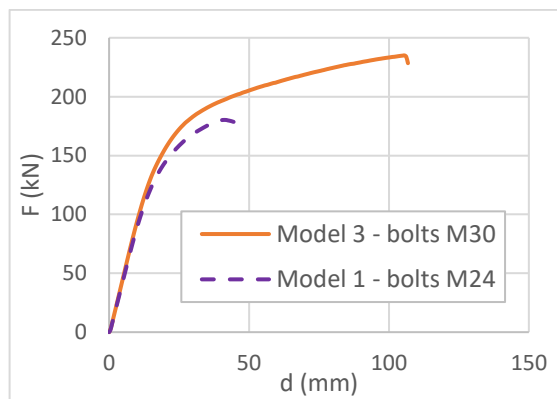

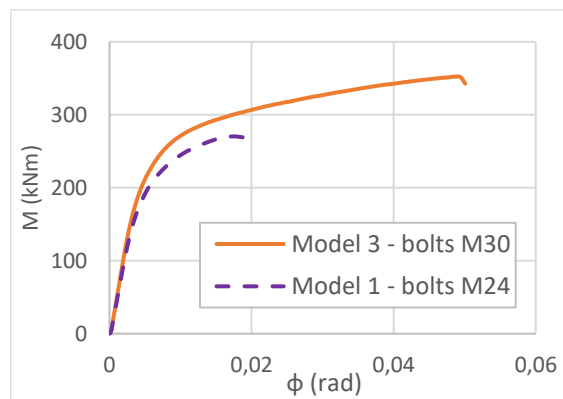*Figure 49. Force-displacement diagram – Model 3-Model 1 comparison – end-plate's thickness 20mm*

Figure 50. Moment-rotation diagram – Model 3-Model 1 comparison – end-plate's thickness 20mm

However, in order to obtain the failure mode and fully understand its reaction throughout the loading procedure we should observe the Figures presented herein. This will allow us to evaluate the efficiency of the alteration of the bolt's diameter when the end-plate's thickness is rather thin (20mm). What one can notice from the comparison being made in Figure 51, is that in Model 3, due to the strengthening of the bolts, there has been a large expansion of stress in the column web, something that was not significantly affected in Model 1 (M24 bolts). However, these stresses do not lead to the development of plastic strains, so

51

the column web is considered to be almost intact. This alteration in the bolt's diameter, has led to an excessively deformed connection that ultimately fails from the development of a plastic hinge in the end-plate and the rupture of the bolts. Nevertheless, Models 1 and 3 incorporate an end-plate of 20mm thickness and therefore these extreme deformations are somewhat justified. The compared results clearly demonstrate the inefficiency of this configuration due to the relatively inadequacy of the end-plate and bolts.
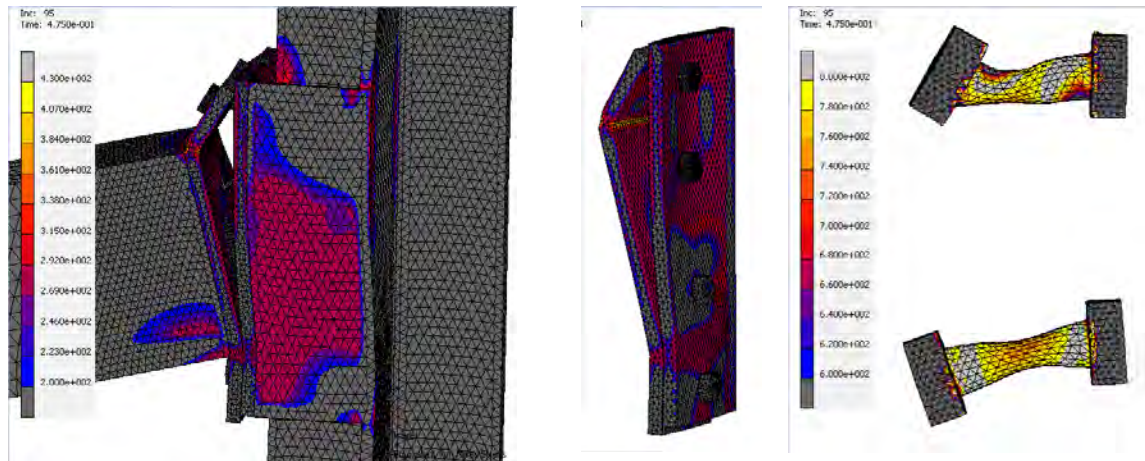
Figure 51. Von Mises stress of Model 1 (bolts M24) at $M_{j,u1}$ =273,04kNm (x10)
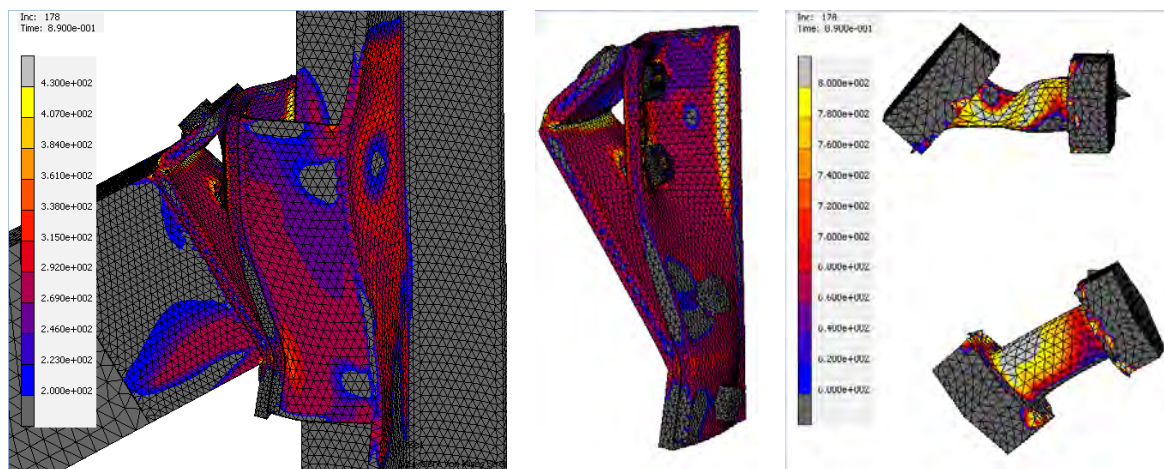
Figure 52. Von Mises stress of Model 3 (bolts M30) at $M_{j,u3}$=352,47kNm (x10)

- Model 2/4 comparison (End-plate's thickness 25mm – Bolts 8.8 M24/M30)

In order to diminish the extreme deformations and the early failure of the connection due to the inadequacy of the end-plate and bolts, Model 4 has incorporated an end-plate with 25mm thickness and bolts of 30mm diameter (M30). Figures 53,54 show that a significant improvement has been achieved, as in the case of a 20mm thickness end-plate. This time though, it seems from the sheer drop in the curves, that probably the cause of failure has been a rather brittle one. The ultimate moment resistance of the Model's 4 connection has been obtained as $M_{j,u4}$=419,36kNm which gives a 81,59% of the beam's plastic moment. It can be indicated that the connection has performed very efficiently. Compared to Model's 2 moment

52

resistance there has been achieved a 34,21% increase (from $M_{j,u2}$=312,46kNm to $M_{j,u4}$=419,36kNm).
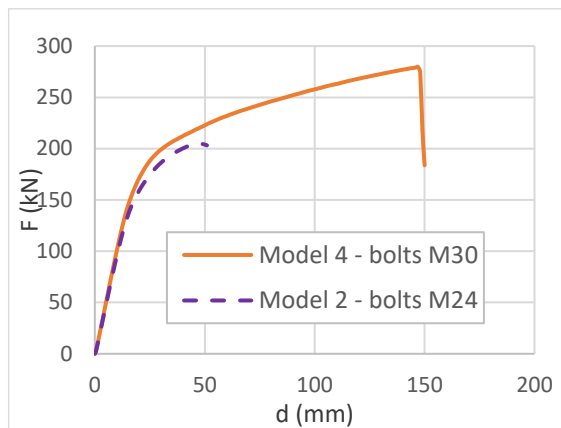

Figure 53. Force-displacement diagram – Model 4-Model 2 comparison – end-plate's thickness 25mm
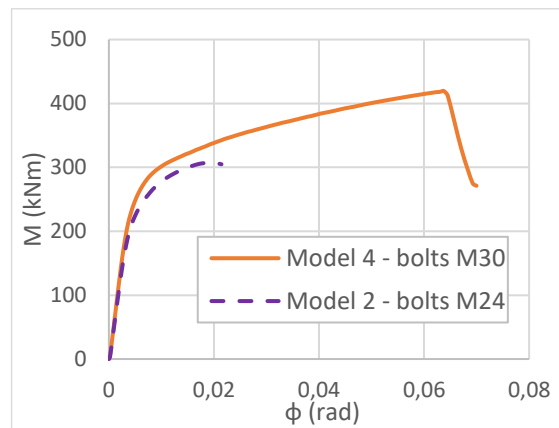

Figure 54. Moment-rotation diagram – Model 4-Model 2 comparison – end-plate's thickness 25mm

From Figures 55,56, we can clearly observe the differentiation in the connections' response. Due to the increase of the bolt's diameter from 24 to 30mm combined with a thick end-plate (25mm), the overall connection has been strengthened considerably and thus stress concentration has been shifted to areas like the edge of the beam, the column's stiffener, column web and the column-attached plate. The stress seems to be significantly increased in these areas by reaching and exceeding the materials yield stress (275MPa). The equivalent T-stub seems to be once again the most critical component and finally due to the relatively thick end-plate, the failure of the connection comes again from the bolt failure in the upper row.
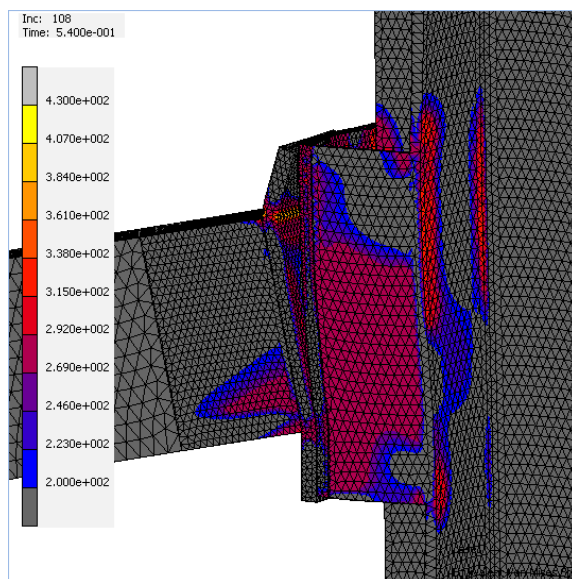

Figure 55. Von Mises stress of Model 2 (bolts M24) at $M_{j,u2}$=312,46kNm (x7)

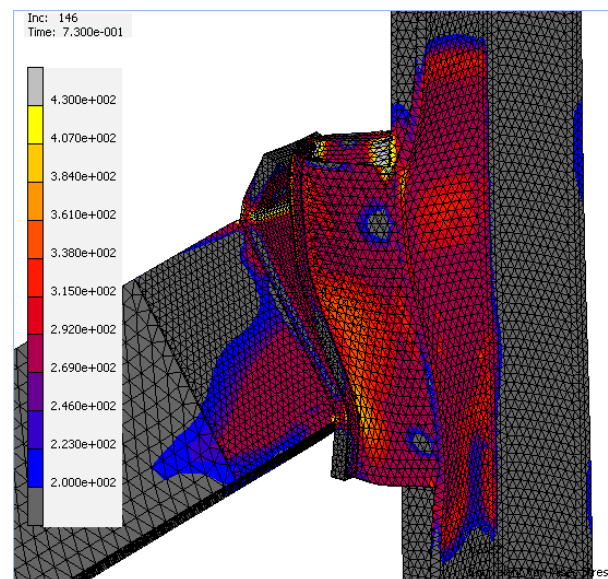*Figure 56. Von Mises stress of Model 4 (bolts M30) at $M_{j,u4}$=419,36kNm (x7)*

53

So far, it can be concluded that the influence of the bolt's diameter is rather stronger compared to the end-plate thicknesses'. The alteration from M24 bolts to M30 ones has given a 20,09% increase in the maximum flexural resistance of the joint when a 20mm thickness end-plate is used and a 34,21% when a 25mm is incorporated in the model. Of course, this can be attributed to the fact that with this specific geometry, bolts are the most critical components. A major drawback with this alteration of the bolts' diameter is the increased stress concentration in the column web and stiffener and their excessive deformation.

4.5 Models 5 and 6 – Influence of bolt's grade

The investigation made in the previous chapters, has revealed the significant influence of the bolts in the connection's overall response. Models with bolts of 24mm diameter have not affected in a great extend critical parts of the connection such as the column flanges and web that should remain as much as intact as possible for a later connection design along the strong axis. However, their ultimate moment resistance is not as high as the ones with bolts of 30mm diameter that unfortunately affect greatly other parts of the connection. In both cases, bolts are considered the reason of failure. In order to avoid bolts with a greater diameter than 30mm it was decided to alter their grade, not only to improve the joints capacity.

The aim of the two new Models (5,6), is also to examine the bolt grade's influence in the joint's ultimate capacity and failure. For this reason, bolts M30 8.8 were replaced with 10.9 ones, the material law of which (stress-strain curve) has been presented in Figure 29a.

- Model 3/5 comparison (End-plate's thickness 20mm – Bolts M30 8.8/10.9)

From the force-displacement diagram (Figure 57), a similarity can be observed in the two curves, until beam reaches the displacement value of 100mm. From this point the connection of Model 5 seems to increase its capacity and ductility.
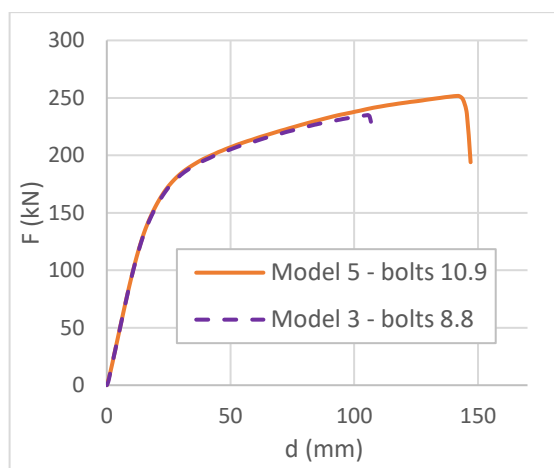

Figure 57. Force-displacement diagram – Model 5-Model 3 comparison – end-plate's thickness 20mm
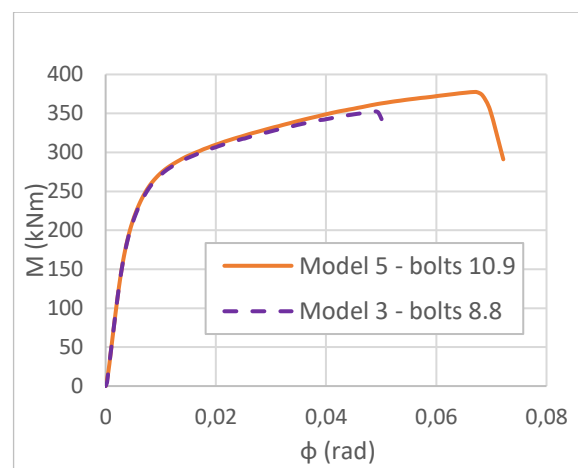
Figure 58. Moment-rotation diagram – Model 5-Model 3 comparison – end-plate's thickness 20mm

54

From the moment-rotation curve (Figure 60) we can obtain the maximum flexural resistance of Model 5 as $M_{j,u5}$=377,40kNm, that gives us an 8,21% increase from the Models 3 moment capacity ($M_{j,u3}$=352,47kNm) and a 44,10% increase in the connection's rotational capacity. From this, it can be concluded that at least for the case of a 20mm end-plate, the alteration of the bolt's grade does not have a major effect in the connection's capacity. This is essential, mainly when a plastic analysis is of concern.

It is now important to observe the stress concentration in Model 5, compared to the one of Model 3 in order to realize the influence of the bolts grade as a parameter. From Figure 59 we can once again observe the heightened stress concentration in the column web as well as the column-stiffener. Figure 60, demonstrates that when the bolt's grade is converted from 8.8 to 10.9, the two later critical component are somehow relieved and stress is expanded clearly in areas like the beam's web and lower flange, the two plates but most importantly in the equivalent T-stub that seems to be highly affected due to this alteration. Of course, this can be partially attributed to the relatively thin end-plate (20mm) and the development of prying forces between the two plates. Finally, Model 5 fails due to the simultaneous bolt rupture and the creation of a plastic hinge in the top part of the end-plate.
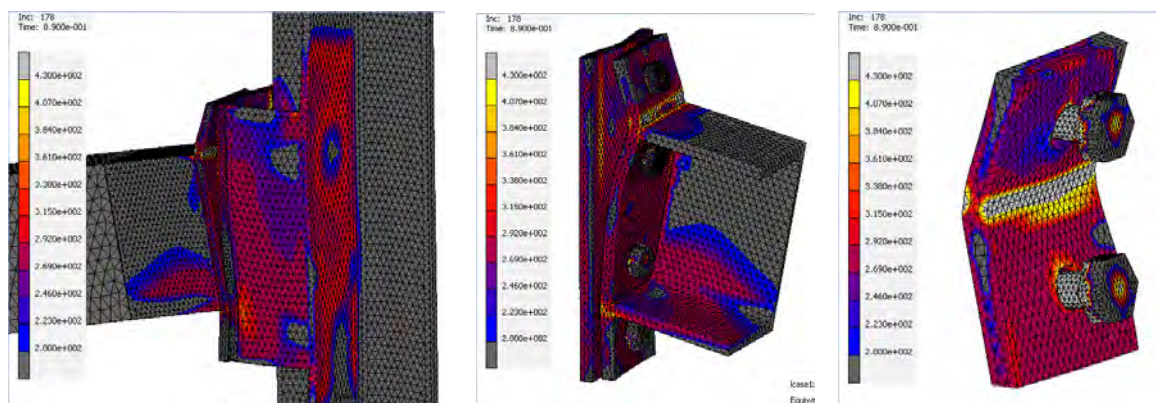

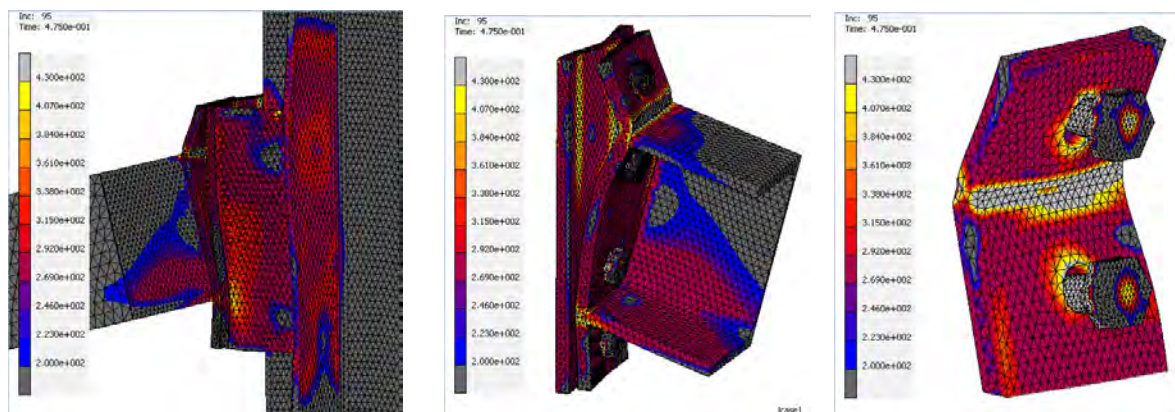*Figure 59. Von Mises stress of Model 3 (bolts 8.8) at $M_{j,u3}$=352,47kNm (x3)*

Figure 60. Von Mises stress of Model 5 (bolts 10.9) at $M_{j,u5}$=377,40kNm (x3)

Regarding Model's 5 behavior comparatively to its previous counterpart, it can be said that bolts 10.9 allowed the connection to relieve the area inside the column. Instead, plastic

55

strains were mainly concentrated at the beam and the T-stub. On the other hand, Model 3 didn't have the opportunity to exhaust in a high level the end-plate due to bending. This is attributed to the relatively weaker bolts. All in all, it should be noted that a major advantage of Model 5 is the column web's low levels of stress and deformation. This would unduly facilitate the design of the second connection in the strong axis of the column.

- Model 4/6 comparison (End-plate's thickness 25mm – Bolts 8.8/10.9)

At this point, a presentation of Model 6 (bolts 10.9) is going to be made and a comparison of its total behavior with its 8.8 bolt grade counterpart. The main characteristic with these two models is that they incorporate a 25mm end-plate.

From the next two diagrams, it can be seen an almost identical behavior until the beam's edge reaches the displacement of 150mm or the connection the rotation of 0,065rad at which point it increases its strength until achieves its ultimate resistance of $M_{j,u6}$=447,69kNm. Considering Model 4's strength at $M_{j,u4}$=419,36kNm we can see a 6,76% increase, which is the smallest from all the previous comparisons. It seems that when the end-plate is rather thick combined with large in diameter bolts (M30), the connection's behavior is barely affected from an alteration in the bolt's grade. However, its ductility in terms of its rotation exhibits a significant increase (53,85%) that undeniably should be taken into account in the design of the connections.
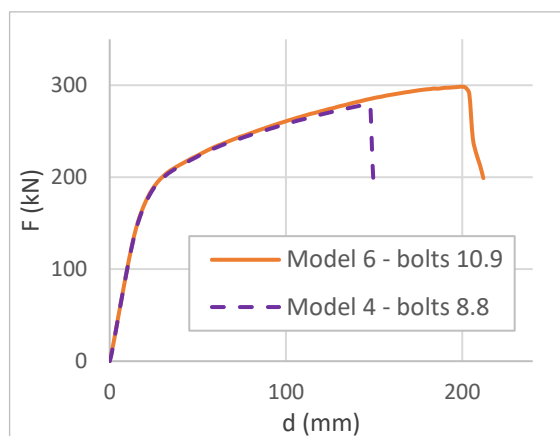

Figure 61. Force-displacement diagram – Model 6-Model 4 comparison – end-plate's thickness 25mm
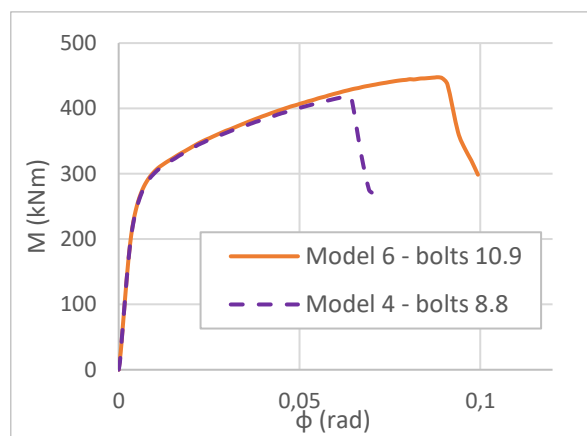
Figure 62. Moment-rotation diagram – Model 6-Model 4 comparison – end-plate's thickness 25mm

Similarly to the previous comparison between Models 3 and 5, we can see that the studied-parameter barely affects the connection's ultimate flexural resistance, the optimization of which is usually the main scope of similar studies. Nevertheless, in order to obtain a clearer image, a comprehensive observation in the connection's condition during the analysis is going to be made in order to establish whether the alteration made, was justified and appropriate and how much has affected the various components.

56

From Figures 63,64, we can first observe the increased stresses in the column flange and the beam. This is something that needs to be avoided and it will be eradicated by strengthening other parts of the connection so that they can receive more of the internal forces. The end-plate, due to its thickness (25mm), does not exhibit an excessive bending like in the case of the 20mm end-plate (Model 5). Instead, the component that undertakes the role of the main stress receiver (except the two plates is the vertical stiffener. It seems that this component which also receives the shear force (created by the tension forces transmitted through the bolts and compression force that passes from the contact between the two plates to the stiffener) needs to be strengthened in order for the connection to be able to perform even better and accept the increased shear. Nevertheless, the failure of the connection comes once again from the inadequacy of the bolts in combination with the plastic hinge in the end-plate and column-attached plate.
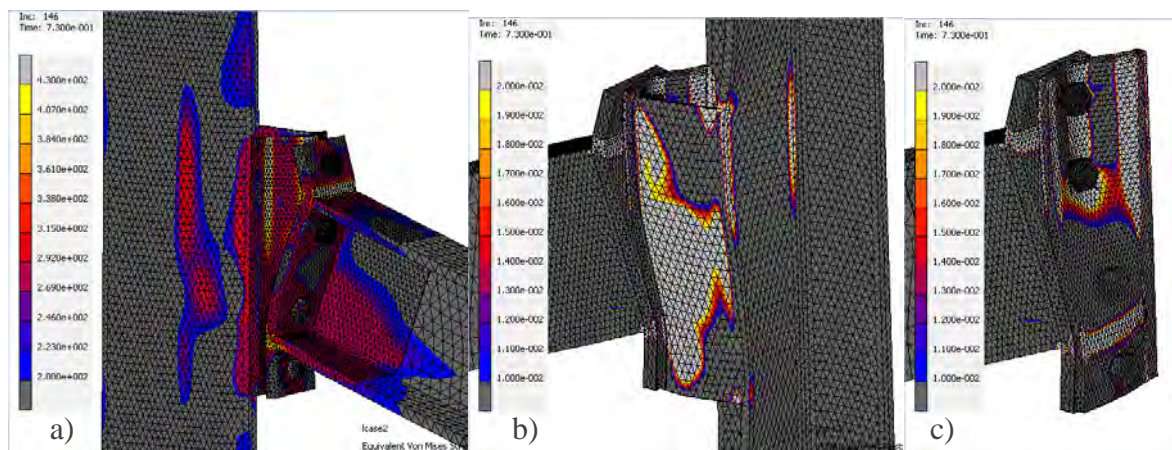

Figure 63. (a) Von Mises stress and (b),(c) equivalent plastic strains of vertical stiffener and column-attached plate (Model 4 bolts 8.8 at $M_{j,u4}$=419,36kNm) (x4)
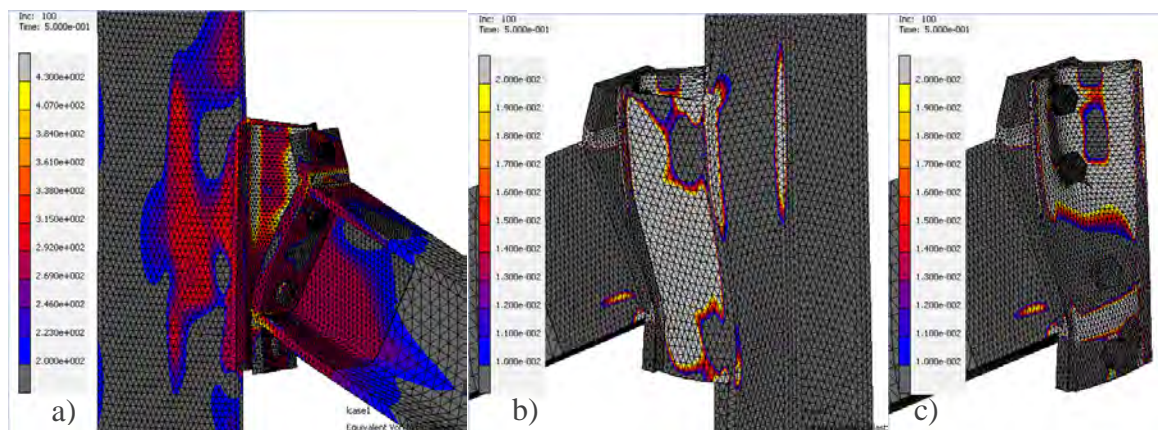
Figure 64. (a) Von Mises stress and (b),(c) equivalent plastic strains of vertical stiffener and column-attached plate (Model 6 bolts 10.9 at $M_{j,u6}$=447,69kNm) (x4)

To sum up, until this part of the investigation, four in total analyses have been performed and presented that have undeniably highlighted the effect of the bolts in the total response of the connections. The bolts diameter was the studied parameter in Models 3 and 4

57

that were then compared with Models 1 and 2 respectively. This comparison showed that the bolts' diameter has a major influence in the overall response due to the fact that bolts were apparently the most critical component. By increasing the bolts diameter, moment capacity was significantly improved. The equivalent T-stub was mainly affected in the part of the end-plate that yielded (especially in the case of a 20mm end-plate) and the main drawback was the development of plastic strains and stresses with increased magnitude in places like the vertical stiffener and the column web. Large and unprecedented displacements were predominantly observed in the column web and stiffener. However, the cause of failure was not altered considerably.

Subsequently, the studied parameter was the bolts grade. This was the case for Models 5 and 6 that were then compared with Models 3 and 4 accordingly. With this alteration, it was clear that the end-plate was largely affected, especially in the second bolt row and a plastic hinge was inevitable. Similarly, the beam's web and lower flange were parts that stress reached very high values something that was observed for the first time. Perhaps the most noticeable differentiation in Models 5 and 6 was the development of large displacements and the excessive bending of the column-attached plate and column web and stiffener. What can be observed especially in Models 4,5,6 is the plastic strains in almost all the body of the vertical stiffener, something that is not appears to happen in the column web despite its large displacements. As it has been discussed in previous chapters, the vertical stiffener acts as a web that the weak-axis connection lacks. Due to that, it plays an imperative role on its overall performance and needs to be strengthened sufficiently.

From Table 8, we can see the final results of the analyses in terms of the Model's moment resistance and the relevant percentage that shows the differentiation with the beam's plastic moment. It can be said that the strongest configurations are the ones that combine a thick end-plate (25mm) with strong bolts. Model 6, performed quite successfully and it is very close to be rendered as full-strength connection. All in all, it can be said that for the Models with a 20mm end-plate the dominant failure mode is the end-plate in bending (equivalent T-stub) with simultaneous rupture of the bolts while in models with a 25mm end-plate, the connections are clearly governed by the failure of the bolts. Nevertheless, in every analysis various components are affected as it has been discussed in the previous sections.

Table 8. Geometry of parameters and response of Models 3-6

	Bolt type	End-plate thickness (mm)	Column-plate thickness(mm)	Column stiffener dimensions (mm)	$M_{j,ui}$ (kNm)	$M_{j,ui}/M_{pl,HEB300}$
Model 3	M30 8.8	20	20	161x500x10	352,47	67,86
Model 4	M30 8.8	25	20	161x500x10	419,36	81,59
Model 5	M30 10.9	20	20	161x500x10	377,40	73,43
Model 6	M30 10.9	25	20	161x500x10	447,69	87,10

58

From all the above, the investigation to be followed is characterized by three new analyses that incorporate a vertical stiffener with dimensions of 161x750x16mm instead of the previous 161x500x10mm. This will theoretically give the connection the advantage of receiving much more effectively the shear force coming from the couple force (tension and compression), increase the flexural resistance of the joint, reduce the excessive rotations and eventually alter the propagation of stresses between the different components.

4.6 Models 7, 8 and 9 – Influence of vertical stiffener's dimensions

In the previous section, the bolt's grade and how it affects the connection's response were discussed. What was essentially revealed, was that it barely alters the joint's maximum capacity but on the other hand it showed that it changed the distribution of the internal forces. The most affected component was the vertical stiffener and column web. However, between those two, only the stiffener developed plastic strains. Due to that and given that the geometry of most of the other parts has been already altered, it was decided to change its thickness and height in order to reduce the stresses and plastic strains. The new thickness of the stiffener is 16mm instead of the previous 10mm and the height 750mm instead of 500mm. This is going to be applied in Models 4,5,6 that will be analyzed once again with this alteration that will theoretically have a significant effect in the overall behavior. It will allow us to examine this parameter's influence in the joint.

- Model 4/7 comparison (stiffener's dimensions 161x500x10 / 161x750x16mm)

The first analyzed model (Model 7) was the one with a 25mm end-plate and M30 bolts of 8.8 grade. From the diagrams in Figures 67,68, a negligible difference can be observed in the two models. More specifically, a mere 2,5% increase in the connection's moment resistance was measured from Model 7's ultimate resistance ($M_{j,u7}$=429,67kNm), that gives a 83,60% percentage compared to the beam's plastic moment (smaller than Model 6's).
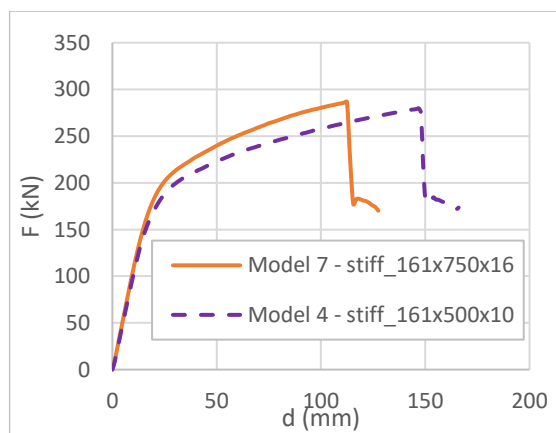

Figure 65. Force-displacement diagram – Model 7-Model 4 comparison – (end-plate 25mm / bolts M30 8.8)
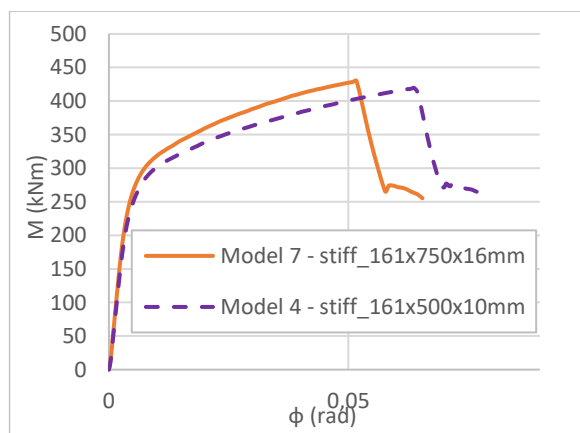
Figure 66. Moment-rotation diagram – Model 7-Model 4 comparison – (end-plate 25mm / bolts M30 8.8)

59

A decrease in the joint's rotational capacity was observed (17,7%). The reduction in the rotation of the joint is apparently attributed to the new stiffener's function that limited the excessive rotation. From the above diagrams, it is clear that the new alteration did not improve the joint's behavior regarding its ultimate moment resistance. However, we shall also observe whether it improved the internal forces state in the crucial components, that is the column web and the vertical stiffener itself. Figures 67,68, demonstrate the enhanced image that we expected firstly at the column web, that has minimized its displacements and plastic strains. The vertical stiffener also exhibits a similar behavior, with small displacements (up to 2,5mm) and almost zero plastic strains. However, both the column web and vertical stiffener receive substantial levels of stress, up to 315kN. A component that is largely affected due to the strengthening of the vertical stiffener, is the column-attached plate that bends around the vertical axis. The connection is finally governed by the rupture of the bolts and once again the studied model incorporates an end-plate with 25mm thickness.

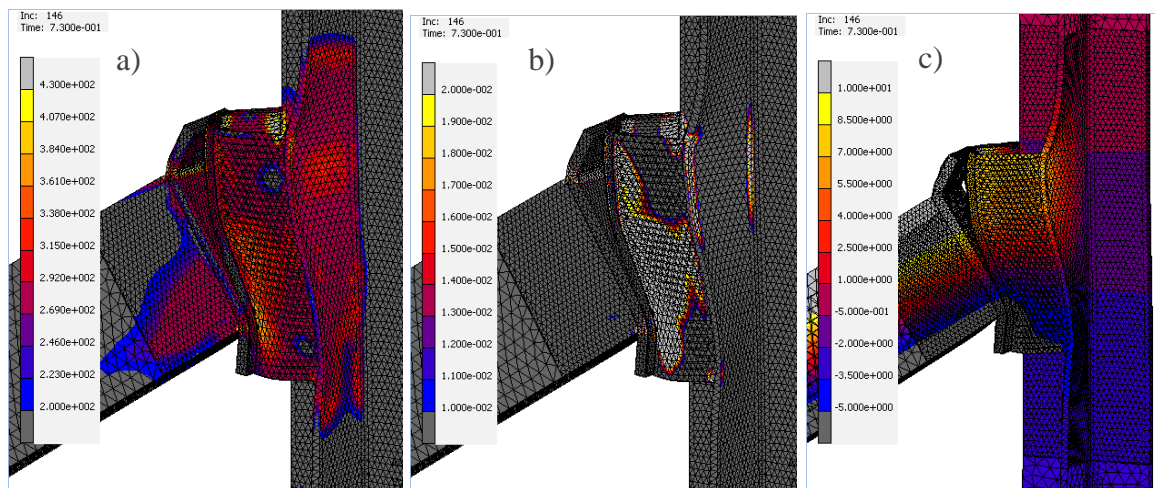*Figure 67. (a) Von Mises stress, (b) equivalent plastic strains and (c) displacements of Model 4 (stiffener 161x500x10mm) at $M_{j,u4}$=419,36kNm (x7)*

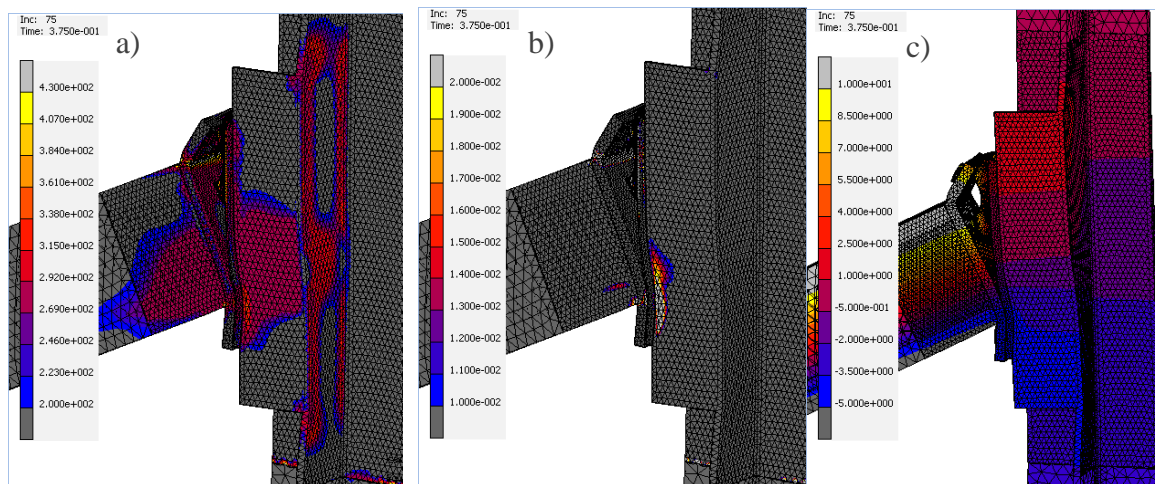*Figure 68. (a) Von Mises stress, (b) equivalent plastic strains and (c) displacements of Model 7 (stiffener 161x750x16mm) at $M_{j,u7}$=429,67kNm (x7)*

60

- Model 5/8 comparison (stiffener's dimensions 161x500x10 / 161x750x16mm)

The two analyzed Models (5 and 8), incorporate a 20mm in thickness end-plate combined with M30 bolts of 10.9 grade. What we expect from this model is once again a significant bend in the end-plate but also an improved condition in the new stiffener and column web. From the observation of the reaction force-displacement and moment-rotation curves (Figures 69,70) we can observe, similarly to the previous comparison between Models 4 and 7, a negligible difference in the connection's ultimate capacity, only 2,2% and a 25% reduction on the joint's maximum rotation. Model 5's flexural resistance has been measured as $M_{j,u5}=377,40kNm$ while Model 8's as $M_{j,u8}=385,82kNm$. Once again this indicates the low effectiveness of the stiffener's geometry as a parameter in the response of the joint. Of course, this happens due to the fact that for the given joint configuration, bolts are the most critical component. However, the fact that the rotation of the joint has been considerably reduced is quite essential and should not be neglected in joint design. Especially for serviceability purposes, it is definitely advantageous for the excessive displacements and rotations to be limited as much as possible.
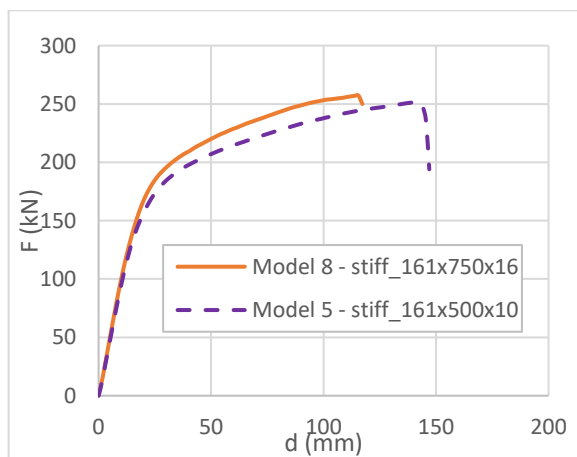

Figure 69. Force-displacement diagram – Model 8-Model 5 comparison – (end-plate 20mm / bolts M30 10.9)
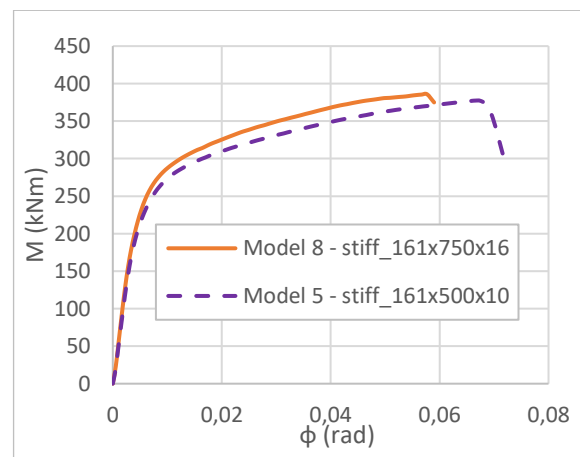

Figure 70. Moment-rotation diagram – Model 8-Model 5 comparison – (end-plate 20mm / bolts M30 10.9)

It is now essential to examine the condition under which the connection of Model 8 has failed and compare it with Model 5's corresponding failure. From Figures 71,72, we can first notice the significant reduction in the deformation of the vertical stiffener and column web. However, the maximum displacement of the beam has not been considerably altered due to the end-plate's ability to bend quite excessively and thus produce a large beam displacement (120mm). Already a major advantage has been achieved that will utterly facilitate the design of a strong connection in the perpendicular axis. A second thing that can be observed, is the lower stress levels in the vertical stiffener. In addition, high stress values in the column web have been limited only in the areas that it is welded to its flanges and to the stiffener. As in the case of the previous comparison, the column-attached plate has been remained rather

61

vertical and has not exhibited a significant bending around the horizontal axis. Nevertheless, it still yields due to bending around the vertical stiffener and seems that needs to be strengthened in the sequel. Finally, plastic strains have been limited only in the two plates and have been almost disappeared from the stiffener and column web. Bolts in the two upper rows exhibit large elongation and reach high levels of stress (up to 1000MPa). The failure of the connection is caused due to the creation of a plastic hinge in the end-plate in combination with bolt rupture.
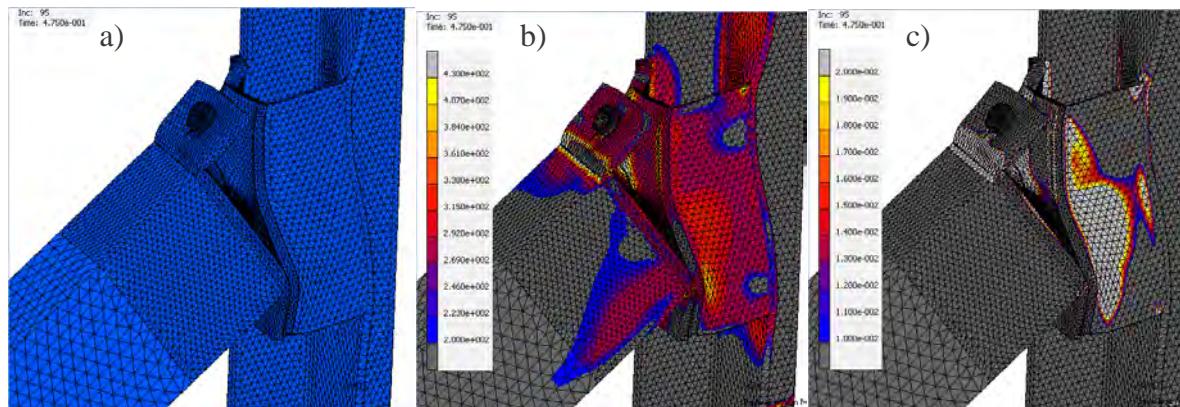

Figure 71. (a) Deformation, (b) Von Mises stress and (c) equivalent plastic strains of Model 5 (stiffener 161x500x10mm) at $M_{j,u5}$=377,40kNm (x8)

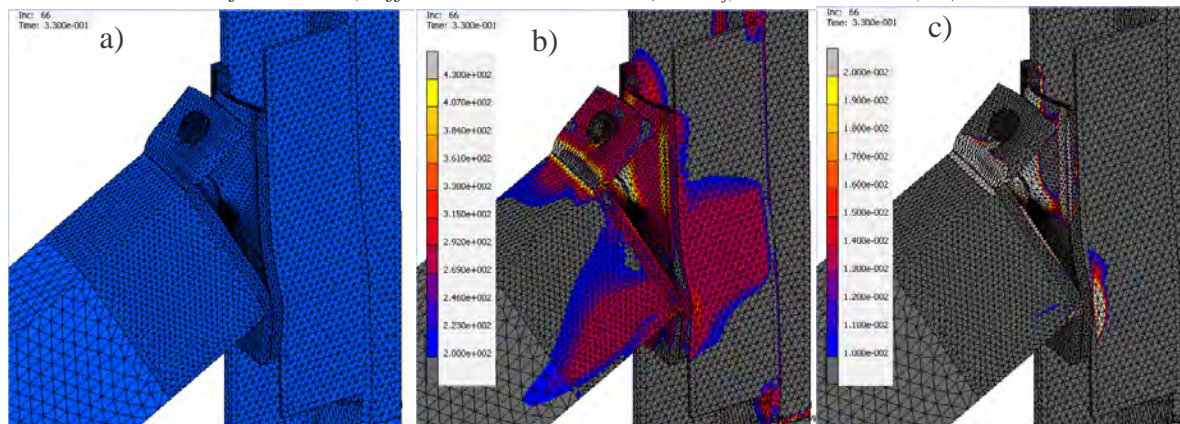*Figure 72. (a) Deformation, (b) Von Mises stress and (c) equivalent plastic strains of Model 8 (stiffener 161x750x16mm) at $M_{j,u8}$=385,82kNm (x8)*

Finally, in order to achieve a more holistic understanding on the influence of the vertical stiffener's geometry a review on Model 9's behavior needs to be made with a relevant comparison to Models 6's results.

- Model 6/9 comparison (stiffener's dimensions 161x500x10 / 161x750x16mm)

The final comparison that is going to be made at this part of the investigation is the one between Models 6 and 9. From this, we will achieve a better understanding in the effectiveness of a strengthened stiffener in the behavior of a rather strong connection (Model 6) that incorporates a thick end-plate (25mm) and strong bolts (M30 10.9). Figures 73,74, demonstrate the behavioral curves that indicate a rather similar behavior between the two models. More specifically, Model 6's resistance ($M_{j,u6}$=447,69kNm), with the new stiffener's

existence has now reached the value of $M_{j,u9}=459,59kNm$ which corresponds to an 89,42% of the beam's plastic moment. Regarding the ultimate moment, there is a 2,7% increase and for the maximum rotational capacity, a 42,86% decrease by comparing the two curves. From the examination made in the two previous comparisons this was quite expected. The connection cannot increase at a great extent its flexural resistance due to the fact the equivalent T-stub remains the critical component. However, it has probably enhanced the performance of the model regarding the plastic strains created previously in areas like the column web and stiffener.
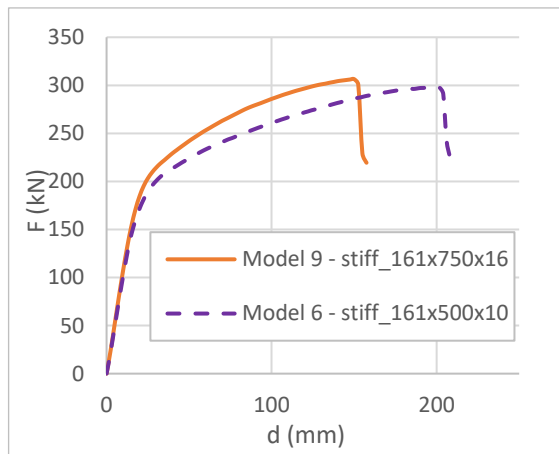

Figure 73. Force-displacement diagram – Model 9-Model 6 comparison – (end-plate 25mm / bolts M30 10.9)
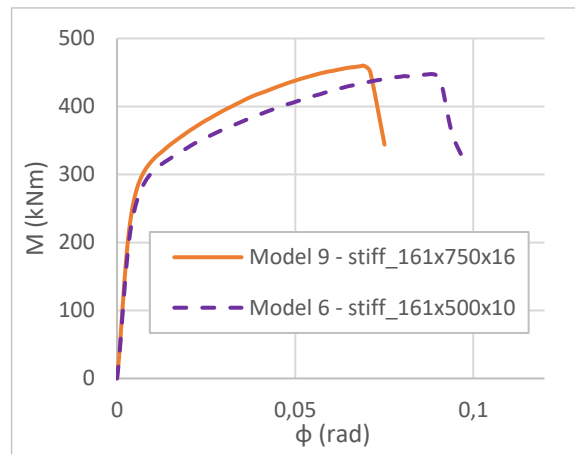
Figure 74. Moment-rotation diagram – Model 9-Model 6 comparison – (end-plate 25mm / bolts M30 10.9)

The first thing that can be noticed from Figures 75,76, is probably the reduced displacements of the beam that obviously stem from the slight rotations that the column web of Model 9 exhibits. For this reason, the height and thickness of the new stiffener can be rendered sufficient enough. By comparing the new model's deformation to the models of the previous comparison (Models 5 and 8), we can observe a reduction in the end-plate's bending that is of course caused by its thickness. However, in the connection there is one mechanical component that appears to be insufficient and be the cause for the small reduction in the beam's ultimate translation from Model 6 to Model 9. This component is the column-attached plate that in Models 5-9 seems to be relatively weak and its thickness will be the studied parameter in the sequel of this chapter.

From the Figures below (75,76), we can see that plastic strains have been limited only in a small part of the vertical stiffener, and have disappear from the column web. If the connection is ever loaded in a high level, it is essential to be able to limit the development of plastic strains in components near or at the column, especially in the case of a seismic load (usually lateral to the connection). In this case, a plastic hinge in the beam, away from the connection would be ideal and would prevent in the relevant frame or structure a lateral collapse. Therefore, the column with its components, should be first protected.
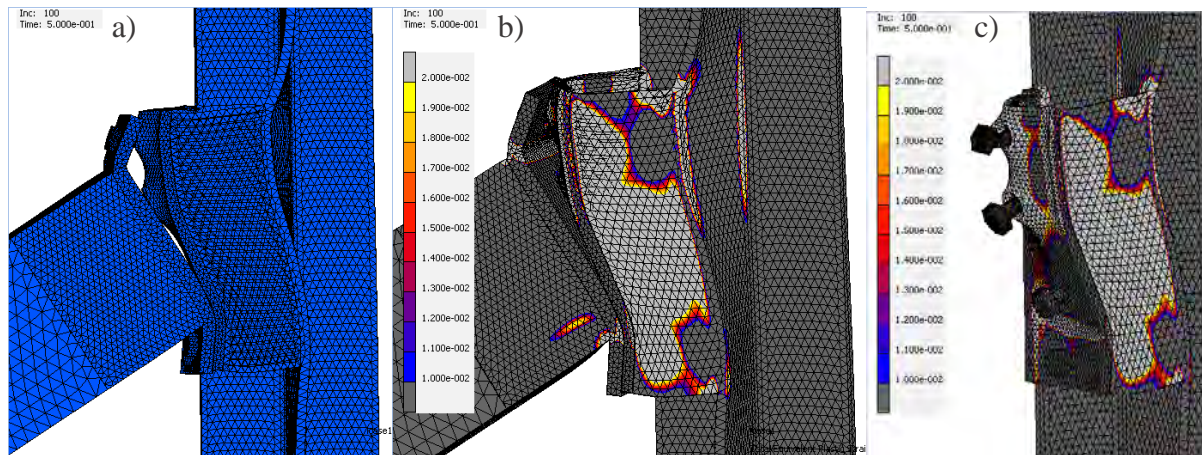
63

*Figure 75. (a) Deformation, and (b),(c) equivalent plastic strains of Model 6
(stiffener 161x500x10mm) at $M_{j,u6}$=447,69kNm (x5)*

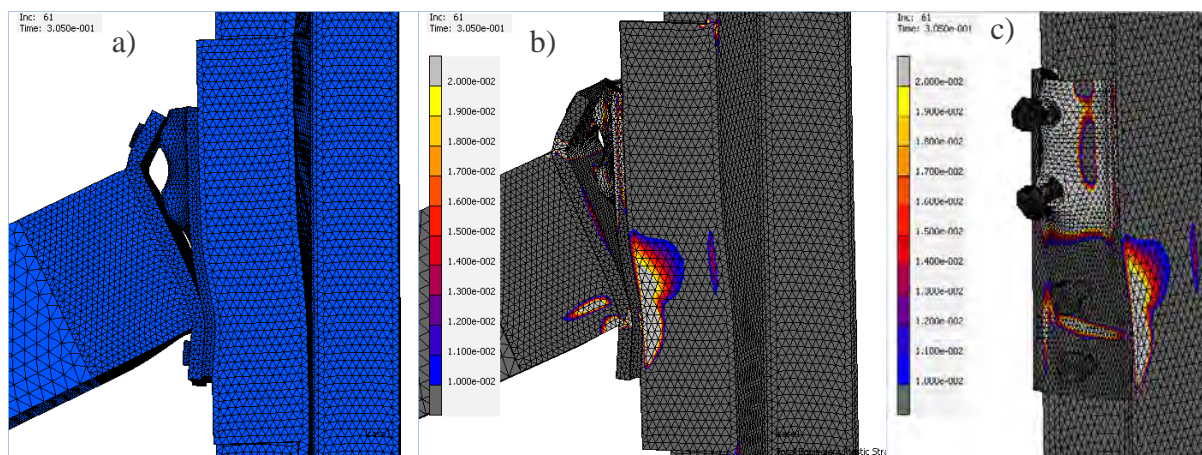*Figure 76. (a) Deformation, and (b),(c) equivalent plastic strains of Model 9
(stiffener 161x500x10mm) at $M_{j,u9}$=459,59kNm (x5)*

4.7 Models 10, 11 and 12 – Influence of column-attached plate's thickness

The presentation made in the previous section with the relevant comparisons, made clear that the vertical stiffener's geometry plays a major role in the distribution of stresses and strains and in the magnitude of deformations particularly in the column web, a highly important component in joint design. Nevertheless, the ultimate capacity of all three models did not have a considerable difference. In addition, the failure modes of the models remained as they were with a failure in the equivalent T-stub and bolts. Finally, the maximum displacement of the beam in all three cases remained relatively large due to the excessive bending of the column-attached plate around the vertical axis.

Before considering improving the equivalent T-stub's performance by strengthening its components (end-plate and bolts), it was decided to examine the behavior of the connection by altering the thickness of the column-attached plate that exhibited significant bending and thus plastic strains in the three previous models (7,8,9). By that, we should comprehend the

64

necessity of the joint regarding this parameter and of course improve its performance during the loading procedure and at failure.

The aim of this section, is to present three new analyzed models that incorporate a column-attached plate of 25mm thickness. The vertical stiffener will remain constant with dimensions 161x750x16mm. The new Models 10,11,12 will be compared with Models 7,8,9 accordingly in order to examine and evaluate this parameter's influence in the response of the connections.

- ### Model 7/10 comparison (Column-attached plate's thickness 20/25mm)

The first presented model of this section is Model 10, and it is compared with the results of the corresponding that includes a 20mm column-attached plate instead of 25mm.

To begin with, Figures 77,78, demonstrate the behavioral curves of the new model with comparison to the previous. It can be noticed, that the general form of the two curves have a discernible difference. Model 10 seems to have failed rather smoothly, in contrast with Model 7's final increment, at which point the connection seems to have failed abruptly. From the previous moment capacity $M_{j,u7}$=429,67kNm, the new configuration led to a slight reduction (0,46%) in the maximum flexural resistance with the value of $M_{j,u10}$=427,69kNm. Given that, it can be said that no improvement was achieved by altering the plate's thickness.

However, something that cannot be neglected is the significant reduction in the joint's rotational capacity. This reduction reached the impressive of value of 91,67%. It is now important, to made a thorough observation of the stresses of the new model in order to understand the second in row component likely to develop plastic strains (after the column-attached plate that has already be strengthened).
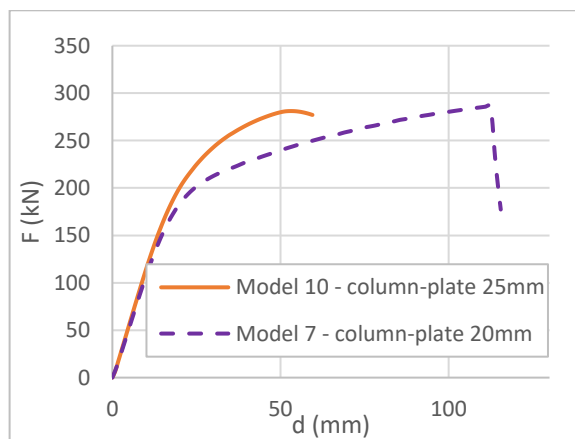

Figure 77. Force-displacement diagram –
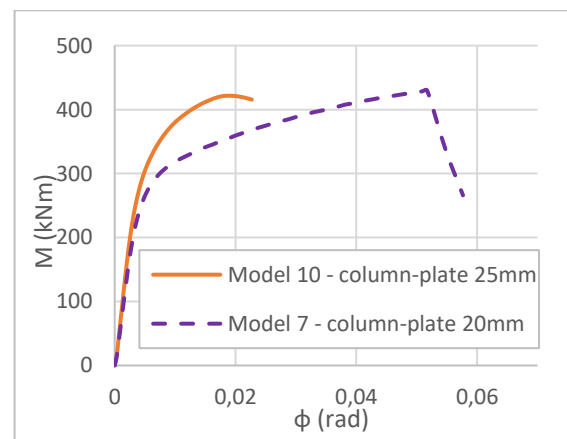Model 10-Model 7 comparison –
(end-plate 25mm / bolts M30 8.8)

Figure 78. Moment-rotation diagram –
Model 10-Model 7 comparison –
(end-plate 25mm / bolts M30 8.8)

By observing Figures 79,80, we can clearly notice the behavioral differentiation of the two models that stem from the alteration made in the column-attached plate's thickness. In

Model 7's Figures, an extreme bending in the studied plate can be seen that ultimately leads to the development of plastic strains in almost every section at its upper part. Due to that, bolts seem to follow this horizontal displacement and therefore exhibit small elongation but on the other hand significant bending due to the deformation of the end-plate. All these, explain why this Model gave a relatively large maximum rotation (at the final increment). It is reminded that the failure of this connection is provoked due to rupture of the bolts in the upper row. When the column-attached plate has been strengthened, it is obvious that its bending has been exceedingly reduced. Only small displacements seem to have been developed and thus the highly stressed zones have been shifted. All these excessive internal forces have been received by the bolts in the two upper rows.
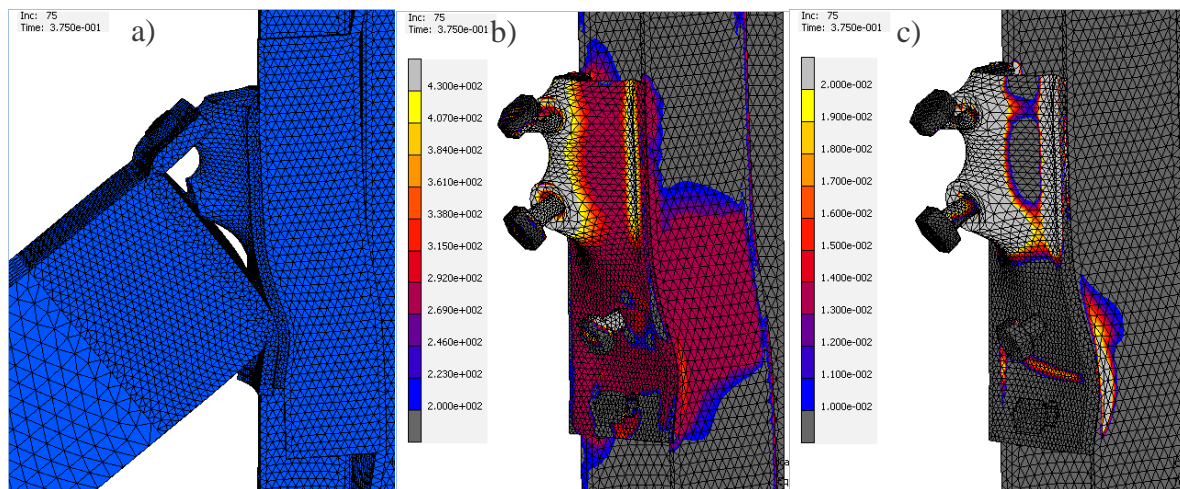
Figure 79. (a) Deformation, (b) Von Mises stress and (c) Equivalent plastic strains of Model 7 (column-attached plate 20mm) at $M_{j,u7}$=429,67kNm (x12)

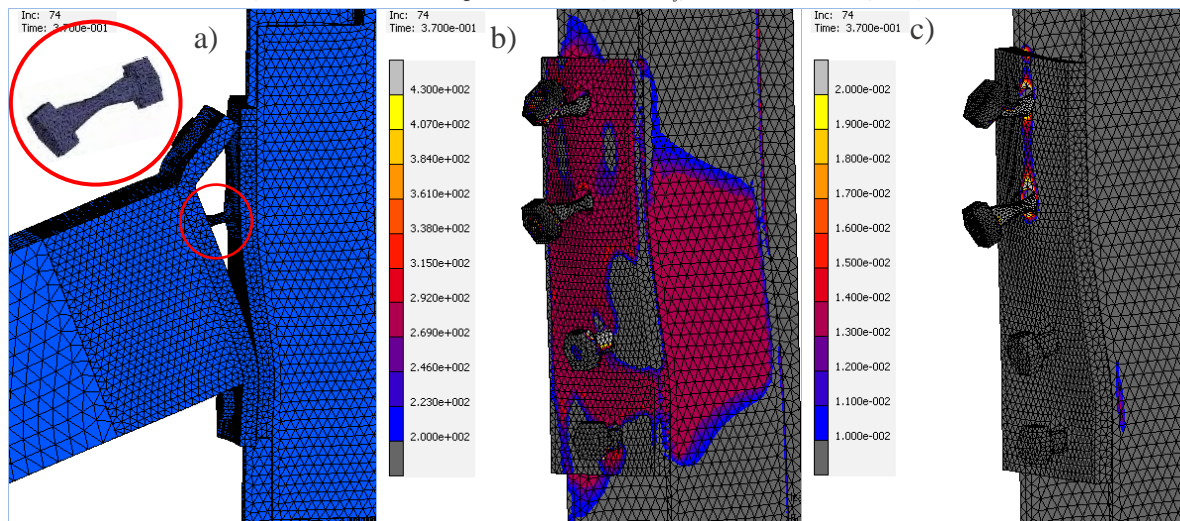*Figure 80. (a) Deformation, (b) Von Mises stress and (c) Equivalent plastic strains of Model 10 (column-attached plate 25mm) at $M_{j,u10}$=427,69kNm (x12)*

This is quite obvious by observing the relevant figures, from which we can see the substantial elongation that cause a relevant tension. However, only the bolts in the second upper row exhibit a pure elongation, in contrast with the upper row's bolts that display an

66

additional bending. Finally, the connection is governed by the rupture of the bolts in the second row as it can graphically be explained in the figures above.

- Model 8/11 comparison (Column-attached plate's thickness 20/25mm)

The previous comparison showed us the significant effect that the alteration of the column-attached plate's thickness had on the distribution of internal forces and finally the failure mode of the connection. The two models to be compared in this subsection, incorporate a 20mm in thickness end-plate and M30 bolts of 10.9 grade. Once again, the effectiveness of the two different thicknesses of the column plates, is going to be examined and evaluated.

By observing Figures 81,82, we can clearly notice that the two curves exhibit a considerable similarity regarding the initial stiffness which is the slope of the linear part of the curves. Model 8's moment resistance ($M_{j,u8}$=385,82kNm) has been slightly increased to $M_{j,u11}$=406,78kNm, which corresponds to a 5,44% percentage. The new flexural resistance also gives a 79,14% regarding the beam's plastic moment. It can be noticed that this percentage is smaller than the relevant of Models 6,7,9,10. This can be attributed to the fact that Models 5,8,11 incorporate a 20mm end-plate, which ultimately and consistently leads to lower levels of maximum resistance of the joint. For all these it can be concluded, that when a 20mm end-plate is included in the joint, the equivalent T-stub instantly becomes a critical part of it (given that bolts are already considered critical) and does not allow a more efficient exploitation of the joint's various components and a more uniform distribution of the internal forces.
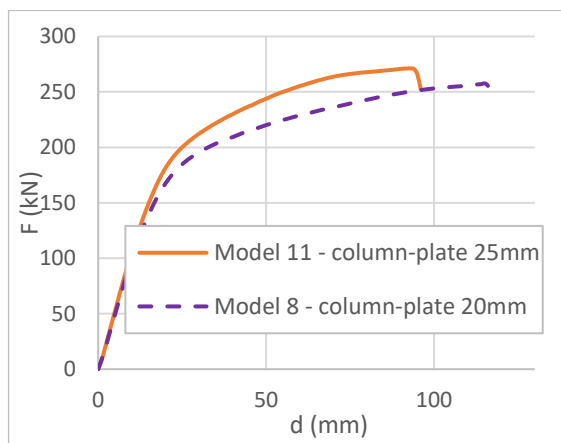
Figure 81. Force-displacement diagram – Model 11-Model 8 comparison – (end-plate 20mm / bolts M30 10.9)

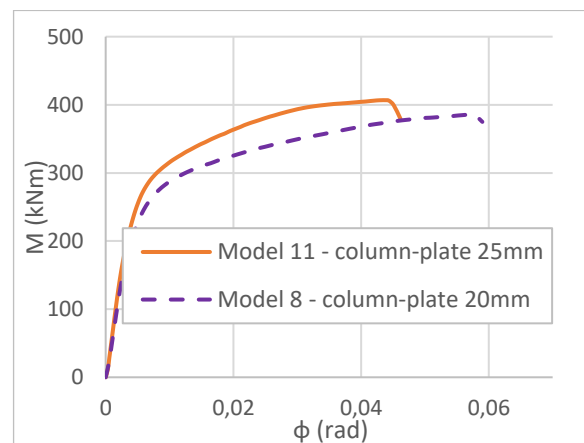*Figure 82. Moment-rotation diagram – Model 11-Model 8 comparison – (end-plate 20mm / bolts M30 10.9)*

Regarding the new Model's plasticity, a 30,43% reduction in the joint's ultimate rotation has been measured. Nevertheless, it can be concluded that a design that incorporates a 20mm end-plate constantly leads to a decreased resistance and a guaranteed failure of the bolts or equivalent T-stub.

67

Until now, an obvious similarity in the two Model's behavior has been observed. However, we should also examine whether this alteration has improved the plastic strains in other parts of the connection. Figures 83,84, demonstrate the Von Mises stresses and equivalent plastic strains of the two plates in the final increment of the analysis (at failure). Perhaps the most noticeable thing is the fact that the column-attached plate of Model 11, has exhibited only a slight deformation in contrast with Model 8's plate that bends excessively around the vertical axis and thus yields quite significantly.

More specifically, in the case of a 20mm column-attached plate (Model 8), we can see that plastic strains arise in both plates, with the biggest magnitude at the end-plate. This leads to an increased rotation of the joint and less elongation in the bolts that follow the displacements of the two plates. One the other hand, when a 25mm column-attached plate is of concern (Model 11), no plastic strains are observed in the plate's most stresses vertical section. Due to the strengthening of the column-plate and the relatively thinner end-plate, the later seems to absorb all the stress from the beam's bending and exhibit a deformation that ultimate leads to the development of a plastic hinge.
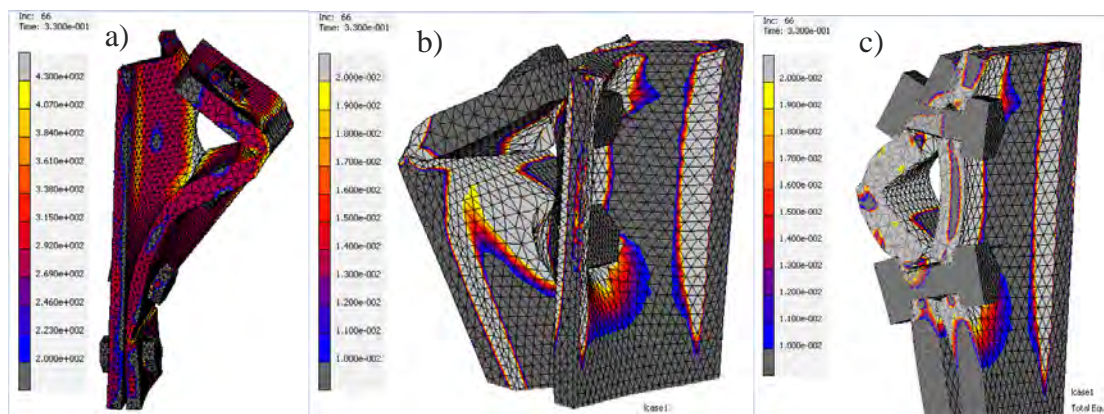

Figure 83. (a) Von Mises stress, and (b), (c), Equivalent plastic strains of Model 8 (column-attached plate 20mm) at $M_{j,u8}=385,82kNm$ (x10)
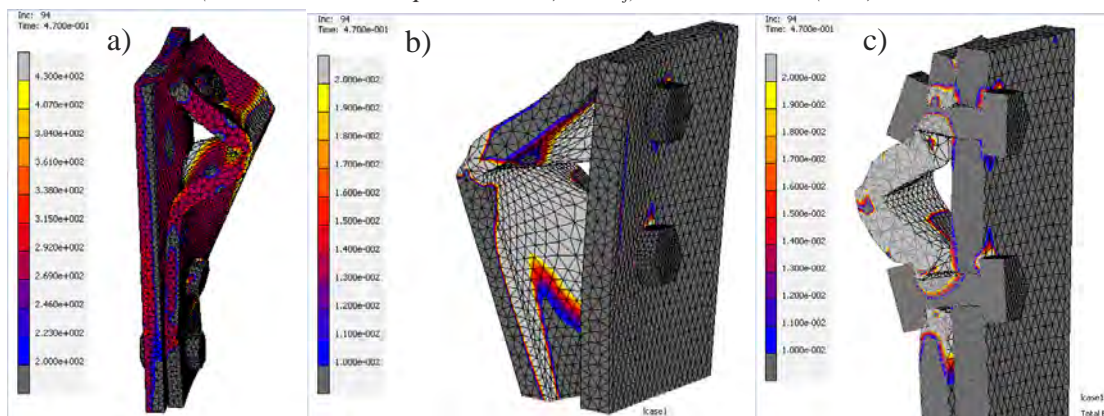

Figure 84. (a) Von Mises stress, and (b), (c), Equivalent plastic strains of Model 11 (column-attached plate 25mm) at $M_{j,u11}=406,78kNm$ (x10)

68

In addition, due to the static mode that the column-plate displays, bolts seem to be elongated and bend around the horizontal axis. It can be concluded though, that the ultimate failure mode of the two Models has not considerably changed. The connection finally fails due to the simultaneous rupture of the bolts in the upper row and the development of a plastic hinge in the end-plate's most stresses section (section between the two upper bolt rows). It should not be neglected that the plastic strains in all other parts of the connection have remained at low levels (<0.5%), and thus the joint design in the column's weak-axis should not impede the strong-axis design. To sum up, a relatively thin end-plate leads to a rather quick failure and impedes the process of a more uniform distribution in other parts of the connection.

- Model 9/12 comparison (Column-attached plate's thickness 20/25mm)

The previous subsection showed that when a 20mm end-plate is incorporated in the Model, the connection exhibits a rather weak response. The alteration of the column-attached plate's thickness induced a different force distribution in the two plates, reduced the joint's maximum rotation but did not increased in a desired level the flexural resistance of the joint.

The final comparison to be presented hereafter concerns Models 9 and 12, that both comprise a 25mm in thickness end-plate and M30 bolts of 10.9 grade. Given the characteristics of Model 12's connection, it is expected to perform well and give a plastic moment ($M_{j,u12}$) very close to the beam's ($M_{pl,EHB300}$).
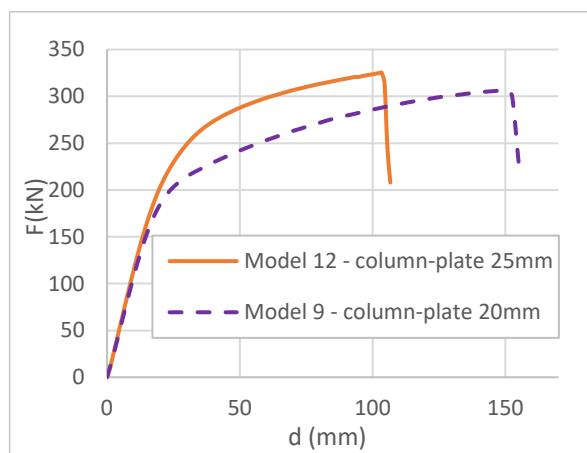
Figure 85. Force-displacement diagram –
Model 12-Model 9 comparison –
(end-plate 25mm / bolts M30 10.9)
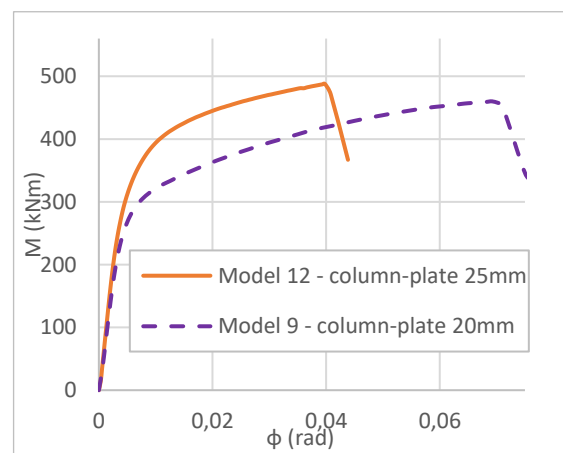
Figure 86. Moment-rotation diagram –
Model 12-Model 9 comparison –
(end-plate 25mm / bolts M30 10.9)

Figures 85,86, show an obvious difference in the two curves that indicate a different behavior from the two models after the linear elastic part. Model 9's moment resistance ($M_{j,u9}$=459,59kNm), has now become $M_{j,u12}$=487,66kNm, which gives a 6,11% increase. The capacity of the new model corresponds to a 94,88% percentage regarding the beam's plastic moment, which renders this connection as the strongest among Models 0-11. A significant

69

difference can be also observed in the two Models rotational behavior. The maximum rotation of Model 12 has been almost decreased in half (43%), which again indicates the strong response that the connection exhibited during the displacement of the beam. In the sequel, a presentation of the model's most stressed regions will be made by emphasizing the cause of failure in order to then try to achieve a full-strength connection.

The Figures below (87,89), clearly demonstrate the tendency of Model 12 to exploit parts of the connection that remained intact in the previous analyses. We can observe a significant part of the beam to develop stresses up to 220-290Kn, as well as the column's stiffener and flanges stresses up to 315Kn. The column-attached plate's bending has been considerably reduced and its plastic strains have remained only in the middle section. It can be concluded therefore, that the new thickness of the plate (25mm) is not completely adequate. However, the most inadequate part of the connection are probably the bolts, especially in the upper row that seem to fail once again.

Figure 87. (a) Von Mises stress, and (b), (c), Equivalent plastic strains of Model 9 (column-attached plate 20mm) at $M_{j,u9}$=459,59kNm (x8)

Figure 88. (a) Von Mises stress, and (b), (c), Equivalent plastic strains of Model 12 (column-attached plate 25mm) at $M_{j,u12}$=487,66kNm (x8)

70

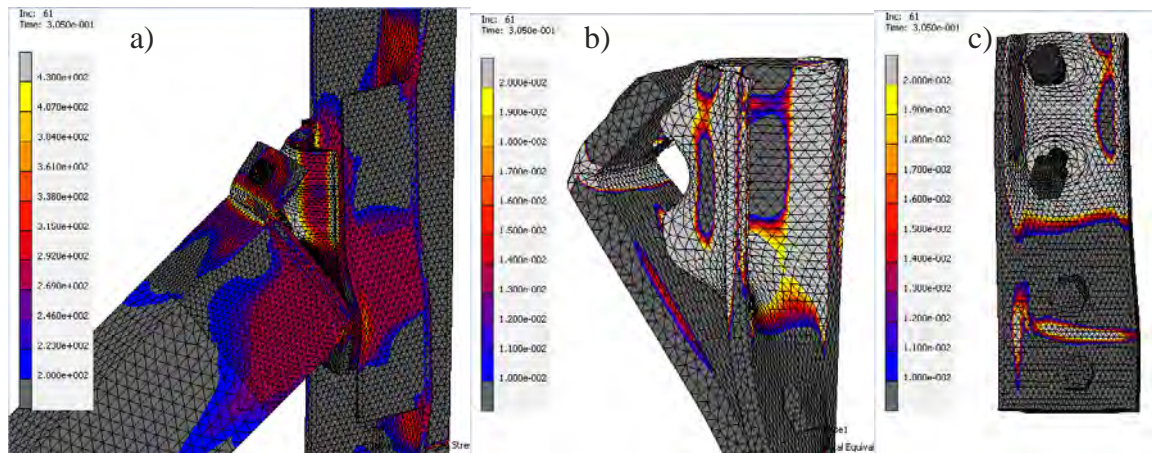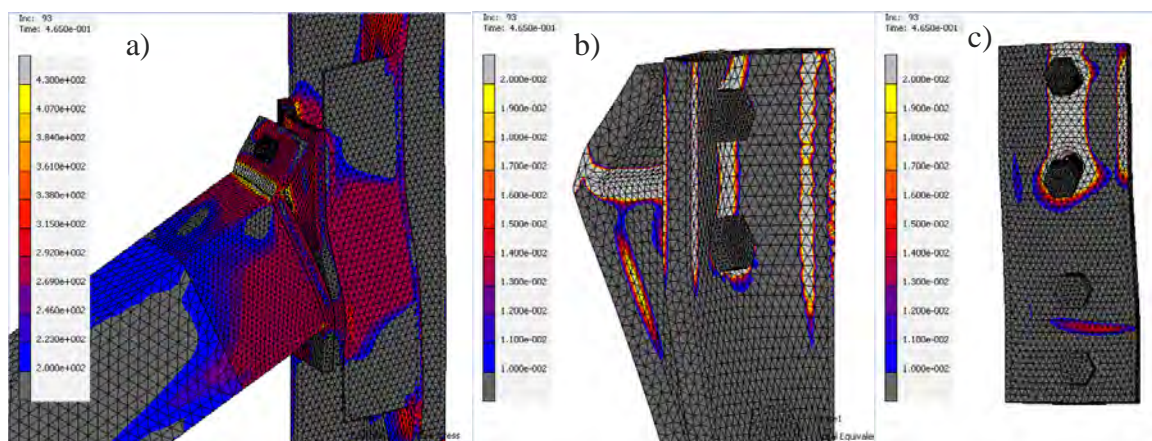To sum up, the six last analyzed Models showed the significant influence of the vertical stiffener and column-attached plate's dimensions in the response of the studied connection. More specifically, the first studied parameter (Models 7,8,9) demonstrated the resulted difference, not in the connection's capacity but rather in the distribution of stresses and the development of plastic strains in the various components. In all three models, the maximum rotation was significantly reduced and the column's web and flange remained almost intact in terms of both strains and displacements. The second studied parameter (Models 10,11,12), showed that again the maximum capacity of the joint was not considerably altered, however the new plate's behavior (column-attached plate), was enhanced at a great extent and thus the internal forces were expanded in the beam. Model 12 in particular, developed a flexural moment resistance of 487,66kNm and thus its connection is considered almost a full-strength one. Table 9 displays Model 7-12 geometric characteristics and final response values with comparison to the beam's strength. What can be noticed, is that when a 20mm end-plate is incorporated in the model, the final strength is relatively low and so is the relevant percentage $M_{j,ui}/M_{pl,HEB300}$.

Table 9. Geometry of parameters and response of Models 7-12

	Bolt type	End-plate thickness (mm)	Column-plate thickness(mm)	Column stiffener dimensions (mm)	$M_{j,ui}$ (kNm)	$M_{j,ui}/$ $M_{pl,HEB300}$
Model 7	M30 8.8	25	20	161x750x16	429,67	83,60
Model 8	M30 10.9	20	20	161x750x16	385,82	75,07
Model 9	M30 10.9	25	20	161x750x16	459,59	89,42
Model 10	M30 8.8	25	25	161x750x16	427,69	83,21
Model 11	M30 10.9	20	25	161x750x16	406,78	79,14
Model 12	M30 10.9	25	25	161x750x16	487,66	94,88

4.8 Model 13 – Achieving a full-strength connection

After thoroughly examining the connection's response by altering five in total of its parameters and exporting notable conclusions, it was considered essential to modify the model in order to produce a full-strength connection. To achieve that, a modification of Model's 12 ($M_{j,u12}$=487,66kNm) geometry was made. The procedure followed, included an identification of the joint's most stresses components whose geometry was then increased accordingly.

The connection of Model 13, incorporates bolts M36 of 10.9 grade. It was considered extremely essential to increase the diameter of the bolts due to the strong influence that this parameter exhibited in the relevant section (4.4). In addition, bolts remained critical in all the analyses and played the role of the weakest component therefore in order to strengthen the

connection's response, bolts' diameter was altered. The second most critical component of the connection during the current investigation was the end-plate in bending. It is undoubtable that a 20mm end-plate was inefficient and a 25mm was still developing significant plastic strains, so in the final model a 32mm in thickness end-plate is going to be integrated. The combination of these new alterations will produce a rather adequate equivalent T-stub. Regarding the column-attached plate and from the last analyses the proven ability of the plate to receive internal forces and not to yield at any point was undeniable therefore this plate will remain to 25mm in thickness. Finally, given that in the last presented model (Model 12), increased stresses were emerging once again in the vertical-stiffener, it is necessary to strengthen it as well, thus its width/height will remain at 161/750mm respectively, whereas its thickness will be increased from 16 to 20mm.

At this point, it is reminded that regarding the finite element model of the connection, the column was divided into three sections. The upper, middle and lower part whose different meshes were then connected using the built-in capability of MSC Marc to connect non-conforming meshes. However, when the new strong model was analyzed, a brittle abruption was detected in these connections. Therefore, in order to avoid this unpleasant result, the column was now modeled as a single uniform component that was then meshed with the use of ten-node isoparametric tetrahedral elements. By that, it was possible to obtain trustworthy results and the realistic failure mode.

The presented curve below (Figure 89), demonstrates the behavior of the final model in terms of the beam's reaction force-displacement and connection's moment-rotation curves. In the second curve, the plastic moment of the beam HEB300 is presented as an upper bound that indicates the strong behavior that the connection exhibited. The flexural capacity of the model was measured as $M_{j,u13}=540,55kNm$, which corresponds to a 105,36% percentage compared to the beam's plastic moment ($M_{pl,HEB300}=513,05kNm$). Due to that, the connection can be rendered as a full-strength one, according the classification of EC3 regarding typical major-axis connections.
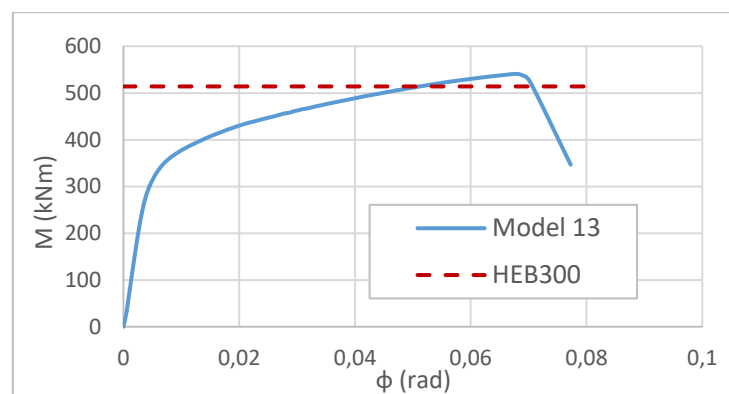

Figure 89. Moment-rotation curve of Model 13 and plastic moment of beam HEB300

From all these, it can be assumed that the distribution of internal forces in the final model will be rather different and a new failure mode might appear. For a better understanding of the connection's response a presentation in several increments of the analysis is going to be presented hereafter by emphasizing the development of plastic strains and highly stressed zones throughout the joint.
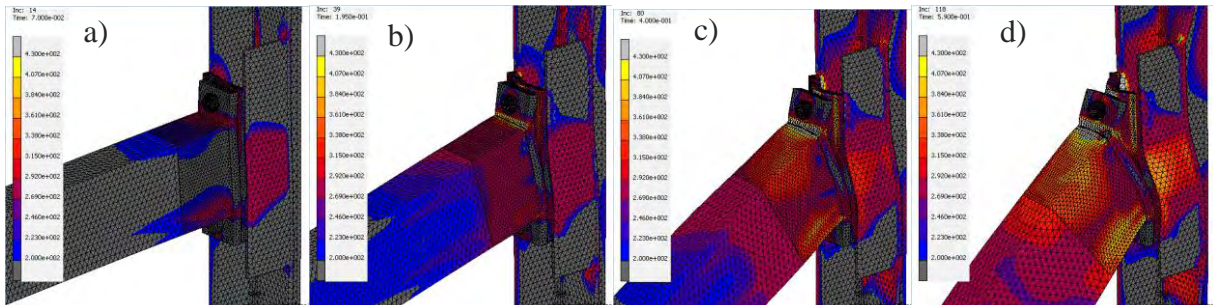

Figure 90. Von Mises stress of Model 13 at a) 12%, b) 33%, c) 67% and d) 100% of the analysis (x5) (maximum stress value-430MPa)

As demonstrated in Figure 90, the connection of Model 13 can be characterized by the development of significant stresses predominantly in the beam. This suggest that the connection itself (plates, bolts, stiffener, column) is adequate enough and the joint needs to exploit the existence of the beam and its ability to bend. At the last increment of the analysis the beam has developed very high stresses that mostly affect its two flanges due to the tension in the upper and compression in the lower zone. Therefore, were an analytical computation of the connection's capacity to be made, based on the component method, the new components that appeared in the analysis, would have to be considered (beam web in tension, beam flange in tension/compression). However, not only the beam receives significant stresses.

It should not be neglected that the resulted flexural resistance of the connection was very close to the beam's plastic moment. Given that, it is obvious that the failure is caused due to a combined rupture of different elements (components) rather than an exclusive beam failure. Were the connection to be strengthened even more, (by increasing the thickness of the plates, stiffener or change the bolt's diameter) and thus exceed considerably the beam's plastic moment, its failure would be probably caused exclusively due to the inadequacy of the connected beam.

Besides the highly stressed response of the beam, it is clear that from an early stage of the analysis the vertical stiffener and plates also develop significant stresses. On the other hand, the column flange as well as the welds between the column and its flanges start to be deformed and thus approximate and consequently exceed the yield stress. Finally, bolts seem to have played an imperative role during the analysis and exhibited sufficient endurance (since the tension is now causing significant issues to the beam and not only to the bolts).

73

Hereafter, the equivalent plastic strains are presented (Figure 91), in three increments of the analysis (33%, 67% and 100%). The development of strains initiates in the beam's upper and lower part as well as the middle part of the vertical stiffener. During the analysis, strains seem to be propagated predominantly at the beam and at the final increment, several sections of the beam have been completely yield, at which point the connection fails. However, the cause of failure is attributed both to the development of plastic hinge in the beam and the rupture of the bolts in the upper row.
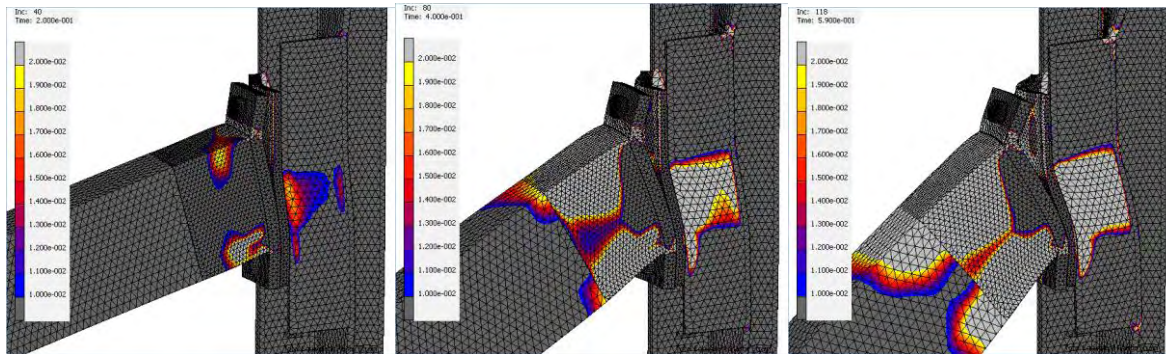
Figure 91. Equivalent plastic strains of Model 13 at a) 33%, b) 67% and c) 100% of the analysis (x5) (maximum strain value 2%)

Finally, in Figure 92 we can clearly observe the development of plastic strains in the end-plate and column-attached plate at the final increment of the analysis. Despite the alteration made in these plate's dimensions they are still develop significant plastic strains due to their bending. What is also considered essential to be noted is that the beam's lower flange due to the excessive amount of compression that receives, seems to almost buckle. For this reason, it is imperative to pay much attention in the selection of a beam with adequate thickness of flanges and web in order to avoid such unpleasant buckling effects.
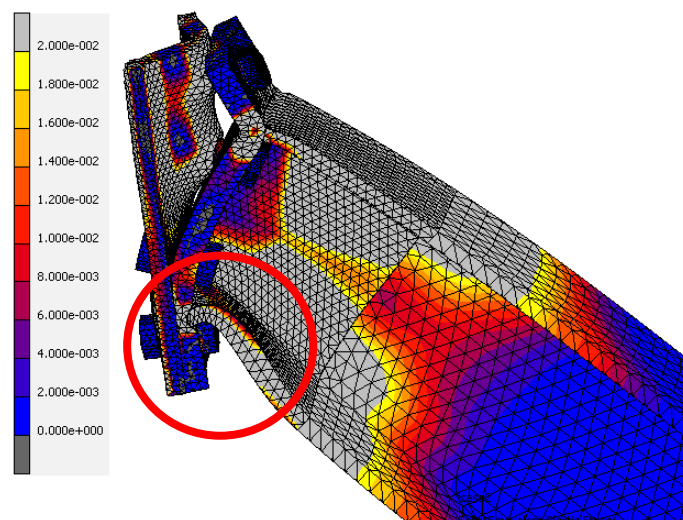
Figure 92. Equivalent plastic strains of the two plates and beam at final increment (x5) (maximum strain value 2%)

74

Therefore, it is clearly demonstrated, that the use of such sophisticated numerical models can ultimately reveal the connection's different phenomena that may arise, such as non-linear effects (buckling). However, as it has been discussed in Section 3.2.3, the computational cost and the time-consuming parameters must be taken into consideration as well.

4.9 Overall comparison

The investigation made in Chapter 4, aimed at understanding the behavior of the under-study weak-axis connection by means of numerical models from a parametric analysis. The analysis was focused in the study of five in total parameters. Each of the tested models exhibited a unique behavior which can be characterized by a moment resistance, a stiffness or rigidity and a rotational capacity. However, when a plastic analysis is of concern, the most important value to be calculated is the moment capacity. In Table 10, a presentation of all the analyzed models is being made, that highlights the procedure followed in order to achieve a full-strength connection which is occasionally the main case study in joint design.

Table 10. Geometric details and response of Models 0-13 - Overall comparison

	Bolt type	End-plate thickness (mm)	Column-plate thickness(mm)	Column stiffener dimensions (mm)	M_{jRd} (kNm)	$M_{jRd}/M_{pl,HEB300}$ (%)
Model 0	M24 8.8	20	20	-	226.66	44.10
Model 1	M24 8.8	20	20	161x500x10	273.04	53.12
Model 2	M24 8.8	25	20	161x500x10	312.46	60.79
Model 3	M30 8.8	20	20	161x500x10	348.77	67.86
Model 4	M30 8.8	25	20	161x500x10	419.36	81.59
Model 5	M30 10.9	20	20	161x500x10	377.40	73.43
Model 6	M30 10.9	25	20	161x500x10	447.69	87.10
Model 7	M30 8.8	25	20	161x750x16	429.67	83.60
Model 8	M30 10.9	20	20	161x750x16	385.82	75.07
Model 9	M30 10.9	25	20	161x750x16	459.59	89.42
Model 10	M30 8.8	25	25	161x750x16	427.69	83.21
Model 11	M30 10.9	20	25	161x750x16	406.78	79.14
Model 12	M30 10.9	25	25	161x750x16	487.66	94.88
Model 13	M36 10.9	32	25	161x750x20	540.55	105.17

From the Table above, we can observe several things. First and foremost, it is clear that the use of a vertical stiffener is highly essential as it increases the moment resistance by almost 10% and at the same time it impedes the development of plastic strains and ultimately the abruption of the column-attached plate that is welded to the column's two flanges.

75

Furthermore, one can notice that the biggest amplification in the connection's capacity was when M30 bolts were used, instead of M24. On the other hand, parameters such the thickness of the column-attached plate and thickness/height of the vertical stiffener gave an increase up to 5%. This showed us how critical the components "end-plate in bending" and "bolts in tension and bending" were in the failure mode of the connection. Finally, Model 13 gave a moment resistance 5,36% larger than the beam's plastic moment, therefore the connection can be rendered as a full-strength one. From the discussion made on this model it was emphasized that the use of the high-order elements in the numerical model, even though increased significantly the analysis time, made the identification of buckling effects in the beam's flange possible, something that should not be neglected.

Nevertheless, a more thorough understanding in the connections' overall performance can only be achieved by observing their moment-rotation curves, so that additional values such as their stiffness and rotation can be revealed. Figure 93, demonstrates the moment-rotation curves of Models 0-6 with an upper value that corresponds to the beam's plastic moment. From this Figure, one can observe the significant increase in the rotational stiffness, when the vertical-stiffener is incorporated in the models. Furthermore, regarding the connection's rotational performance, it can be noticed that Models 0,4,5,6 exhibit substantial rotation. This can be attributed either in the absence of the vertical stiffener that causes the column-attached plate and thus the beam to be displaced substantially or the excessive rigidity of the connection due to the existence of a thick end-plate (25mm) combined with strong bolts (M30 8.8 or 10.9).
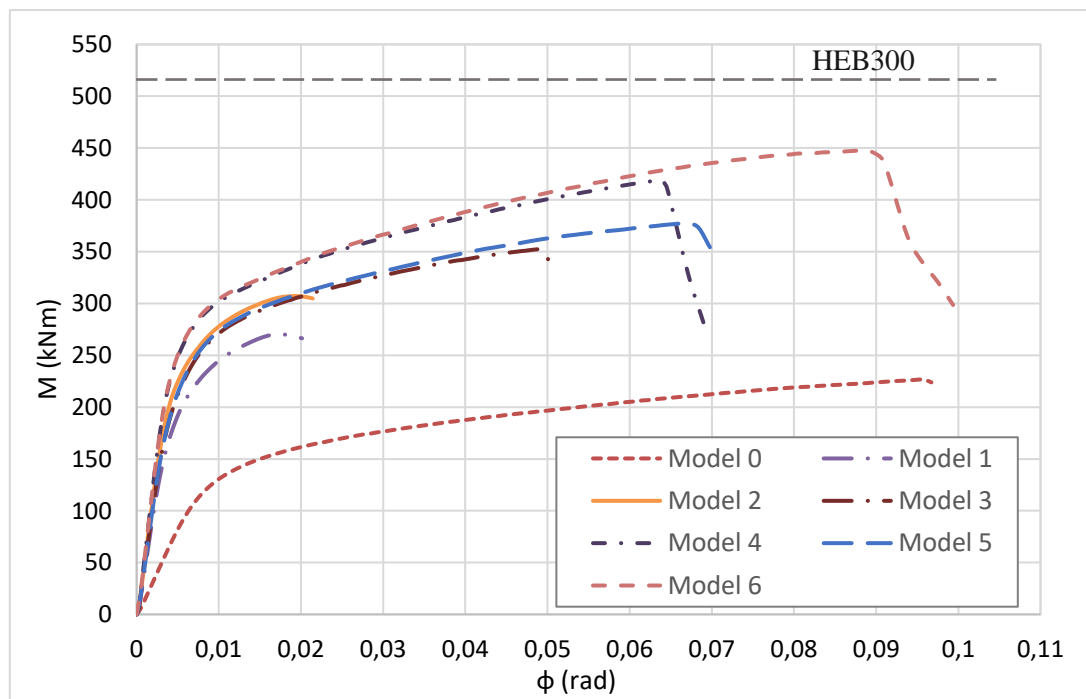

Figure 93. Moment-rotation curves of Models 0-6

76

The performance of the rest of the models, along with the additional plastic moment of the beam are presented in Figure 94. The numerical results of this second group of models show an obvious enhancement in their performance compared to the previous group. One can observe the significant rotational stiffness that these models exhibit and their convergence in the elastic field of the curves. In addition, the three models that stand out regarding their maximum moment resistance are ones that incorporate a column-attached plate with 25mm thickness or both thick end-plates combined. Regarding the ultimate rotational capacity, Models 9 and 13 develop significant rotations at failure, approximately 0,07rad ($\approx$ 4 degrees). An additional characteristic of these curves is their somewhat sheer drop at failure that is apparently attributed to the rupture of the bolts in the upper row that was the most prevalent cause of failure.
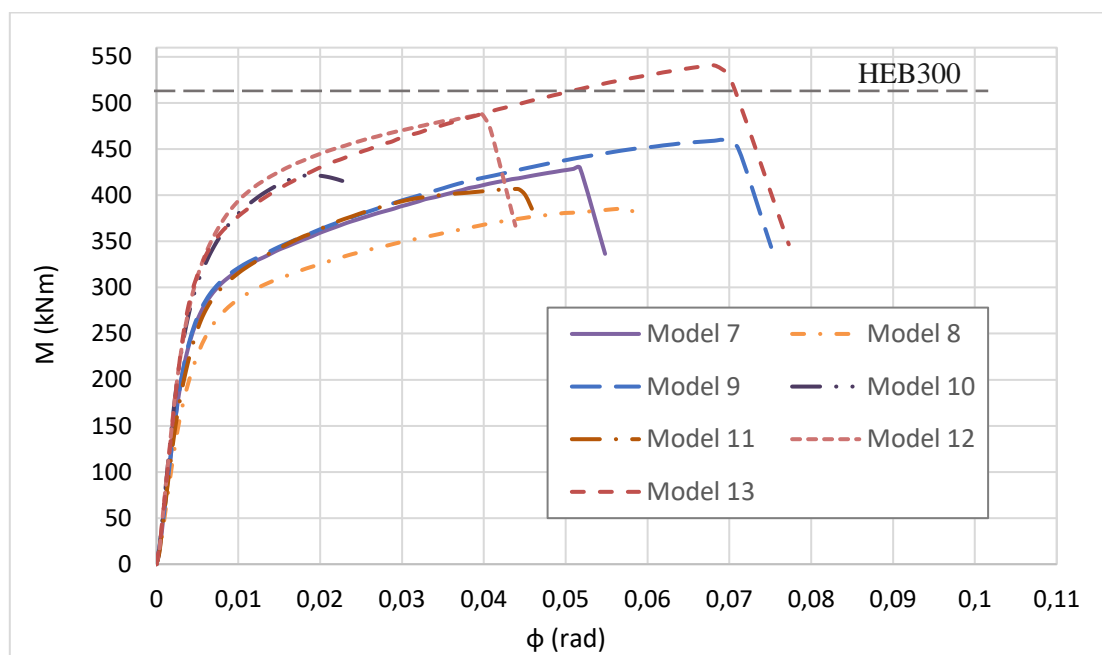
Figure 94. Moment-rotation curves of Models 7-13

Finally, the performance of Model 13's connection renders it as a full-strength one, since its ultimate flexural resistance exceeds the plastic moment of the beam. Nevertheless, this classification concerns solely strong-axis connections, according to EC3, that as it has been discussed in previous chapter has not yet included a design procedure for their weak-axis counterparts. Such connections are predominantly chosen when a plastic hinge in the beam is preferred rather than a failure inside the region of the connection. This ultimately, protects the relevant frame in which the connection is embedded, thus the structure, from a lateral collapse.

77

5. CONCLUSIONS AND SUGGESTIONS

The aim of this thesis was to examine a bolted connection in the weak-axis of the column by means of numerical models. Due to the lack of guidance in the relevant part of EC3 regarding their design as well as the limited literature on the topic a finite element analysis is essential in order to thoroughly comprehend the connection's actual performance. The main concern was to obtain the highly essential moment-rotation curves that uncover their rotational response. A parametric analysis was completed that revealed the connection's critical components and its various failure modes. In addition, an emphasis was given in the perseverance of the column's initial condition in order to facilitate a second connection design in the strong-axis.

A finite element analysis of joints offers the possibility to simulate their actual behavior with good accuracy as it has been proven from various studies that showed a very good agreement with relevant experiment results. The current investigation, demonstrated that a parametric analysis of a connection by means of numerical models is feasible although difficult to be applied in every day practice. A clever exploitation of the model's possible simplifications is of essence if an optimization of the problem is of concern.

In the current investigation, the symmetry of the problem resulted in ultimately analyzing only half of the model, which curtailed dramatically the computational time. At this point, much attention needs to be given in the application of the boundary conditions to accurately simulate the actual degrees of freedom. Another fact that was already known prior to the investigation was that significant stresses and plastic strains would appear solely in the connection zone rather than the entire model. Due to that, high-order elements were only used in this zone and thus an additional reduction of the analysis time and data results that needed to be post-processed, was once again achieved. Nevertheless, given the excessive need of several components to be modelled accurately due to their substantial deformation during the analysis, a highly dense discretization couldn't be avoided that contrariwise increased the computational time. Furthermore, the curves in the bolt-holes of the plates demanded an even denser grid. Therefore, the final selection of the elements' order and grid density should be done wisely by considering all the aspects of the problem at hand. Finally, the accurate representation of the non-linear material curves (constitutive relationships), is essential for the development of a trustworthy model, thus a thorough literature review to obtain the appropriate curves is imperative.

Regarding the results of the investigation, it is obvious that the proposed configuration can be characterized by several advantages. First and foremost, by connecting the beam to the column flanges by means of two end-plates, instead of directly connecting it to the column web, an enhancement in the overall behavior and a more efficient exploitation of the components is achieved. Not only the out-of-plane deformation of the column web that causes

78

the development of significant plastic strains is avoided, but also a utilization of the column flanges that now bend along their strong-axis, is achieved. By retaining the column's web intact throughout the analysis, we facilitate a possible design in the strong-axis of the column, as the component "column web in shear" is normally a critical one. In addition, the construction of this second connection in the strong-axis becomes much more convenient, as the two designs do not hinder with each other. A second, and perhaps more important finding, as it is the novel contribution of this thesis, is the imperativeness in the use of the vertical stiffener, especially in joints with column sections of significant heights. Were this stiffener not to be used in the model, large displacements of the components and excessive bending of the column-attached plate around the vertical axis and thus substantial plastic strains in the welds between the column-flanges and plate would appear. In addition, the use of the stiffener resulted in a substantial increase in the connection's rotational stiffness. Given that a connection in the weak-axis of a column lacks the important existence of a web, the stiffener essentially acts like a web and receives a significant amount of the shear force.

However, it is essential to address that the use of the proposed configuration demands highly strong welds in the connection between the column flanges and its attached-plate. The use of simple fillet welds, seemed to be inadequate as it resulted into local plasticity at this zone and caused and early failure of the connection without allowing it to utilize its several components. Instead, the use of full penetration welds was proven to be highly effective and led to a more uniform distribution of the internal forces. In general, this last finding is also consistent with previous research on a similar configuration.

As far as the specific geometry of sections and components that was analyzed is of concern, the parametric analysis showed that Models 0-12, exhibited a partially-strength behavior. The prevailing failure mode of the models was the one due to the rupture of the bolts in the upper row. However, not only bolts, but also the equivalent T-stub formed by the end-plate and beam's upper flange seemed to be critical as well. Especially in cases were the model incorporated a 20mm in thickness end-plate, the failure of the connection was rather early and this can be partially attributed to the development of prying forces between the two plates, that stressed additionally the bolts. When bolts are designed stronger, stress is mainly concentrated on the plates and vertical stiffener. By increasing the stiffener's height and thickness, plastic strains are then observed in the column-attached plate and stress is once again shifted to the bolts and the beam end-plate. It can be concluded that the critical components by which such connection can be designed are the bolts in the upper row in tension and the equivalent T-stub in bending formed by the beam and its attached end-plate. For this reason and a when a high moment capacity connection is needed, attention should be given to these components. Finally, through Model 13, one can observe the ability of the proposed configuration to realize a full-strength connection.

At this point, I would like to address some future research suggestions that were mainly arisen out of the limitations that I have identified during my research on the topic. Since the calculation of a connection's most essential features (moment-capacity, rotational stiffness and capacity) by means of numerical models is highly time-consuming, perhaps a similar procedure followed in the design of strong-axis connections is needed. However, only few studies have developed mechanical models for the calculation of the stiffness, rotational capacity, ultimate load and failure mode for the new components that appear in such connections (e.g. the so-called E-stub that appears in 3-D joints). If more studies were to be performed, EC3 part 1.8, would expand its design guideline to include weak-axis connections as well. In addition, given that in the current investigation, a single connection was analyzed and evaluated, a study that includes both strong and weak-axis connections in corner and internal joints is essential in order to examine the coupling effects and behavioral differentiations of the weak-axis connection when the strong one is subjected to various levels of loading and vice versa. Finally, it would be interesting to examine the behavior of the studied joint in the presence of a constant compressive load in the column which is the main column load in structural frames.

80

REFERENCES

[1] CEN, Eurocode 3: Design of steel structures, Part 1.8: Design of joints. EN-1993-1-8. Brussels: European Committee for Standardization; 2005.

[2] Gomes FCT, Jaspart J. P, Maquoi R.: Moment capacity of beam-to-column minor-axis joints. In: Proceedings of the IABSE international colloquium on semi-rigid structural connections. Istanbul (Turkey): IABSE; 1996. pp. 319–26.

[3] J. P. Jaspart, Recent advances in the field of steel joints — Column bases and further configurations for beam-to-column joints and beam splices, Professorship Thesis, Department MSM, University of Liege, Belgium, 1997

[4] D. A. Nethercot, T. Q. Li and B. Ahmed (1998): Unified Classification System for Beam-to-Column Connections, *Journal of Constructional Steel Research,* Vol. 45, No. 1, pp. 39-65.

[5] C. Faella, V. Piluso, G. Rizzano : Structural Steel Semirigid Connections. Theory, Design and Software, CRC Press, Bica Reton, FL, 2000 (ISBN: 0-8493-7433-2).

[6] Frye, M.J. and Morris, G.A. (1975): Analysis of Flexible Connected Steel Frames, *Canadian Journal of Civil Engineering,* Vol. 2, pp. 280-291.

[7] Krishnamurthy, N., Huang, H., Jeffrey, P.K. and Avery, L.K. (1979): Analytical *M-φ* Curves for End-Plate Connections, *Journal of the Structural Division,* ASCE, January, Vol. 105, pp. 133-145.

[8] Kukreti, A.R., Murray, J.M. and Abolmaali, A. (1987): End Plate Connection Moment-Rotation Relationship, *Journal of Constructional Steel Research,* Vol. 8, pp. 137-157.

[9] Faella C., Piluso V., and Rizzano G. (1997): A new Method to Design Extended End Plate Connections and Semirigid Braced Frames, *Journal of Constructional Steel Research*, Vol. 41, No.1, pp. 61-91.

[10] Chen, W.F., Kishi, N., Matsuoka, K.G. and Nomachi, S.G. (1988a): Moment Rotation Relationship of Top and Seat Angle with Double Web Angle Connections, in *Connections in Steel Structures: Behavior, Strength and Design,* Elsevier Applied Science, London.

[11] Chen, W.F., Kishi, N., Matsuoka, K.G. and Nomachi, S.G. (1988a): Moment Rotation Relationship of Single/Double Webuble Web Angle Connections, in *Connections in Steel Structures: Behavior, Strength and Design,* Elsevier Applied Science, London.

[12] Yee, K.L. and Melchers, R.E. (1986): Moment-Rotation Curves for Bolted Connections, *Journal of Structural Engineering,* ASCE, Vol. 112, pp. 615-635

[13] Wales, M.W. and Rossow, E.C. (1983): Coupled Moment-Axial Force Behavior in Bolted Joints, *Journal of Structural Engineering,* ASCE, Vol. 129, pp. 1250-1266.

[14] Chmielowiec, M. and Richard, R.M. (1987): Moment Rotation Curves for Partially Restrained Steel Connections, Report to AISC, University of Arizona, p. 127.

[15] Tschemmernegg, F. and Humer, C. (1988): The Design of Structural Steel Frames under Consideration of the Non-linear Behavior of Joints, *Journal of Constructional Steel Research,* Vol. 11, pp. 73-103.

[16] Bose SK, McNeice GM, Sherbourne AN. Column webs in steel beam to column connections. Part I: formulation and verification. *Computers Structures* 1972;2: 253–72.

81

[17] Krishnamurthy N, Graddy DE. Correlation between 2- and 3-dimensional finite element analysis of steel bolted end-plate connections. *Computers Structures* 1976;6(4–5):381–9.

[18] Sherbourne AN, Bahaari MR. 3D simulation of end-plate bolted connections. *J Struct Eng* 1996;120(11):3122–36.

[19] Bursi OS, Jaspart JP. Benchmarks for finite element modeling of bolted steel connections. *Journal of Constructional Steel Research* 1997;43:17–42.

[20] Bursi OS, Jaspart JP. Calibration of a finite element model for isolated bolted end plate steel connections. *Journal of Constructional Steel Researc*h 1997;44(3):225–62.

[21] Bursi OS, Jaspart JP. Basic issues in the finite element simulation of extended end plate connections. *Computer Structures* 1998;69:361–82.

[22] Choi CK, Chung GT. Refined three-dimensional finite element model for end-plate connection. Journal of Structural Engineering ASCE 1996;122(11):1307–16.

[23] Bahaari MR, Sherbourne AN. Behaviour of eight-bolt large capacity endplate connections. *Computers Structures* 2000;77:315–25.

[24] Sumner EA, Mays TW, Murray TM. End-plate moment connections: test results and finite element method validation. *4th International Workshop on Connections in Steel Structure*s; 2000. p. 82–93.

[25] Swanson JA, Kokan DS, Leon RT. Advanced finite element modeling of bolted Tstub connection components. *Journal of Constructional Steel Research* 2002;58(5–8):1015–31.

[26] Gantes CJ, Lemonis ME. Influence of equivalent bolt length in finite element modeling of T-stub steel connections. *Computers Structures* 2003;81:595–604.

[27] Abolmaali A, Matthys JH, Farooqi M, Choi Y. Development of moment–rotation model equations for flush end-plate connections. *J Constructional Steel Res* 2005;61:1595–612.

[28] Maggi YI, Gonçalves RM, Leon RT, Ribeiro LFL. Parametric analysis of steel bolted end plate connections using finite element modelling. *J Constructional Steel Res* 2005;61:689–708.

[29] Kukreti AR, Zhou FF. Eight-bolt endplate connection and its influence on frame behaviour. *Eng Structures* 2006;28:1483–93.

[30] Dai XH, Wang YC, Bailey CG. Numerical modelling of structural fire behaviour of restrained steel beam-column assemblies using typical joint types. *Eng Structures* 2010;32:2337–51.

[31] Concepción Díaz, Mariano Victoria, Pascual Martí, Osvaldo M. Querin , FE model of beam-to-column extended end-plate joint. *Journal of Constructional Steel Research* 67 (2011) 1578-1590.

[32] J. P. Jaspart, (2000): General report: session on connections, *Journal of Constructional Steel Research,* Vol. 55, pp. 69-89.

[33] Young CR, Jackson KB. The relative rigidity of welded and riveted connections. *Canadian Journal of Research* 1934;11(1–2):62–134.

[34] Rentschler, G. P.; Chen, W. F.; and Driscoll, G. C. Jr., "Tests and analysis of beam-to-column web connection, June 1977" (1977). *Fritz Laboratory Reports*. Paper 2164

[35] Chen WF, Lui EM. Static web moment connections. *Journal of Constructional Steel Research* 1988;10:89–131.

[36] Janss J, Jaspart JP, Maquoi R. Strength and behaviour of in plane weak axis joints and 3D joints. In: Proc. of the state of the art workshop on connections and the behaviour, strength and design of steel structures. 1987. p. 60–8.

[37] Davison JB, Kirby PA, Nethercot DA. Rotational stiffness characteristics of steel beam–column connections. *Journal of Constructional Steel Research* 1987;8:17–54.

[38] Kim YW. The behaviour of beam-to-column web connections with flush end plates *M.Sc. thesis*. University of Warwick; 1988.

[39] Steenhuis M., Jaspart J. P., Gomes F., Leino T.,: Application of the Component Method to Steel Joints, *Proceeding of the Control of the Semi-Rigid Behavior of Civil Engineering Structural Connections Conference,* COST C1, Liege Belgium, 1998, pp 125-143.

[40] Lima LRO de, Vellasco PCG daS, Andrade SAL de, Silva LAPS da. (2001): Experimental and mechanical model for predicting the behaviour of minor axis beam-to-column semi-rigid Joints. *International Journal of Mechanical Sciences* 2002 Vol. 44(6) pp. 1047–65.

[41] Neves, L.F.C, and Gomes, F.C.T.: Semi-Rigid behaviour of beam-to-column minor-axis joints. In: Eth-Honggerberg, Zurich, Switzerland, *Proceedings of the IABSE International Colloquium on Semi-Rigid Structural Connections*, Istanbul, Turkey, 1996. p. 207–16.

[42] Neves, L.F.C, and Gomes, F.C.T.: Parametric study on the behavior of minor-axis joints. COST C1 WG2 Meeting, Coimbra, November 1994, Doc. COST C1/WD2/94-14.

[43] Luciano R.O. de Lima, Jose L. de F. Freire, Pedro C.G. da S. Vellasco, Sebastiao A.L. de Andrade, Jose G.S. da Silva,: Structural assessment of minor axis steel joints using photoelasticity and finite elements, *Journal of Constructional Steel Research*, Vol. 65 (2009) 466–478.

[44] L. Simoes da Silva, Towards a consistent design approach for steel joints under generalized loading, *Journal of Constructional Steel Research*, 2008 Vol. 64 1059–1075.

[45] MSC.Marc 2015, User's Guide, "Volume A: Theory and User Information", MSC.Software Corporation

[46] Cabrero J, Bayo E. The semi-rigid behaviour of three-dimensional steel beam-to-column joints subjected to proportional loading. Part I. Experimental evaluation. J Constr Steel Res 2007;63(9):1241–53.

[47] Cabrero J, Bayo E. The semi-rigid behaviour of three-dimensional steel beam-to-column steel joints subjected to proportional loading. Part II: Theoretical model and validation. J Constr Steel Res 2007;63(9):1254–67.

[48] Loureiro A, Moreno A, Gutierrez R, Reinosa J. Experimental and numerical analysis of three-dimensional semi-rigid steel joints under non-proportional loading. Eng Struct 2012; 38:68–77.

[49] Loureiro A, M. Lopez, Gutierrez R, Reinosa J Experimental and numerical analysis of E-stubs in three dimensional joints: A new analytical formulation for the stiffness calculation. Eng Struct 2013; 1:9–53.

[50] Linfeng Lu, Yinglu Hu, T.H. Zhou et al..: Experimental research on box strengthen joint connection for weak-axis of I-section column-H-shaped beam, *Journal of Constructional Steel Research*, 2016 Vol. 37 (2) pp. 73-80.

[51] Linfeng Lu, Yinglu Hu, Hong Zheng.: Investigation of composite action in seismic performance of weak-axis column bending connections, *Journal of Constructional Steel Research*, 2017 Vol. 129 pp. 286-300.

[52] A.K. Dessouki, A.H. Youssef, M.M. Ibrahim, Behavior of I-beam bolted extended end-plate moment connections, Ain Shams Eng. J. 4 (4) (2013) 685−699.

[53] International Standard ISO 898-1: Mechanical properties of fasteners made of carbon steel and alloy steel. Part 1: "Bolts, screws and studs with specified property classes - Coarse thread and fine pitch thread", 2009.

[54] Ying Hu, Buick Davison, Ian Burgess and Roger Plank.: Multi-Scale Modelling of Flexible End Plate Connections under Fire Conditions, *The Open Construction and Building Technology Journal*, 2010, 4, 88-104.